Uncertainty analysis of acoustic flow measuring instruments for characterization of high energetic river flow

by

Kaisar Ahmed Bhuyan

A Thesis Submitted to the Faculty of Graduate Studies of
the University of Manitoba
in Partial Fulfilment of the Requirements of the Degree of

MASTER OF SCIENCE

Department of Mechanical Engineering
The University of Manitoba
Winnipeg

Abstract

Velocity and turbulence measurement uncertainty using acoustic methods in highly energetic river flows are quantified by performing measurements to isolate specific error terms, and by applying analytical methods and statistical analysis to recorded data. A MATLAB code is developed for motion compensation and data filtering. The methodology adopted is to perform acoustic measurements in a controlled laboratory setting and in an energetic river test site at Reynolds number from 0.05×10^7 to 3×10^7. As the performance of hydrokinetic turbines operating in highly energetic flows depends on localized velocity and turbulence parameters, uncertainty analysis contributes to improving river site characterization for the marine industry. The uncertainty analysis applies to acoustic instruments deployed from a stationary platform, a moving vessel, or alternatively, suspended in the water column via a cabling system in energetic river flows, which are typical configurations required by this industry. A methodology to conduct measurement and estimate the uncertainty is presented for these three configurations. The uncertainty analysis results are dependent on multiple inputs which are processed using algorithms made accessible online. A typical result of the error analysis at a velocity of 1.10 m/s a maximum deviation of 23% is observed between the measured and expected streamwise velocity at an instrument pitch angle of 45°. After implementing angle compensation the uncertainty reduces to 4%. Furthermore, by applying an IMU correction algorithm, the maximum velocity error is reduced by 29.3% and the turbulence by 77.0% after applying the motion compensation to river surface measurements. Processed flow results from an energetic river test site show the ADV overestimate streamwise mean time-averaged velocity and underestimate turbulence intensity measurements with an average of 4.6% and 27.4%, respectively.

Acknowledgements

I would like to sincerely thank my supervisor Dr. Eric Bibeau for the opportunity and freedom he gave me to develop my expertise in instrumental analysis. Without his wisdom and experience advice it would not be possible for me to finish my thesis. I would like to thank Samuel d'Auteuil and Jody Soviak for their advice and assistance. I would like to acknowledge the technical support of Zeev Kapitanker in my experimental set-up and instrumentation. I would also like to thank Sixtus Ekezie, Raul Vaid, Nick Jackimec and all the member of CHTTC research center for their continuous support throughout data acquisition and analysis.

Also, I am thankful for all of the undergraduate student research assistants who helped me throughout each summer especially Michel d'Auteuil for helping me with signal processing and development of the motion compensation code. I would like to thank NSERC discovery grant and GETS for their financial support of the project. Finally, I would like to thank my dearest friends and family for their encouragements, inspiration and supports.

Contents

List of Tables

List of Figures

Nomenclature

English Symbols

A	Energy captured area
u, v, w	Instantaneous velocity components in x, y and z directions
X, Y, Z	Streamwise, spanwise and vertical directions respectively
E, N, U	East, north and up directions in earth frame respectively
I	Turbulence intensity
K	Turbulence kinetic energy
U	Expanded standard uncertainty
k	Coverage factor
c	Speed of the sound
f	ADV frequency
g	Gravitational constant
P	Pitch angle
R	Roll angle
H	Heading angle

Greek Symbols

A_s	Cross sectional area
ρ	Fluid density
μ	Dynamic viscosity
ϵ	Turbulence dissipation
λ	Wave length
ω	Angular rate

Subscripts and Superscripts

C_p	Performance coefficient
R_e	Reynolds number
R_{eh}	Reynolds number based on channel hydraulic radius
R_h	Hydraulic radius
P_{wt}	Wetted parameter
$\bar{(\cdot)}$	Average quantity
$(\cdot)'$	Fluctuating quantity
c_i	Sensitive coefficient
u_c	Combined uncertainty
D_p	Diameter of the particle
a_{IMU}	IMU acceleration recorded in x,y and z coordinate
$\overline{a_{IMU}}$	IMU mean acceleration recorded in x,y and z coordinate

Abbreviations

ECA	Energy Captured Area
TI	Turbulence Intensity
CHTTC	Canadian Hydrokinetic Turbine Test Center
ADV	Accoustic Doppler Velocimetry
ADCP	Accoustic Doppler Current Profiler
TKED	Turbulent kinetic energy dissipation rates
IMU	Inertial Measurement Unit
ISO	International Standard Organization
AIAA	American Institute of Aeronautics and Astronautics
ASME	American Society of Mechanical Engineers

Chapter 1

Introduction

1.1 World energy demand

According to the 2015 United Nations projections, the world population is expected to rise to $9,725$ million by 2050 [6]. With this population rise, world energy consumption is also expected to increase to 239 trillion kWh by 2040 at 1.4 % per year [7]. To address this energy demand, stakeholders have identified renewable energy sources in addition to fossil fuels and nuclear energy. Amongst energy resources, fossil fuel is the most commonly used. In 2014, 78% of the total energy consumed in the world was harnessed from fossil fuel [7–9]. This poses a problem as excessive use of fossil fuels and nuclear causes not only global warming, but also causes environmental issues such as air pollution, acid precipitation, ozone depletion, forest destruction, and emission of radioactive materials [10]. However, the amount of fossil fuel resource available is limited in quantity and is on a steady decline [11]. These environmental effects of fossil fuel and increased energy demand makes renewable energy sourcing a necessity [10].

According to the 2016 Renewable Energy Policy Network for the 21st Century

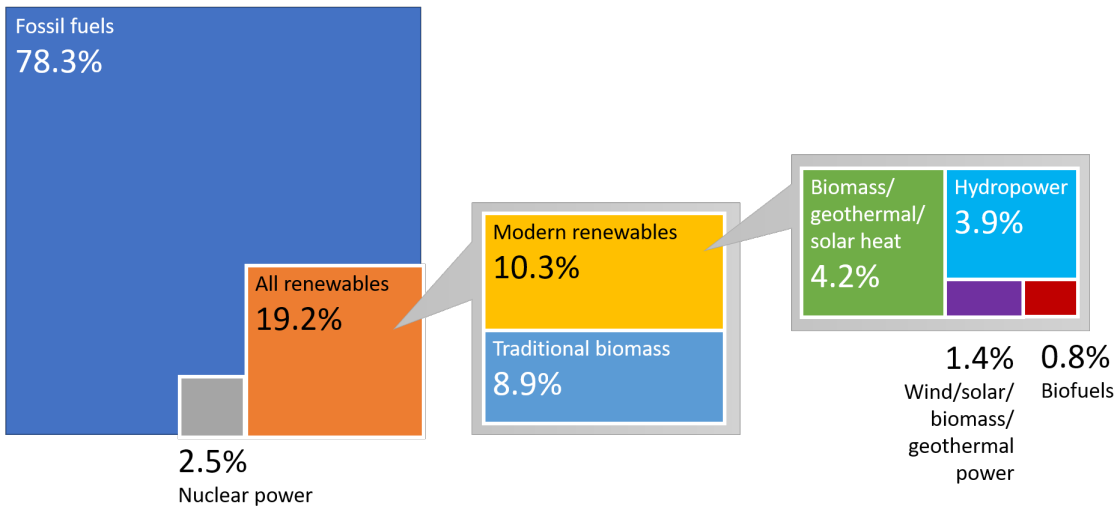

Figure 1.1: Estimated renewable energy share of global energy consumption at the end of 2014 [4]

(REN21)'s report [4, 7], renewable energy contributes 19.2% of the global energy consumption with a growth rate of 2.6% per year, as shown in Figure 1.1. Unlike fossil fuel, renewable energy sources have limited impact. Use of renewable energy sources contributes to reduce global CO_2 emissions and adds flexibility to the energy resource mix by decreasing dependence on the limited reserves of fossil fuels [12]. Different renewable energy sources such as solar, wind, hydro, and biomass are already displacing fossil fuels [13]. Renewable sources can effectively and economically meet energy demands. However, due to the supporting policies from the government for establishing sustainability, energy security, and cost reduction, the difference in generation cost between fossil fuel and renewable energy is decreasing, with many renewable options now achieving at a much lower cost [14]. Attention of researchers, energy companies, and stakeholders are moving towards renewable energy sources to meet growing energy demand and climate change challenges. Hydrokinetic energy is part of the renewable energy portfolio that is emerging.

1.2 River hydrokinetic turbine

Energy generation from hydro can be through a classical approach where potential energy of water is extracted using suitable turbo machinery [15], or through conversion of kinetic energy of flowing water using a hydrokinetic turbine (HKT) [16]. An electromechanical energy converter used in harnessing kinetic energy from flowing water source to generate electricity is known as a HKT [15]. The flowing water sources are tidal, ocean, river or channels [17].

The working principle of a HKT and a wind turbine are similar, but higher power density can be obtained from a hydrokinetic turbine compared to a wind turbine. A HKT operating in a 2 to 3 m/s flow velocity region can generate four times higher power density compared to a similarly rated wind turbine as the density of water is higher than that of air [18]. Multiple turbines also can be installed in a multi-array arrangement like in a wind farm to increase energy extraction or power production from a specific location [19]. However, HKTs are limited by the total rotor area when compared to wind energy. Power generation using HKT system also requires minimum civil work [20]. For remote communities where transmission lines are not available, developing HKTs can provide off-grid electricity because of its simplicity and cost effectiveness [21]. From a deployment standpoint, HKTs can be deployed in an energetic river site, but it is necessary to carry out a site characterization to determine the viability of HKT operations.

Power generation from HKTs depends on the energy available in the flowing water at the deployment location with performance varying depending on mechanical and electrical components, as well as system design specifications. The kinetic energy of flowing water is used to rotate the turbine blade secured to an electro-mechanical generator to generate electricity. The geometry of turbine blades and their interaction with the flow characteristics impacts the performance of HKT. These impacts faced by

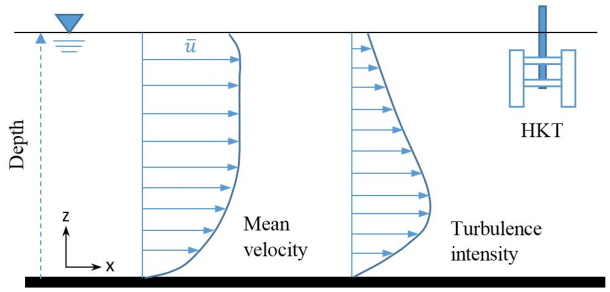

Figure 1.2: Typical distribution of velocity and turbulence profile in a highly energetic River flow of HKT application

operating turbines makes the velocity and turbulence characterization of a potential HKT location a necessity when planning a turbine project.

Figure 1.2 represents a typical velocity and turbulence intensity profile which impacts the Energy Captured Area (ECA) of a HKT in a highly energetic river flow. Flow characteristics varies with depth, location, and season. ECA is defined as the cross-sectional area of a turbine's rotor and calculated as

$$ECA = \pi r^2 \tag{1.1}$$

where r is the radius of the turbine blade from the center of the rotor.

The performance of a deployed turbine depends on the mean velocity and turbulence statistics acting on the ECA of a HKT. The minimum workable flow velocity is above 1.5 m/s, but 2.5 m/s is preferable [22]. For higher speed river flow, more engineering is required, and fewer sites are available. It is essential to characterize flow velocity accurately as the power density is related to the cube of the velocity as

$$P = \frac{1}{2} C_p \rho A u^3 \tag{1.2}$$

where ρ is water density, u is instantaneous velocity component, A is ECA, and C_p

is the performance coefficient.

The performance or power coefficient, C_p, of a turbine is defined as the ratio of actual electric power produced by a turbine to the total power supplied to the turbine blade. The maximum value of C_p is 0.59 which is referred to as the Betz limit. Change in flow direction plays a role in the selection of a HKT. For example, vertical-axis turbines are deployed in a flow region where the direction of the flow can change frequently, and the addition of a shroud makes the turbine less influenced by flow directions.

Many other factors impact the performance of HKTs. Impacts of different flow and site parameters on HKTs performance are stated in Table 1.1; Figure 1.3 shows the characterization of a highly energetic river site and different flow features encountered during the process. These include anchoring of the measurement platform, deployment of the instruments, large forces on deployed instruments, instrument vibration, unsteady velocity, turbulence, river bed roughness, water level, and measurement platform instability. These factors complicate characterization in a high energetic river environment. Hence, the characterization of a HKT deployment site is performed in three stages:

1. initial characterization,
2. detail characterization, and
3. long-term characterization.

Instruments such as an Acoustic Doppler Velocimetry (ADV), Acoustic Doppler Current Profiler (ADCP), sonar, and shear probe are used for such characterization. An ADCPs provides a velocity profile, uses a monostatic diverging beam pattern, and typically samples a larger spatial region for velocity estimation while an ADV is a point measurement system, uses a bistatic converging beam pattern, and samples a small volume of water.

Table 1.1: Effect of different flow and site parameters on HKT performance and site selection

Characterization	Tested parameter	Instrumentation	Effects
Initial	Bathymetry	Sonar ADCP	Safety Site selection Deployment Mooring system
	Depth	Sonar ADCP	Safety Site selection Deployment Turbine design
	Width	Range finder	Safety Mooring system Deployment
	Mean velocity	ADV ADCP Flowmeter Velocity meter	Turbine capacity Mooring system
Detail	Velocity profile	ADV ADCP	Turbine position Turbine design Turbine capacity
	Flow direction	ADV	Turbine design
	Turbulence intensity	ADV ADCP Shear probe	Safety Mooring system Turbine blade fatigue
	Time scale	ADV Shear probe	Turbine wear Cyclic load on turbine Turbine design
	Length scale	ADV Shear probe	Turbine wear Cyclic load on turbine Turbine design
	Dissipation	ADV Shear probe	Turbine wear Cyclic load on turbine Turbine design
	Boundary layer	ADV ADCP	Turbine position Turbine design
Long term	Flow velocity variation	ADV ADCP Velocity meter	Yearly power production
	Water depth variation	ADCP	Safety Turbine design
	Ice cover	Satellite	Safety Placement

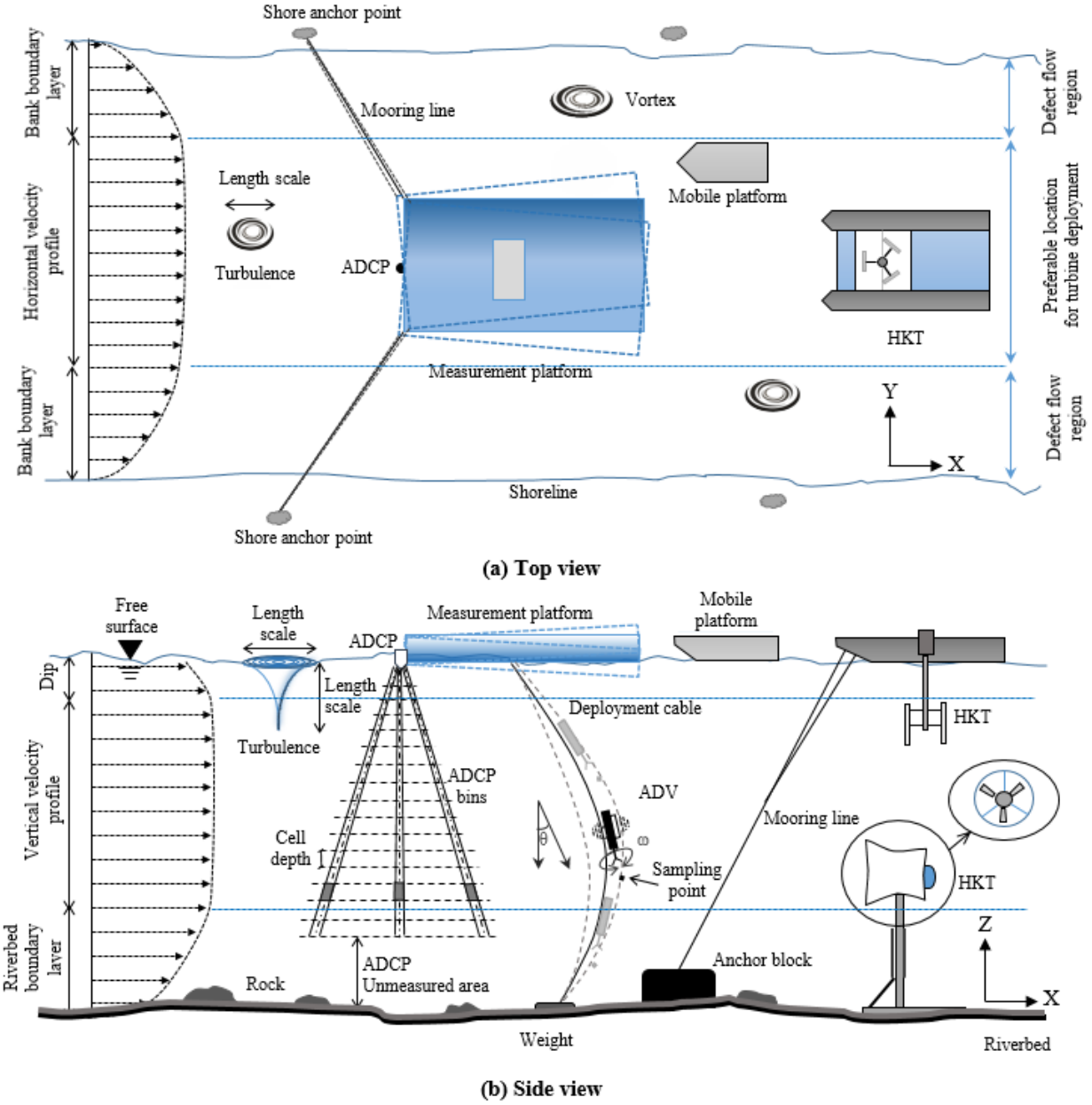

Figure 1.3: Schematic view of a river site characterization where ADV and ADCP are deployed from the measurement platform to obtain flow velocity and turbulence profile: (a) top view of a potential HKT site characterization, and (b) side view of the site characterization. The position of ADCP is fixed and deployed at the front of the measurement platform while the ADV-a point measuring device-is deployed to different depths through the water column during the characterization exercise using a cable. In between the dip and the boundary layer is the region with the highest velocity and is preferable for HKTs placement.

The ADCP is predominantly used for flow velocity distribution and discharge measurements in open channel, river, and tidal applications [1, 23–28] while ADV dominates laboratory environments [23, 29–35]. However, in recent times there has been a surge in characterizing flow in high energetic riverine environments using ADV [36–38]. This increase is because of ADV's higher resolution in velocity and turbulence measurement. In this study, the performance of ADV is tested in controlled laboratory settings, and then ADV's field measurement is compared with the ADCP measurement data.

1.3 Energetic river site characterization

Flow velocities in energetic river site are three-dimensional with significant flow fluctuations. They are affected spatially and temporally depending on flow interaction with the river bank, rocks, surface, and bottom roughness of the flowing water [39,40]. In addition, surface wake, vortex shedding, and increased turbulence are generated due to riverbed alignment, and in-stream structures like a dam, bridge piers, docks, rocks greater than 500 mm in diameter, submerged cobbles, boulder, pebble clusters [41, 42], large woody debris, and aquatic vegetation. These in-stream structures impact on turbine deployment and performance. Therefore, it is important to perform a bathymetry analysis of the energetic river site before deployment of a HKT. Bathymetry provides information on geometry, riverbed roughness and depth of the river. Furthermore, it also provides information regarding the potential site hazards and helps to identify the type of turbine design suitable for that specific location.

In addition to bathymetry, free stream velocity measurement is another important factor that is determined during the characterization of an energetic river site. Free stream velocity can be measured with an ADV and an ADCP. As part of the initial

characterization, the velocity of different sections of the river is measured to identify the region with the highest velocity and sufficient depth for HKT installation. After identifying the locations with the highest velocity, a detailed in-depth analysis of the selected locations is performed.

A detailed and long-term assessment of the flow characteristics is required to obtain information at different depths of the selected locations. For this stage of characterization, flow statistics such as boundary layer thickness, Turbulence Intensity (TI), Turbulence Kinetic Energy (TKE), length scale, time scale, Reynolds stresses, and dissipation rate are measured. The boundary layer is defined as the region close to the bottom of the river bed where flow velocity varies from zero at the bed to 99% of the free stream velocity or the maximum velocity [43]. This distance is the boundary layer thickness, δ. Near the free surface, the velocity decreases again and is known as a dip, as shown in Figure 1.3b. At the bank of the river, another boundary layer occurs. This type of boundary layer is known as the bank boundary layer, as illustrated in Figure 1.3a. For HKT applications in an open channel and rivers, the boundary layer thickness is considered not suitable for turbine deployment. It is recommended to place a HKT in high velocity regions so that more power can be extracted.

Meanwhile, turbulence impacts performance and operational lifetime of a turbine [44, 45]. This makes turbulent statistics calculations an important concept when planning a HKT deployment in an energetic river site. According to Reynold's decomposition [46], a turbulent flow is the combination of average component and a fluctuating component of flow velocity, defined as

$$u = \overline{u} + u'; \quad v = \overline{v} + v'; \quad w = \overline{w} + w' \tag{1.3}$$

where $\overline{u}$, $\overline{v}$, and $\overline{w}$ represents average streamwise (longitudinal), spanwise (transverse) and vertical (depth) velocity components, while their corresponding fluctuating components are u', v', and w', respectively. Root-mean-square (RMS) of fluctuating components are known as the strength of turbulence and are represented as $u_{rms} = \sqrt{\overline{u'^2}}$, $v_{rms} = \sqrt{\overline{v'^2}}$, and $w_{rms} = \sqrt{\overline{w'^2}}$. TI and TKE can be calculated using the mean fluctuation and RMS values of velocity components. A larger RMS value represents a higher TI although they have the same mean velocity.

The Reynolds normal stresses, also known as mean pressure stresses, are defined as $\overline{u'^2}$, $\overline{v'^2}$, and $\overline{w'^2}$, whereas Reynolds shear stress or mean stresses are defined as $\overline{u'v'}, \overline{v'w'}$, and $\overline{w'u'}$. The difference in mean shear load induced on the blades causes the rotation of the blade while the orientation of the eddies in the flow is identified from Reynold's shear stresses. These differently oriented eddies and forces impact the performance of a turbine. Therefore, it is important to quantify the potential eddies and the load they induce on the turbine [47].

1.4 Measurement uncertainty in an energetic river-ine application

Velocity measurements in energetic river sites require the capturing flow features such as flow velocity, turbulence, surface and riverbed roughness. In a river site, these flow features are variable. Therefore, any measurement technique adopted for velocity flow characterization must be able to work in high velocity and river depths. The flow velocity of an energetic river site varies from 2 to 3 m/s which results in high drag effects on instruments such as the ADV, ADCP, and their support structure. Drag force experienced by these measurement instruments and support components can be calculated by

$$F_D = \frac{1}{2} C_D \rho U^2 A \tag{1.4}$$

where C_D is the drag coefficient of the body, and A is the ECA. For example, an ADV submerged in a river site with an average velocity of 2.5 m/s experiences drag force of approximately 100 N, considering a value of C_D as 0.35 obtained from Fox and McDonald [48]. With this force acting on a body, it is difficult to keep such instruments in a stationary position during measurements. Moreover, from a recent test conducted at energetic river sites it was observed that when the ADV is deployed near the riverbed with a cable, it experiences a large force and hence lifts the ADV upwards, as shown in Figure 1.3. This has made obtaining the boundary layer data a more difficult task. A possible solution to this could be achieved by adding more weights at the end of the ADV deployment cable. The sources of uncertainty in energetic riverine measurements are listed in Table 1.2. However, this research focuses on particle size, turbulence, motion, vibration, and instrument orientation uncertainty, as highlighted in Table 1.2, as these are prevalent in the riverine application.

Furthermore, flow measurements in high energetic river environment require personnel training, safety, knowledge of underwater hazards such as rocks, environmental conditions like rain, flood or ice formation, transportation, logistics, and access to the measurement site. Other factors include rugged instrument support and their ongoing maintenance, workforce, slipping and tripping hazards, and anchoring of the measurement platform. For such measurement the marine Industry needs to develop best practice to reduce the uncertainty in velocity measurement in energetic rivers.

Table 1.2: Measurement uncertainty of acoustic instruments in an energetic riverine application highlighting the five terms addressed in this study as these are prevalent in HKT riverine application. Other error sources are covered in the literature already.

Source	Uncertainties	Remarks
Instrument	Doppler noise	Error sources are covered in the literature already. Section 2.4
	Sampling volume	
	Sampling frequency	
	Sampling time	
	Spatial and temporal resolution	
Environment	Particle size	Section 2.5, 3.3.1, and 4.2
	Turbulence	Section 2.5, 3.3.2, and 4.3
	Air bubbles	Literature. Section 2.5
	Sound speed	
	Presence of magnetic field	
Deployment	Instrument inclination	Section 2.6, 3.3.3, and 4.4
	Motion	Section 2.6, 3.3.4, and 4.5
	Vibration	Section 2.6, 3.3.4, and 4.5
Data analysis	Coordinate transformation	Literature. Section 2.7
	Post processing	

1.5 Objectives

The focus of this research is to perform an investigation on flow measuring instruments such as ADV in a high energetic riverine environment. This involves inherent uncertainty of the instrument and the measurement procedure employed during site characterization, including:

1. Identify the sources of ADV uncertainty during deployment and environmental impacts on the ADV in high energetic flow applications,
2. Determine the effect of particle size, turbulence, instrument orientation, vibration, and motion in ADV measurement in a controlled laboratory setting by isolating each error terms, applying analytical methods, and statistical analysis,
3. Develop a MATLAB code to compensate ADV's motion and instrument orientation in high energetic flow characterization, and

4. Evaluate the compensation method developed for the ADV uncertainties for the high energetic riverine application and comparing with the ADCP measurement data.

5. Develop best practice for these type of flow measurements in energetic rivers.

1.6 Methodology

To achieve research objectives, the following methodology was applied. Tests investigating the effect of seeding particle size, instrument orientation, motion, and vibration were performed in a controlled environment using a water tunnel and shaker table. During laboratory tests, the value of the parameters such as vibration frequency and displacement, water flow velocity, instrument motion, position, and bed roughness were controlled and isolated to find their effect on measurement uncertainty. Field experiments were carried out in high energetic river site at the Canadian Hydrokinetic Turbine Test Center (CHTTC) and the results obtained compared with the results obtained from the controlled environment experiments. Finally best practice is developed for the field experiments to minimize uncertainty of the measurement. The methodology applied in this study is illustrated in Figure 1.4.

1.7 Thesis contribution

Performance of the ADV was tested in a controlled laboratory setting with different seeding particle, turbulence level, and surface roughness. Different sized seeding particle was used to increase the signal strength of the ADV, while rocks of various size and shape were used to change the roughness and turbulence statistics of the water tunnel. In this study, five measurement uncertainty were quantified: particle size, turbulence, instrument orientation, vibration, and motion.

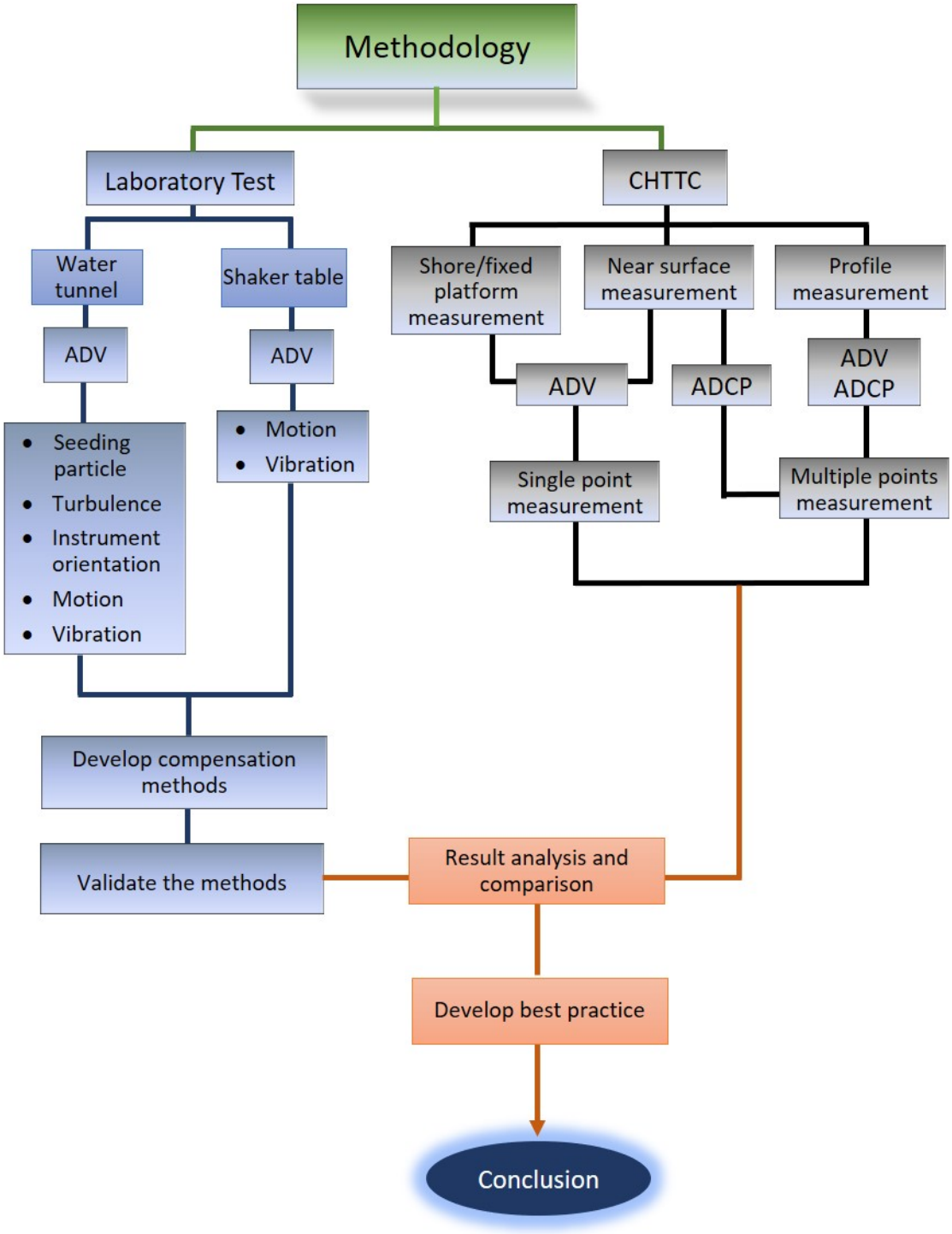

Figure 1.4: Methodology to estimate uncertainty of velocity measurement in high energetic river flow

A MATLAB code was developed to detect and correct angular position and remove ADV movements due to the high energetic flow velocity. The code uses the Inertial

Measurement Unit (IMU) data for compensation. The performance of this IMU unit was tested and validated using a uniaxial shaker table in this study. Then the performance of the Matlab code developed was tested in a water tunnel with known flow specification. This code was then applied in less controlled environments at the CHTTC. To demonstrate the flexibility of the compensation code developed, measurements were performed from a platform using three point anchoring system, two points anchoring with support from a rigid structure, one point anchoring system, and without any anchoring point. The code has been documented and is available online and detailed in Appendix B.

Factors were identified and compensated to enhance the accuracy of the measurements applied to energetic river flows. Site characterization with the analysis performed will help companies to perform accurate turbine performance predictions and contribute to International Electrotechnical Commission TC−114 marine energy−wave, tidal and other water current converters standard certification. Best practice are listed in the conclusion in term of data post processing and how to minimize the uncertainty.

Chapter 2

Sources of uncertainty in energetic riverine measurements

2.1 Measurement uncertainty of acoustic instruments

The measurement of a physical quantity has uncertainty. Measurement uncertainty is the chance that an error physically exists in a measurement [49]. There are many factors that may influence measurements. Although measurement conditions can be controlled, they cannot be predicted completely, leading to additional error associated with the results. Error and uncertainty are not the same. The error is the difference between the true value and the measured value. The true value is the actual value of the measured parameter. Identifying the true value is the first step of uncertainty analysis. As there is no method to measure true value, an accepted reference value established from the repeated measurements is considered as the true value. However, uncertainty is the value of a result within which the true value is asserted with a specified level of confidence. Two numbers are required to quantify an uncertainty,

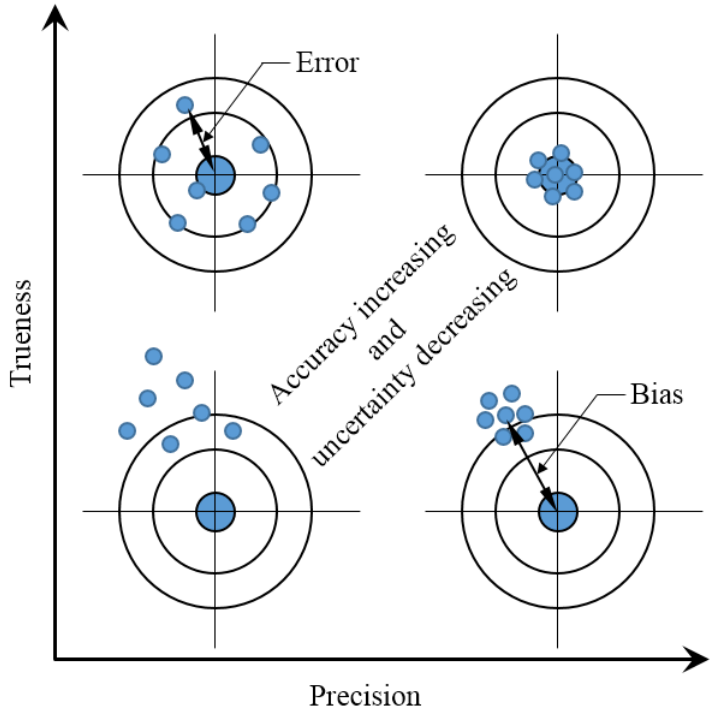

Figure 2.1: Error terminologies showing error, uncertainty, and bias

the margin of value or interval and the confidence level. For example 2.00 ± .01 m/s at 95% level of confidence means that the true value lies between 1.99 to 2.01 m/s with a certainty of 95%. The relationship between different error terminology is illustrated in Figure 2.1. Trueness is the closeness between the average value of multiple test results and the accepted true value; the closeness of independent measurements with its true value, is known as precision. Low uncertainty is achieved when precision and accuracy of the test result are high.

2.1.1 Uncertainty of acoustic Doppler velocimeters

Laser Doppler velocimetry and particle image velocimetry are used in laboratory settings for measuring flow velocity and turbulence but are difficult to apply in riverine environments due to the their complexities. Hot-wire is also another popular instrument for flow characterization with a good temporal resolution but preferably used in laboratory settings. On the other hand, ADV can be used in laboratory

and field applications in river [25, 28, 38, 50–52], tidal [26, 53–57], estuaries [58, 59], and in open channels [60] with good accuracy. The ADV can be used in a wide range of operations due to its robustness, ability to measure three-dimensional instantaneous velocities, high sampling rate, with no calibration needed, and relatively low cost.

Acoustic methods offer the ability to perform point and profile measurement. ADV is a single point measurement instrument. So multiple ADVs have to be used for velocity and turbulence profile measurement of a river site, or the position of the ADV changed within the water column. Using multiple ADVs or changing the ADV position during measurement process in high energetic river site is difficult and adds more uncertainty to measurements. Other sources of instrument uncertainty are Doppler noise, sampling frequency, time, and volume as well as spatial, and temporal resolution.

Performance of an ADV is also affected by flow conditions, deployment techniques and the post data analysis method. For example, according to the manufacturer guide, ADV can auto correct pitch angle of the instrument up to 10° angle [2]. For full profile measurement in a high energetic river, it is difficult to maintain below the recommended value of 10° angle. In that case, if the pitch angle is more than the limit recommended by the manufacturer, an external correction routine needs to be implemented to reduce the uncertainty.

2.1.2 Uncertainty of acoustic Doppler current profilers

ADCP can be used to obtain the velocity and turbulence profiles of a river or channel. Deployment of an ADCP is relatively simple compared to an ADV as the position of an ADCP does not have to be changed while measurements are carried out. Amongst other factors considered in choosing an ADCP over

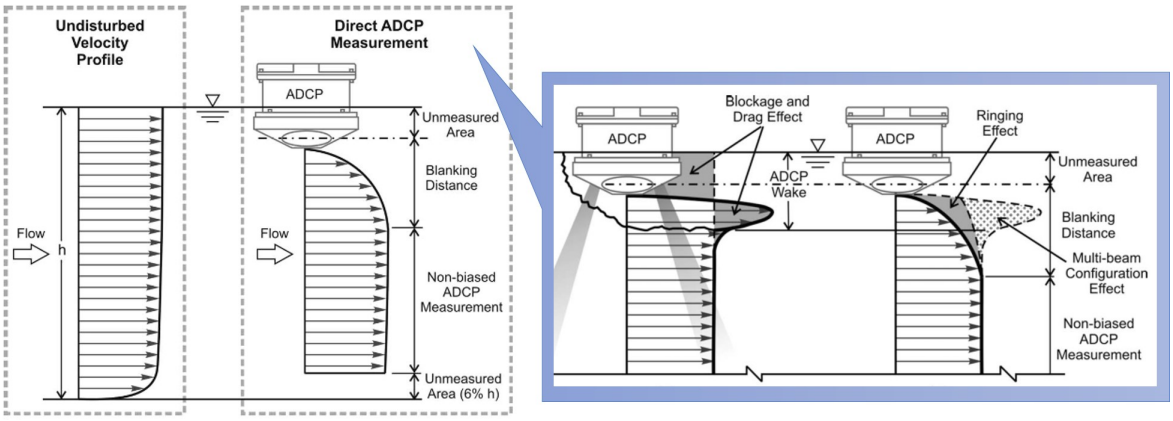

Figure 2.2: Schematic view of the ADCP uncertainty in vertical profile measurement in an undisturbed channel flow (not to scale). The uncertainty includes an unmeasured area at top and bottom of the test section, blockage effect, ringing effect, and blanking distance [1].

other acoustic instruments, ADCP is robust and has good resolution. Hence, it is commonly used for site resource assessment like river discharge measurement, streamwise velocity distribution, turbulence characteristics, sediment transportation, the spatial distribution of velocities, riverbed survey, and longitudinal dispersion estimation [61, 62].

ADCP measures flow velocity by averaging flow velocity over a relatively large volume of water. With increase in the separation distance between the sensor and the volume of the water, the sampling volume increases. This leads to higher uncertainty due to the spatial resolution at a longer distance from the deployment point. At the longer distance, the acoustic signal has to travel a longer length, decreasing the ability of ADCP to measure the higher frequency range. The accuracy of the measurement especially decreases near the riverbed and wake region [63]. However, ADCP uses internal velocity distribution model to estimate the velocity of the unmeasured area near the river bed and the free surface, as shown in Figure 2.2. Doppler noise in the ADCP data set also causes inaccuracy in velocity measurements [64].

There are other factors which affect ADCP measurements. Muste [1] identified

nineteen sources of error in ADCP for discharge measurement which are common for velocity and turbulence profile measurements in an energetic river site. In addition, instability of the measurement platform adds more uncertainty to the measurement. Muste [1] classified the sources into three groups- major, significant, and minor factors. Some of them can be controlled or limited by changing the settings or by post-processing parameters such as noise, velocity ambiguity, sampling time, depth, temporal resolution, and edge estimation. Others are difficult to control or to estimate like side lobe-interference, blanking distance, vertical profile model, beam angel effect and discharge model. A visual representation of some factors are presented in Figure 2.2.

2.2 Error sources of acoustic instruments

Muste [1] classified measurement uncertainty of the acoustic flow measuring instruments into three major rank based on their influence in the overall characterization process and mentioned in Table 2.1. Some of the major error terms are discussed in this section.

2.2.1 Doppler noise

ADV works on Doppler shift concept. Initially ADV transducer transmits short periodic acoustic pulses, a small portion of the acoustic pulse reflected form suspended water particles of the small sampling volume. These pulses are then reflected back to the ADV, where the frequency of these pulses are then measured. ADCP also works on the same principle with relatively wide sampling area. The actual flow velocity is calculated based on change in the Doppler shift between the sent and return acoustic signal of particle within the sampling volume. The return signal contain noise and spikes along with the velocity recordings. This noise creates an insignificant effect on

Table 2.1: Error sources of the ADCP and their ranking for characterization proposed by Muste [1]. Table also shows if error term is relevant to ADV measurements. Highlight sections are addressed in this study.

S/N	Uncertainty	Error rank	Total uncertainty	ADV relevance
1	Spatial resolution	Significant: can be limited	NA	√
2	Noise	Major: can be imited	Variable	√
3	Velocity ambiguity	Significant: can be limited	Variable	√
4	Side-lobe interference	Major: difficult to control/limited	NA	×
5	Temporal resolution	Minor: can be limited	NA	√
6	Sound speed	Significant: can be limited	Variable	√
7	Beam angle	Minor: difficult to control/limited	1%	×
8	Boat speed	Major: can be limited	Variable	√
9	Sampling time	Significant: can be limited	3% to 21.9%	√
10	Reference boat velocity (bottom-track profiling)	Major: can be limited	NA	×
11	Blanking distance	Major: difficult to control/limited	NA	×
12	Depth (bottom-track profiling)	Significant: can be limited	2%/ping (RDI-ADCP)	×
13	Time	Minor: difficult to control/limited	0.01 sec	√
14	Rotation	Minor: difficult to control/limited	NA	√
15	Edge	Minor: can be limited	NA	×
16	Vertical profile model	Significant: difficult to control/limited	1% to 4.3%	×
17	Discharge model	Minor: difficult to control/limited	-0.2% to -0.6%	×
18	Finite summation	Minor: can be limited	<1%	×
19	Site selection & vessel navigation	Significant: can be limited	NA	×

Table 2.2: Vector ADV wake spots [2]

Nominal velocity range (m/s)	Wake spots (m)
7.00	0.02, 0.04
4.00	0.03, 0.06
2.00	0.05, 0.09
1.00	0.08, 0.20
0.30	0.20
0.10	0.46
0.01	3.12

the mean statistics of the flow.

2.2.2 Sampling volume

The sampling volume of the ADV instrument is a 0.015 m diameter cylinder with 0.005 - 0.020 m in height, located 0.15 m away from the ADV transmitter. These sampling volume can be adjusted from ADV settings by changing the height of the cylinder. A small sampling volume will lead to weaker signal strength. Micro turbulence characteristics may not be captured when using a large sampling volume. Furthermore, if the sampling volume is close to the solid boundary it may increase uncertainties in velocity measurements. This phenomenon is known as wake spot. Wake spot depends upon the nominal velocity selected in ADV configuration setup and it can varies from 0.02 to 3.12 m. A complete chart of the relation between wake spot and nominal velocity is given in Table 2.2.

2.2.3 Signal-to-Noise Ratio (SNR)

The consistency of returned signals within the sample volume in the sample period is measured by the percentage correlation and SNR value. These are primarily used to identify the quality of the measurements and accuracy of the acoustic instruments. SNR value indicates the strength of return signals compared it to the instrument noise level and calculated by

$$SNR = 20\log_{10}(Amplitude_{signal}/Amplitude_{noise}) \tag{2.1}$$

Percent correlation indicates the relative consistency of the signal from the scattered particle within the sampling volume [65]. Manufacturer recommended SNR value is greater than 5 dB for mean velocity measurement and for turbulence measurement it is greater than 15 dB [2,66]. A correlation greater than 70% is also recommended to achieve good data [67].

2.2.4 Sampling frequency and time

Sampling time also plays an important role in determining of the turbulence characteristics of the flow velocity [1]. Biased error of the mean flow measurement results due to the insufficient sampling time. This bias error can be minimized by sampling long enough at the highest sampling frequency so that a statistically large sample of the flow structures is captured. At the mean time, faster sampling frequency is required for small sample volumes [68] and sampling time should be long enough to capture all turbulence properties. These sampling volume, time, frequency and location of the sampling volume all are correlated. Limited sampling also biases the discharge estimation through the unmeasured layers as the ADCP extrapolation algorithms does not apply to the instantaneous velocities.

2.3 Flow characterization in high energetic sites

The importance of site characterization was presented in Section 1.3, and the difficulty associated with these measurements were discussed in Section 1.4. Many studies have focused on coastal and tidal flow measurement for marine energy [69–71]. Relatively little development has been done in the field of a riverine hydrokinetic

energy field. Among them, the best practice for tidal and riverine HKT is outlined by the researchers at Oakridge National Laboratory [63, 72, 73]. In their study, they discuss acoustic instrumentations like ADV and ADCP, deployment procedure, and also the methods for post-processing the data. These practices are not universally adopted, and developments are still ongoing [74]. Some of the research work and their findings are summarized in Tables 2.3 and 2.4.

Gunawan et al. [74] investigate a tidal site to deploy up to 30 turbines in different array positions. This study focused on the instantaneous velocity component, direction, turbulence characteristics, and hydrodynamic power density of the site at rotor hub height. During the study period, the maximum velocity of the tidal site was 2.4 m/s with an average velocity of 1.4 m/s. A comparison of the experimental analysis and model base resource assessment of the site was conducted and found that the calculated power density of 2.26 to 2.31 kW/m^2 was one order higher than the model predicted power density. The main reason behind the deviation was assumed to be the spatial and temporal resolution of the numerical model. Finally, it was recommended to use the model-based result for initial assessment, but to obtain an accurate estimation of the flow characteristics and site measurement with appropriate instruments is required. This study shows that resource assessment at the tidal site can be challenging.

Researchers from Acadia University, Dalhousie University, Mavi Innovations, and Fundy Tidal conducted researches at Petit Passage to characterize tidal flows and maximize turbine power generation [27]. ADCP data were collected and compared with computer models. During the experiment, the flow speed varied from 0.25 to 4.0 m/s. There was a good agreement observed between the computer model's prediction and the field experiments data at higher flow speeds in the tidal cycle. Later computational fluid dynamics model was used to configure two 10 m diameter

Table 2.3: Summary of literature review of ocean and tidal site flow characterization

Author	Instrumentation	Site specification	Findings
Guerra et al. [75]	ADV and ADCP	U = 1 to 4 m/s	Vessel-mounted ADCP was used for the long-term velocity measurements whereas Tidal Turbulence Moored ADV was used for turbulence measurement. The results showed that the mean kinetic power density was above 5 kW/m^2 found at a depths less than 60 m.
Karsten et al. [27]	ADCP and computer-aided model	U = 4 m/s (max)	Computer-aided models under-predicted the flow velocity at the early stage while the flow was slow but with the increase in the flow speed better agreement was observed between the models and the ADCP dataset. Later these data were used to simulate two 500 kW turbines in an array arrangement to maximize energy extraction by avoiding wake interaction.
Gunawan [74]	ADV	U = 2.40 m/s (max)	ADV at HKT hub height was used to estimate current speeds, current directions, turbulence intensities, and power densities for a tidal energy site and compared with the national tidal resource assessment data. A significant difference was found between power density calculated using model and site assessment.
Matt et al. [56]	ADV, Shear probe, and Underwater imaging	NA	Optical signal transmission technology was used to characterize turbulence properties (TKED and TD) then compare with share probe and ADV data. ADV estimate TKED successfully in the high energetic environment then comparison with share probe to estimate error.
Hay et al. [26]	ADV and ADCP	U = 1.60 m/s (max)	ADV velocity data found noisy, the average correlation was below 60%, and the variance method was used in ADCP velocity spectra to estimate turbulence properties.
Georgia TecResearch Corp [55]	Numerical	Varied	Regional ocean modeling system numerical model is used to predict the tidal current and power density of the Georgia coast of the USA. No characteristics data was provided.
Thyng and Riley [54]	Numerical	NA	From this study, they were able to find out the region with the highest mean kinetic power density which will eventually help to narrow down the region where proper realistic site characterization is required before turbine deployment.

turbines rated at 500 kW in 3 m/s flows in three different array arrangement. From the experiment, it was found that turbine performance is affected by the wake interaction if they were placed in the same streamline, which was avoided by changing turbine configurations. At the end of the study, researchers recommended more R&D works to improve computer models and more field experiments to provide accurate information.

Arango [50] performed a numerical assessment of hydrokinetic power located downstream of a dam to examine the performance of the turbine in a riverine setting. The average mean river velocity of the site was around 2.70 m/s calculated based on the discharge rate and the cross-sectional area of the dam while Reynolds numbers of the site varied from 1×10^7 to 3×10^7. The power density of the site and the performance parameter provided by the turbine developer were used to calculate the performance of the turbine. Higher power density was observed in the upper section of the water column, and this location was recommended for the surface mounted turbine to maximize turbine performance. It was also found that the capacity factor of the turbine decreases with increasing rotor size and capacity of the turbine. In the study, there was no discussion on turbulence phenomena, and it's the effect on the turbine performance.

Birjandi [51] performed a field survey upstream of a 25 kW turbine on Winnipeg river. The site water depth varied from 7 to 10 m while the average velocity of the river was over 2 m/s, and turbulence intensity varied from 2.5% to 15.4%. Subsequently, scaling law was used to model river condition in a controlled laboratory where more experiments were performed with a small-scale model turbine to understand it's performance effect with different solidity, pitch angle, free surface, and Reynolds number. The study shows that a low-velocity region was generated at one diameter upstream of a turbine which causes higher fluctuation in the turbine power output

Table 2.4: Summary of literature review of river site flow characterization

Author	Instrumentation	Site specification	Findings
Gunawan et al. [76]	Eco sounder, survey boat, ADV, and ADCP	NA	Provided an overview of the properties of a potential HKT site and deployment methods of instruments for flow characterization. ADCP was suggested for velocity measurement while ADV was proposed for high-resolution velocity and turbulence measurement.
J. Woods [28]	ADCP	U = 2.1 m/s (max)	5 and 25 kW vertical axis hydrokinetic turbine were tested at -36°C to 30°C and 2 to 2.6 m/s. Experimental results showed that HKT could provide reliable power in cold climates if they were deployed below the water surface.
Samuel [38]	ADV, ADCP, and Shear probe	U = 0.8 - 2.70 m/s Depth = 11 m Re = 1.34 - 1.86×10^7 Fr = 0.27 (max)	Developed a new method of ADV and ADCP deployment in an energetic riverine environment. Form analysis 4.38% difference was found between ADV and ADCP velocity data whereas for turbulence the maximum difference is 87.74%.
Karsten [27]	CFD and ADCP	U = 1 - 1.8 m/s Depth = 4.5 - 11.5 m	A correlation of 0.96 was found between the ADCP measured flow rate and simulated velocities. A power curve was generated using these velocities. Power generation of the ten turbines located downstream of the dam was calculated by using a computer model and found that 2.04 GWh of electricity could be generated from the available energy resource. This result demonstrated the potential of the available energy downstream of a hydroelectric plant.
Birjandi [51]	ADV, ADCP, and Shear probe	U = 2.1 - 2.5 m/s Depth = 7 to 10 m	A vertical axis hydrokinetic turbine of 25 kW capacity was tested upstream of a dam and near a walking bridge. From the experiment, it was found that at x/D = 1 upstream of the turbine turbulence kinetic energy of the flow increases whereas the mean velocity dropped by 20%.
Arango [50]	Numerical	U = 1.57 - 3.5 m/s Depth = 5.4 - 9.88 m Re > 3×10^7	A 50 kW horizontal axis turbine was deployed at low flow but higher depth region and a 25 kW vertical axis turbine deployed at high velocity and shallow area to analyzed their performance at the downstream of a dam. Average power was calculated by 8 kW and 31.5 kW respectively.
Toniolo et al. [25]	ADCP, multi-beam echosounder, and numerical	Depth = 5 - 15 m Width = 90 - 190 m U = 1.90 m/s (max) Fr = 0.30	Provided information about river discharge, velocity, power density, Fr number, and suitability of installing and operating HKT. Maximum velocity was found at 0.6 m depth from the riverbed.

when the turbine was in an operational state.

2.4 Acoustic instrument uncertainty

The uncertainty of acoustic flow measuring instruments are Doppler noise, sampling volume, frequency, time, spatial and temporal resolution, near transducer error, side lobe interference, and blanking distance, as mentioned in Table 1.2. The ADV measured data contain Doppler noise aliases from the return signal over the Nyquist frequency. This Nyquist frequency is defined as the minimum sampling frequency without introducing errors, which is twice the highest frequency present within the signal. It occurs if the flow velocity reaches above or below the nominal velocity range [77]. Scattered velocity signal variance of the particles in the sampling volume creates a immense velocity gradient in the acoustic beam, which is source of Doppler noise in the acoustic instrument velocity measurements [78]. Some of the research work and their findings are summarized in Table 2.5.

According to McLelland *et al.* [33] turbulence decorrelation, the phase difference of particles between the measurements of transmitter and receiver beam divergence are the sources for the scattered velocity signal. McLelland *et al.* also found that, with the increase in sampling rate from 25 to 100 Hz average Reynolds normal stresses of $\overline{u'^2}$, $\overline{v'^2}$ and $\overline{w'^2}$ velocity component increased by 10%, 4% and 40% respectively. However, Reynolds shear stresses are less affected by increasing Doppler noise and sampling rate, which is less than 1%. At the end of the study, the authors recommended using high-frequency noise filter to achieve a good result. Furthermore, K. Miller [80] found that Doppler noise decreases with the increase in SNR value up to a 420 dB and subsequently a little change was observed in Doppler noise.

The ADCP's has a lower sampling frequency with a higher sampling volume, while ADV's has a higher sampling frequency with a smaller sampling volume;

Table 2.5: Summary of literature review of acoustic instrument uncertainty in laboratory and field experiments

Author	Instrumentation	Specification	Findings
Voulgaris [32]	ADV and LDV	Open-channel flume experiment	Found out three causes of the Doppler noise as (1) flow turbulence and scattering particles (2) probe beam divergence and (3) mean velocity variance of the particles within the sampling volume.
Chanson [35]	ADVP	Open-channel	Developed a method to reduce noise level from the 3D acoustic velocity profiler in mean turbulence measurement with a relative error lower than 10%.
McLelland et al. [33]	ADV	Statistical and laboratory experiment	The error associated with Reynolds normal stress was higher as compared with Reynolds share stress in ADV measurements, which was improved by filtering higher frequency noise, using higher sampling frequency instruments and replacing removed data.
Richard [79]	ADV, ADCP	Statistical and experimental	Developed a method to estimate Doppler noise.
McLelland et al. [33]	ADV	Statistical and laboratory experiment	Measurement uncertainty increases with the increases in the sampling frequency as instrument noise increases, but it also increases the resolution of the measurement which helps to understand the different flow phenomena correctly.
Muste [1]	ADV, ADCP	Open-channel	Error magnitude depended upon the measurement depth and turbulence intensity of the measurement site. For the tested site, error varied from 3% to 21.9% in velocity measurement for measurement time greater than 3 minutes.
Koch and Chanson [34, 35]	ADV	Laboratory and field experiment	Discussed the effect of near wall boundary proximity on the sampling volume location. A laboratory experiment showed that streamwise velocity was affected by the boundary proximity if the location of the sampling volume was less than 30 to 45 mm.
Nystrom et al. [23]	ADCP and ADV	Laboratory experiment	Found out spatial averaging of the ADCP bin data caused bias estimation of the highly three-dimensional mean flow and also limited the ability of ADCP of turbulence characteristics measurements.

measurements are affected by Doppler noise. Doppler noise can be estimated from sensor configuration or manufacturer information. Alternatively, if the sampling frequency is high enough, it also can be calculated from the signal spectra of the instrument [81]. An alternative method for estimating Doppler noise is proposed by Richard [79] for an instrument with lower sampling frequency like the ADCP.

2.5 Environmental uncertainty

In laboratory settings, flow velocity, turbulence, the roughness of the boundary layer, and the orientation of instruments can be controlled as per the experimental requirement. The quality of the water can be controlled by using filters, and seeding particles can be added to increase instruments performance. However, the flow velocity of the river is always changing due to precipitation and upstream dam operations. Large obstructions and river bank change the flow direction. There is limited opportunity to add seeding particle, although Milk can be added as in Reference [37]. Thus in riverine measurements, there is limited control over the environments, and this creates complexity and uncertainty in instrument measurements. Some of the research work and their findings on the environmental effect on instrument performance are presented in Table 2.6 and 2.7, and some of the important findings are reviewed below.

Nikora [31] performed experiments with salty water, 8 - 10 μm sized hollow glass sphere seeding particles, air bubbles, and organic particle in laboratory settings to calculate measurement errors of ADV in turbulence measurement. The average velocity of the test ranged from 0.003 to 0.90 m/s. Results show that even in highly turbulent flow, seeding particle has a significant influence on noise detection, which is 4 - 5 times higher than air bubbles and 2 - 3 times more than fine silt particles.

In rivers seeding particles or any foreign materials cannot be added due to the

Table 2.6: Summary of literature review of environmental uncertainty for acoustic devices in flow measurements

Author	Instrumentation	Site specification	Findings
Under-wood [30]	ADV, LDP, and pitot tube	Wave tank and wave flume, U = ±(0.10 - 1.0) m/s	10 μm sized seeding particle was used for the experiment and found that in some cases obtained SNR value was below 20 dB which caused noisy data. To achieved velocity data with low variance, higher sized seeding particle with a nominal velocity close to the actual velocity was proposed.
Nikora [31]	ADV	Storage tank, and laboratory flume, U = 0.90 m/s Particle size = 8 - 10 μm	Performance of ADV measurement in high turbulent flow was influenced by seeding particle or air bubble presence in water. Results showed that the presence of seeding particle was 4 - 5 times effective than air bubble in noise detection.
Buykx et al. [82]	Laser light scattering	River and lake	Found that for of the river the particle size falls one range and particle size distribution of the river falls between 3 to 300 μm. For all of the tested river site has a higher percentage particle size of 20 μm or more.
Mori et al. [83]	ADV, DVP	Wave Flume Slope = 1/30 Wave height = 0.115 - 0.163 m Wave period = 1.6 - 3.8 s	Found that the formation of air bubble larger than 0.1 mm was independent of water depth and location. Strong turbulence was generated when these air bubble break near surface region. The dual-tip resistive void probe was used to measure the size of bubbles. Experimental results showed that a linear relationship between void fraction and TKE.
Blanck-aert and Lem-min [84]	ADV, ADVP	Open-channel laboratory U = 0.62 m/s Re = 108×10^3 Fr = 0.47	Developed a non-polluting method of generating micro hydrogen bubble in the flow to improve acoustic scattering level. Laboratory test shows that measurement with the hydrogen bubble increase signal strength and contains considerably less noise in turbulence estimation.
Bibeau et al. [36]	ADV	Laboratory and river U = 0 m/s (lab) U = variable (river)	ADV recorded dataset has different size of spikes on the velocity component depending on the location and the size of the air bubbles. Although it does not affect the mean velocity components measurement, while power spectra and autocorrelation are affected by it.
Bir-jandi [37]	ADV	Laboratory and river U = 0 m/s (lab) U = 2.4 m/s (river)	A hybrid despiking method is proposed and analyzed to remove spikes generated in the velocity component due to bubbles in the flow. With the implementation of the despising routine on most noise river dataset skewness and kurtosis value improved from -10.92 and 310.30 to -0.7 and 0.03 respectively, which support Gaussian distribution.

sensitivity of the environment and volume flow rate. To solve the problem Blanckaert and Lemmin [84], developed a technique to generate micro hydrogen bubble to improve acoustic instrument performance by increasing acoustic scattering level in the flowing water. Laboratory test results indicate improvement in turbulent normal stress measurement as compared with low scattering level. Signal above 1 Hz contains most of the noisy data in both cases. This method is non-polluting but cannot be used in practical fields like river or ocean due to its complexity to deploy.

Woods et al. [51] use milk upstream of the flow to improve ADV measurement performance during winter conditions when there is no algae in rivers as milk is not toxic and has almost same density as of water. The largest amplitude counts was achieved from 1:1 and 1:2 milk to water ratio. From the study it is found that milk improves the auto-correlation and the signal-to-noise ratio. However, larger particles of the milk can be the source of unwanted signal.

Buykx et al. [82] studied particle size in water samples from rivers and lakes. The measurements were done with a laser light scattering method to identify the particle concentration in the surface water. From the analysis, it was found that particle size distribution of all of the tested river fell between 3 to 300 μm and had one typical particle size range except for one river. The three tops particle size for the examined rivers were 0.45, 9.7, and 125 μm. The typical particle size range of the river was around 20 μm. For this reason, 20 μm was selected as the highest particle size for the laboratories experiment in this research work.

However, sediment particles, organic particles, and air bubbles of the river water act as seeding particles and improve the performance of acoustic devices. Birjandi [37] conducted a comprehensive study on the effect of air bubbles on ADV performance. Experiments were performed in a controlled laboratory water tunnel with 1.5 cm average sized air bubbles and stagnant water. From the study, it was found that

if the size of the air bubble was larger then the size of the sampling volume, large spikes were generated in the ADV measurement. Furthermore, if the air bubble passed through the sampling volume, all three velocity component was affected, and if bubbles passed in between the ADV probe and sampling volume, one or two velocity components were affected whereas other remains unaffected.

Turbulence is characterized by the chaotic flow or irregular fluctuation of the flow. In the laboratory when the flow is slow, and there is no disturbance between the layer, laminar flow can be achieved. In all other cases, the flows are turbulent. Level of turbulence in different media may be different which is measured by TI. If the TI is lower than 1%, it is regarded as low-turbulence and is achievable in a controlled laboratory [90]. If the TI is between the 1% to 5% like in the deep-wide rivers or shallow rivers with low velocity, the flow is considered as medium-turbulence [91,92]. High turbulence is observed near the surface-zone, and near the gravel bed or any obstacle in the flow and the TI is between 5% and 20% [93–95].

Martin et al. [85] suggested that even when the correlation of the measurement drops below the manufacturer recommended 70% [2] the data set can still be valid to be considered for characterizing the flow. Possible reasons for the low correlation are turbulent flow, flow near the boundary layer, large velocity gradient or particle size in sampling volume. For the experiment, the selected velocity range was 0.60 to 0.90 m/s with the sampling time of 60 to 65 s. An uncertainty of 3% to 10% in mean velocity measurement was observed during measurement due to the short sampling time and low sampling frequency as point out by the researchers. At the end of the study, more analysis was recommended for the analysis of the turbulence characteristics of the sampling volume.

Oak Ridge National Laboratory also performed different tests on ADV and ADCP's performance on turbulence measurements and suggested that to resolve small eddies

Table 2.7: Summary of literature review of environmental uncertainty for acoustic devices in flow measurements (continued)

Author	Instrumentation	Site specification	Findings
Martin et al. [85]	ADV	Tilted flume Dimension (L×W): 15.0×0.5 m U = 0.25 m/s (max)	Found out velocity measurement near the boundary becomes less correlated due to the high turbulence level and eddies size similar or smaller to sampling volume. This problem can be solved by increasing velocity range, but attention must be paid as increasing velocity range might also decrease the measurement accuracy.
Gunawan et al. [86, 87]	ADV and ADCP	Flume channel Dimension (L×W×H): 83.80×2.75×1.1 m U = 0.84 m/s	Turbulence creates noise and fluctuation in velocity time series. These noises do not affect mean velocity calculation but must be removed from the velocity time series before turbulence intensity and Reynolds stress calculation. ADV has higher resolution in turbulence measurement compare then ADCP. By using data reduction method, velocity data can be improved by reducing RMS/standard deviation and ADCP data get closer to ADV measurement.
Neary et al. [63]	ADV and ADCP	River	Experimental result showed that longitudinal TI, normal stresses increases exponentially from the free surface of the water and reaches the maximum values near to the riverbed. For first-order approximations of the mean velocity and turbulence intensity profiles in rivers, the authors proposed to use the power law with 1/6 exponent and the semi-theoretical exponential decay model.
Ruonan et al. [88]	ADV and PIV	Open channel U = 0.696 m/s Re = 36,700 Fr = 0.74	Found that ADV turbulence measurement was related to the sampling rate of the instrument. When ADV sampling rate was above 40 Hz, a good agreement was observed with PIV for turbulence intensity and Reynolds stress measurements.
Sutherland et al. [89]	ADV and ADCP	FloWave facility and tidal site U = 0.9 - 1.6 m/s	An area of the tank was selected based on best matched to a specific set of site conditions to compare the results. Same order of magnitude was found between TI of the tank 6% - 7% and the site 5% - 10%, but higher dissimilarity was observed in the Reynolds stresses value and distribution.
Lohrman [29]	ADV	Calibration test	Depending upon the temperature sound speed can vary from 1440 to 1540 m/s. Without calibration, the maximum error of 3.3% can be obtained from measurement; otherwise, the error is limited to 0.2% for the known temperature (within 1°C).

and the turbulent dissipation of the flow, and the measurement must have to be conducted at a high sampling frequency. Further, to resolve the turbulence characteristics, measurements have to be performed for a sufficiently long time [86,87]. So, there is no one perfect configuration to resolve all of the flow properties, it is a combination of a different parameter of the instrument, and it depends upon the site specification and instrument capability.

2.6 Effect of deployment method on uncertainty

Deployment methods for flow characterization with acoustic instruments can be classified into bottom mounted deployment [47, 62, 74, 96] and surface mounted deployment [38, 57, 97, 98]. Bottom mounted deployment from a stable platform is conducted for long-term measurement varying from a couple of days to months. The ADCP is used for full profile measurement whereas ADV is used for one [47, 62] or a couple of fixed-point measurement [74,96] depending upon the number of ADV is used for the experiment. In general, for higher accuracy of ADV in turbulent properties measurement, the instrument is deployed at a turbine hub height of a potential MHK turbine deployment site to get a better resolution of the flow properties. Some of the research work and their findings are summarized in Table 2.8.

Thomson et al. [96] used two versions of Tidal Turbulence Mooring (TTM) system for flow characteristics measurement in a tidal site. TTM-1 has provision for three ADV deployment with the total height of 19 m while the height of the TTM-2 was 12 m with provision for one ADV deployment. Three stacks of wheel anchors of approximately 2500 lbs were attached at the bottom of the mooring system to hold the setup in place, and a steel buoy of approximately 700 lbs buoyancy was used at the top to hold the ADV nearly vertical. A bottom mounted ADCP was used to measure the full flow profile. The mooring system is shown in Figure 2.3. The

Table 2.8: Summary of literature review of deployment methods for flow characterization in river and tidal sites

Author	Instrumentation (profile/point)	Site specification	Measurement setup
Gunawan et al. [74]	ADV: 2 point	Ocean U = 2.40 m/s(max) Duration = 67 days	Two ADV was used at a hub height of a turbine at 4.25 m for 67 days. No difference was found between two ADV dataset due to the small distance between the two of them.
Richmond et al. [62]	ADCP: profile ADV: point	Ocean depth: 22 m (avg) U = 1.5 m/s (max) Duration = 1467 days	A tripod instrumental mount was used to deployment at the bottom of the seabed where ADCP and ADV were used to collect data at a height of 2.6 and 4.6 m from seabed respectively. The result showed that ADV has less noisy data with higher temporal resolution as compare with ADCP.
Thomson et al. [96]	ADCP: profile ADV: 1 or 3 point	Tidal channel U = 3 m/s (max) Depth = 56 m (max) Duration: 2 days	Two versions of the Tidal Turbulence Mooring (TTM) system was used to measure flow characteristics. A 1.15-ton weight at the bottom was used to anchor the TTM on the place while GPS location of the deployment and recovery confirm the stability of the mooring system. The maximum pitch angle of 38° was recorded at 3 m/s flow.
Kilcher et al. [47]	ADCP: profile ADV: point	Tidal channel U = 0.80 to 2 m/s Depth = 50 m	A modified Stable Tidal Turbulence Mooring (STTM), was used to measure turbulence and flow characteristics at turbine hub height. A 1.2 tone weight was used as an anchor for the system where ADP is deployed at the bottom on top of the weight and ADV is deployed on a crossbeam end.
Lueck et al. [57]	ADV, ADCP, and Shear probe	Tidal channel U = 3 m/s Depth = 53 m Duration = 16 days	Performed long-term measurements with ADV, ADCP and share probe. Mooring line was angled about 50° which affect the readings.
Holmes and Garcia [97]	ADCP: profile ADV: 3 point	River U = 1.03 - 1.52 m/s Depth = 4.87 - 6.46 m Fr: 0.149 - 0.20 Duration = 10 min	The stationary boat was used for the measurement. ADCP was deployed from the side of the boat, one ADV was mounted on the boat for surface measurement, and two ADV was mounted on modified P-61 sediment sampler for data collection at 0.06 and 0.42 m height from the river bed. Three-point anchoring was used for the measurement.
Egeland [98]	ADCP: profile ADV: point	Tidal channel U = 2.50 m/s (max) Depth = 304 m	A towfish was designed to hold the ADV for measure velocity at a certain depth from a surface vessel or moored buoy. Experimental results showed that ADV recorded data was affected by the oscillation of the towfish.
Samuel [38]	ACDP: profile ADV: profile Shear probe	River U = 0.8 - 2.70 m/s Depth = 11 m (agv.) Re = 1.34 - 1.86×10^7 Fr = 0.27(max) Duration = 1.5 hr	4.38% difference was found between ADV and ADCP velocity data. ADCP over predict turbulence data and were not recommended for turbulence characteristics measurement.
Lacey [42]	ADV: 3 point	River U = 0.41 - 0.86 m/s Width = 30 m Re = 1.49 - 5.13×10^5 Fr = 0.24 - 0.43	3 ADV was used from a 1.5 m by 1.5 m aluminum support. The support was rigid. It was possible as the maximum depth of the river was only 0.62 m and the three side by side ADV was used to measure velocity at the different height at the same time.

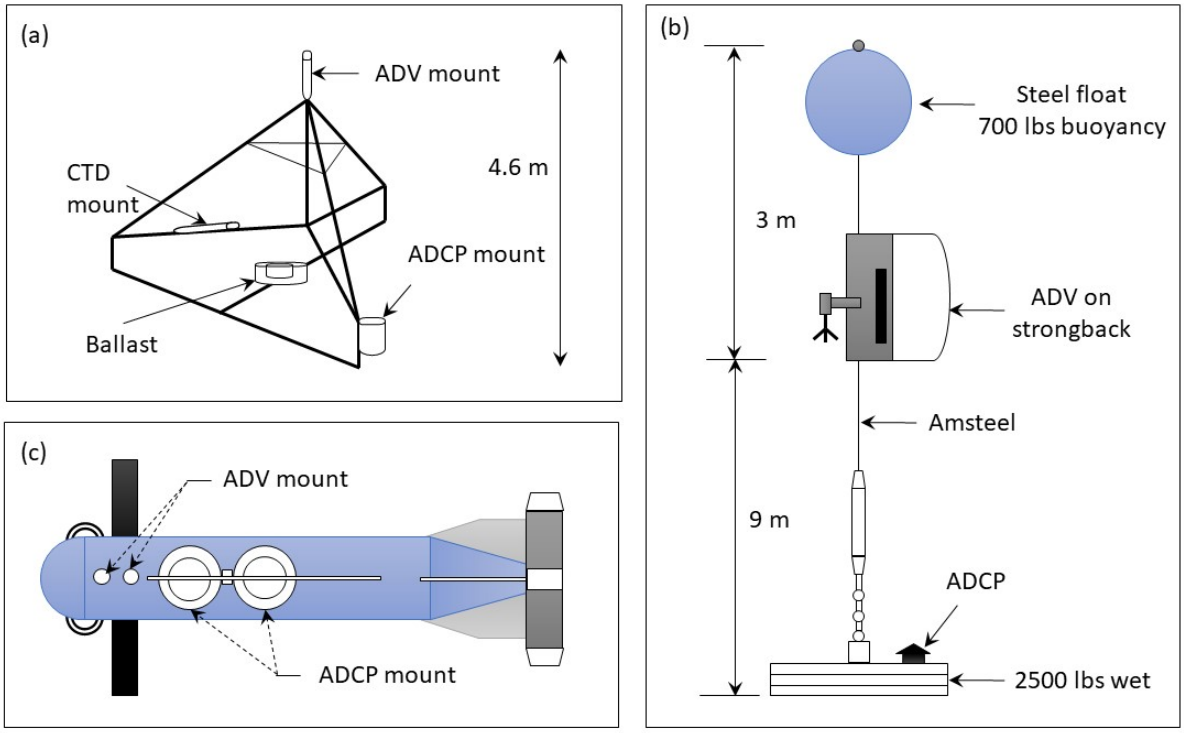

Figure 2.3: Schematic view of different mooring system used for flow velocity characterization (a) Tripod, (b) Tidal Turbulence Mooring (TTM), and (c) Stable Tidal Turbulence Mooring (STTM)

average nominal velocity of the tested site varied from 2.1 to 3.0 m/s and a GPS was used to ensure the stability of the mooring system. During the measurement process, the mooring line was inclined from 22° to 38° as the flow speed varied from 2.0 to 3.0 m/s. This angle of the upper mooring caused problems in ADCP recorded data. Another problem of the system was the impact of vibration and motion of ADV itself during the measurement process. To reduce vibration of the mooring line a filament warp was used. The author also recommends performing motion correction to achieve accurate calculation of flow properties.

Kilcher *et al.* [47] used Stable Tidal Turbulence Mooring (STTM) for turbulence measurement which was an updated version of the TTM system. A buoy of 3.5 m long and 0.46 m in diameter was used for deep-water buoyancy, as shown in Figure 2.3.

The buoy had space for deployment of two ADV and an ADCP at the same time. The ADV was deployed such a way that the probe was pointing upward to measure flow characteristics while ADCP was deployed as pointing downward to the seafloor to measure bottom motion. Velocity measured by ADCP was used to understand the motion of the mooring system and helped to resolve to quantify uncertainty. The author developed a method to perform motion correction and applied for both TTM and STTM deployment method. From the spectral analysis of the systems, the improvement was found in the STTM mooring system. From the further study, the author was able to remove spikes caused by the instrument motion from the energy spectra [99]. However, the author did not present any results of the velocity component after applying motion correction. The downside of the STTM mooring system is the size of the system which adds difficulties in deployment, retrieval, and the fabrication cost, as compared with the TTM system.

Surface mounted measurement is performed by using a mobile boat or a floating platform. The ADV is used for measuring flow properties near the surface, while the ADCP is used for full profile measurements [38, 57, 98, 100]. Towsfish [101] can be used to measure flow statistics of a certain height from a measurement platform. However, as discussed in the section 2.5, ADCP data is not accurate for measuring turbulence characteristics, ADV measurements at different water depth are required for proper assessment of a potential MHK site selection and turbine design.

Homes and Garcia [97] made the first attempted to perform full profile measurement using a stationary boat. However, their data collection was limited to three sampling points with three ADVs. Two of them were positioned near the bottom of the riverbed, and one was placed near the surface region. The method was applied to a river height varying from 4.87 to 6.46 m with a velocity range of 1.03 to 1.52 m/s. A modified version of the P-61 sediment sampler was used for ADV deployment

near the boundary layer and boat mounted ADV was used to take near the surface measurement. The system is not ideal for a high velocity region and deep water depth measurement as for highly energetic flows.

d'Auteuil [38] developed a method for full flow profile characterization of a high energetic river. The average depth of the tested site was 11 m, and flow speed varied from 0.80 to 2.80 m/s. A schematic view of the process is shown in Figure 1.2. In this study, instead of using multiple ADV, the location of the same ADV was changed at different water depths, and measurements were performed for 8 minutes interval. In this case, the effect of the temporal resolution was ignored. Results shows that ADCP was sufficient for mean velocity measurement as 4.38% difference was observed with the ADV recorded streamwise velocity. However, in turbulence intensity measurements the difference was 188%. Therefore, it was recommended to be used ADV for turbulence characteristics measurements. According to the author, the ADV data also contained Doppler noise caused by the instrument vibration and motion, which had to be removed prior to turbulence characteristics calculation to achieve accurate results.

Platform motion, instrument vibration, and angular position are the primary sources of uncertainty in measurements with acoustic instruments like ADV and ADCP [38, 47, 56, 98]. In addition to that, there are other factors like side lobe interference, reference boat speed (bottom-track profiling), blanking distance, near transducer error, cell mapping and orientation of the instrument [24].

A detailed observation of ADCP uncertainty from a moving boat was performed by Gonzalez-Castro [24] to estimate the total uncertainty in the discharge measurement. In the study, an uncertainty analysis standard developed by the American Institute of Aeronautics and Astronautics (AIAA - 1995) was used to develop a framework for estimating total uncertainty in ADCP measurement. The framework was developed

to analytically and statistically estimate total uncertainty based on data reduction equation used for ADCP discharge measurement only. Effect of turbulence was not discussed in the study. The researchers proposed a joint effort between the expert end user and manufacturer for in-depth uncertainty assessment of the device.

Muste *et al.* [102], performed experiments in a channel to observed the ADCP's performance in estimating velocities near the transducer and the bed region. The depth of the rectangular channel varied from 0.3 to 0.9 m while the test velocity varied from 0.3 to 0.9 m/s. A high performance 16 MHz MicroADV was used to collect data at the different depths of the water column and then compared with the data collected by the ADCP. Results showed that, the ADCP measured velocity was biased to have a lower value caused by the flow disturbance introduced by the submerged portion of the device and near transducer error depends upon the probe geometry, magnitude of the flow velocity, the submerged depth of the ADCP, drag force induced by ADCP, ringing effect, signal decorrelation, and signal processing errors.

2.7 Data analysis uncertainty

In addition to Doppler noise, acoustic instruments can contain large amplitude of spikes in the data, which are hard to detect and eliminate from measurement, as sometimes they appear like the natural fluctuation of the flow. Sources and effect of the Doppler noise were discussed in Section 2.4. Different despiking methods can be used to remove these spikes [37,77,103–106]. Despiking a data set consists of detecting spikes and replacing the spikes with a valid data point as to not affect the average and turbulence quantity. Summary of literature review of data analysis uncertainty are presented in Table 2.9.

Goring and Nikora [77] introduced a Phase-Space Thresholding Method where all

Table 2.9: Summary of literature review of data analysis uncertainty of acoustic instrument in flow characterization

Author	Instrumentation	Site specification	Findings
Muste et al. [1]	ADV and ADCP	Open-channel U = 0.09 - 0.15 m/s Depth = 1.22 - 2.13 m Width = 30.48 m	Used RD Instrument (RDI 2001), mid-section and mean-section algorithms to calculate discharge from ADCP measurements and found 0.50% and 0.49% error in mid-section and mean-section algorithm considering RDI algorithm as a reference.
Gonzalez-Castro [24]	ADCP	Analytical method	Developed a framework to calculated total uncertainty in discharge measurement by using data reduction equations following the AIAA standard.
Elgar et al [107, 108]	ADV, ADCP, and EMC	Ocean U = 0.30 m/s Depth = variable	Correlation threshold of 0.7 to 0.3 (for a sampling frequency of 25 Hz) was used to identify inaccurate data. Later 1 s running mean was used to replace incoherent values. The result showed that corrected dataset was more accurate and agreed with the values recorded by the Electromagnetic Current Meter (EMC).
Goring and Nikora [77]	ADV	Not specified	Introduced the phase-space threshold method for removing spikes from the ADV data set and found better results as compared with other conventional despiking algorithms. The final standard deviation of 0.12 m/s was achieved from the threshold method which was lower than the original value of 0.24 m/s. Numerical analysis of the method also showed satisfactory results with 10% higher for iteration greater than 1000.
Birjandi [37]	ADV	Laboratory and river measurement U = 0 m/s (lab) U = 2.4 m/s (river)	Combined phase-space and acceleration threshold and introduce a new hybrid despiking method which was independent of spikes density of the data set. Experimental results showed that the new hybrid method improves the performance of the phase-space method by decreasing the standard deviation of the principal axes of the ellipsoid from 0.047 to 0.04 m/s.
Doroudian et al. [103]	ADV	Open channel U = 0.60 m/s Dimension (D×L×H): 0.60×17×014 m	Suggested to record data in beam coordinates. Then apply despiking routine in beam time series and transformed into Cartesian or ENU coordinates to remove spikes properly.

the data points were plotted in a three-dimensional space, and then points were enclosed by an ellipsoid defined by a criterion. The point outside the ellipsoid was then defined as spikes and replace by using interpolation of the third-order polynomial fit of 12 points before the starting and after the end point of the spike. The author compared the phase-space thresholding method with RC filter [105], turkey 53H [105], acceleration thresholding [104], and wavelet thresholding method [106] with both a clean and contaminated data. Results showed that for clean data filtration method works well except the RC filtration method which detected many false spikes. In the case of contaminated data, acceleration thresholding and phase-space thresholding methods had a low standard deviation of 0.13 and 0.14 m/s compared to the 0.24 m/s of the original signal. Acceleration thresholding had a lower standard deviation, but from the analysis, the author found that in some cases, good data was also detected as spikes. The author also found that for a down facing ADV the vertical velocity component had fewer spikes compared with the horizontal component.

From Goring and Nikora's [77] experimental and numerical analysis, it was observed that phase-space universal thresholding and acceleration thresholding despiking method had better results in the ADV data correction process compare to other conventional methods. Subsequently, Birjandi [37] used these two thresholding methods and introduced a new hybrid method for despiking in bubbly river flow. According to the new method, high amplitude spikes were removed by several iterations until a standard deviation of clean data was achieved. The mean velocity and low frequencies were removed before the phase-space thresholding model was applied; later these values were added again. Phase-space thresholding ellipsoid was used to remove spikes only until a standard deviation of clean data was achieved. Then all the flow statistics were calculated based on these clean data. Linear interpolation was then used to replace spikes for power spectra and autocorrelation coefficient calculations. Like Goring and Nikora [77], the author also tested the new hybrid

method and other methods like simple SNR, acceleration threshold, and phase-space; in clean and contaminated data. For the contaminated data, a standard deviation of 0.04 m/s was achieved in the new hybrid method, whereas the phase-space method obtained a 0.05 m/s standard deviation for principal axes of the ellipsoid calculation. For both cases, the new hybrid method performed better than the phase-space threshold method as the new method was not affected by the spikes density. This despiking method is applied for data analysis in our study.

All acoustic instruments record data in beam coordinates. ADV or ADCP internal algorithm then converts the data into Cartesian or Earth East North UP, whatever was defined by the user. When data is collected in beam coordinates, spikes or noise may occur in the measurement due to different reasons as discussed in Section 2.4, 2.5 and 2.6. Garcia [103] found that these spikes usually appears in one beam coordinates. If the coordinate transformation is performed in those spike time series, spikes from one coordinate may appear in other coordinates. Therefore, it was recommended by the researcher to use despiking method in beam coordinate and subsequently convert into the desired coordinate system.

Chapter 3

Instrumentation, test facilities, and experimental procedures

3.1 Instruments

In order to perform flow characterization in the high energetic river, as shown in Figure 1.3, acoustic instruments are required. ADV and ADCP are used in this study for field measurements and are reviewed here.

3.1.1 Acoustic Doppler velocimeters

The ADV is a point-based flow measurement device which measures flow velocity and turbulence in three directions using the Doppler shift technique. The Nortek Vector ADV with the fixed arm is used for the velocity measurements in this work. The ADV and measurement probe orientation are shown in Figure 3.1. The ADV holds three receiving probes and one transmitting transducer where the probe with red marking represents the streamwise direction. The transmitting transducer sends a short acoustic pulse that travels through the fluid to a sample volume and is

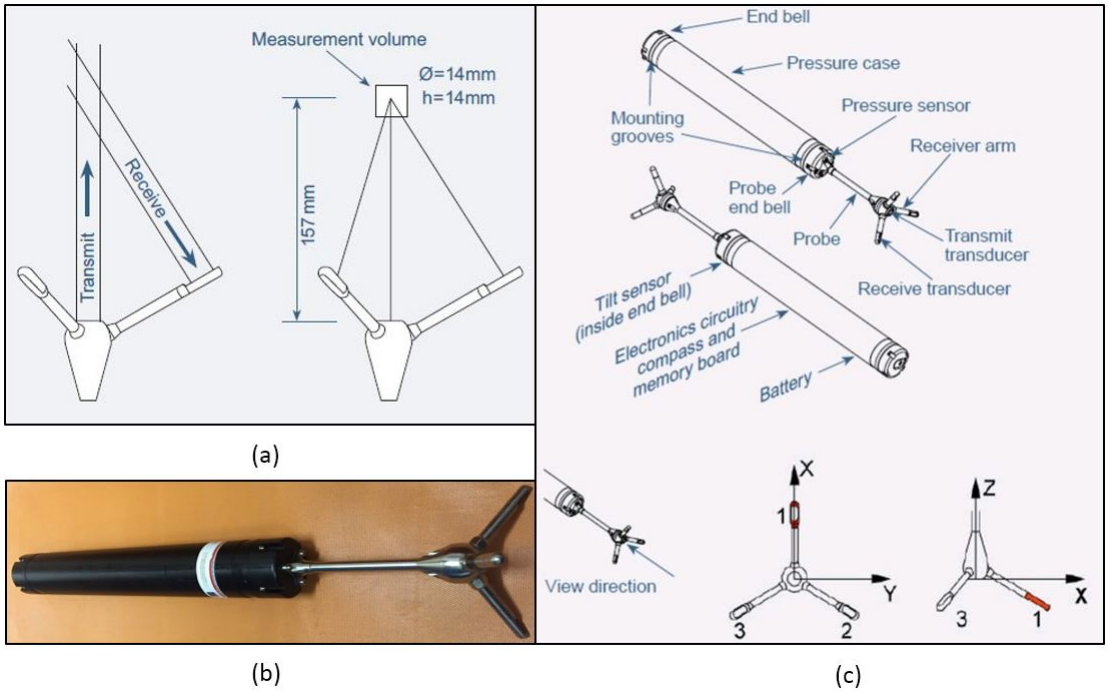

Figure 3.1: (a)Working principle of ADV and location of sampling volume, (b) picture of the Norket Vector ADV, and (c) different component of ADV and axis orientation of the probe [2]

reflected from the scattering particles of the water with a maximum sampling rate of 250 Hz. The particles are assumed to move at the average water velocity and hence the velocity of the flowing water is calculated. Sampling volume is located 157 mm away from the transmitter of the ADV. The shape of the sampling volume is cylindrical with 14 mm in diameter and a height of 5 - 20 mm. According to the measurement requirement, the sampling volume size can be adjusted from the instrument configuration. Parameter setting includes; nominal velocity range, sampling rates, salinity, and measurement time can be changed to obtain accurate results. However, ADV is considered an accurate measurement device with the manufacturer [2] specified relative error of $\pm 0.5\%$ of the measured value and an absolute error of ± 1 mm/s. The specification of the ADV used in this experiment is given in Table 3.1.

The Nortek Vector ADV has an integrated Microstrain Inertial Measurement

Table 3.1: Nortek Vector ADV specification [2]

ADV model	Vector
Velocity Range	$\pm 0.01, 0.1, 0.3, 2, 4, 7\ m/s$ (software selectable)
Accuracy	$\pm 0.5\%$ of measured value, $\pm 1\ mm/s$
Output sampling frequency	$1 - 64\ Hz$
Internal sampling frequency	$100 - 250\ Hz$
Acoustic frequency	$6\ MHz$
Maximum tilt	$30°$

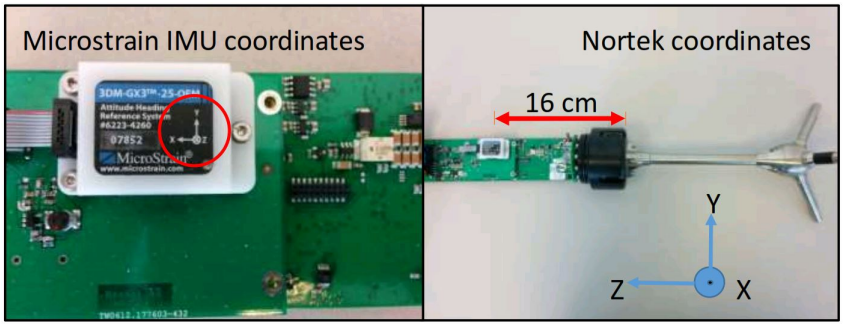

Figure 3.2: Microstrain IMU mounted on circuit board inside ADV pressure housing [5]

Unit (IMU) model 3DM-GX3-25-OEM. This IMU has three sensors: a triaxial accelerometer to measure the linear acceleration, triaxial gyroscope to measure the rotational movement and triaxial magnetometer used for dynamic orientation calculation. The IMU is located inside the ADV housing, as shown in Figure 3.2. This IMU unit motion is considered as the ADV's motion and is used to compensate ADV's motion in high energetic river flow. Instead of compass and tilt sensor, magnetometer measured data is used for coordinate conversion from beam to XYZ or ENU coordinate in an IMU integrated ADV. Note that the IMU and ADV orientations are not the same, as shown in Figure 3.2.

3.1.2 Acoustic Doppler current profilers

The Acoustic Doppler Current Profilers (ADCP) is also an acoustic flow measuring device. ADCP is used to measure discharge rate, 3-dimensional water velocity, depth and bathymetry of a specific location [3]. The difference is the ADCP measures

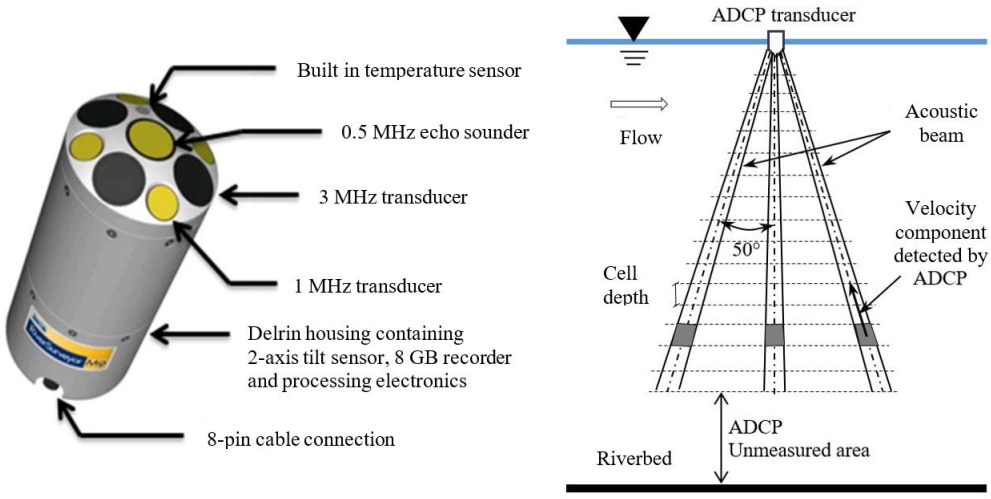

Figure 3.3: Features and working principle of the SonTek M9 ADCP used for the riverine measurements [3]

Doppler frequency shift to calculate velocity whereas ADV measures Doppler phase shift. The SonTek M9 ADCP is used for site characterization at the CHTTC and is too big to be used in the water tunnel. The ADCP contains four transducers which operate at 3.0 MHz, four at 1.0 MHz, and the last sensor is a 0.5 MHz echo sounder, as shown in Figure 3.3. The eight transducer measures velocity while the center echo sounder records depth. The beam from the transducer spreads as it gets further away from the ADCP. The spread angle of the ADCP used in the experiments for this study is 50°. The beam is split up into numerous cells, and the size of the cell gets larger as it goes more in-depth from the device to the bottom of the river. This means that the velocity is averaged over a larger cell as it moves further, which causes a loss in spatial resolution. Specification of the ADCP is given in Table 3.2.

3.2 Test facility overview

To evaluate the 5 uncertainty terms mentioned on Table 1.2 different experiments are performed in a controlled laboratory environment using the water tunnel and shaker table first to investigate the performance of the ADV. Later field experiments are

Table 3.2: Specification of SonTek vertical ADCP [3]

Specification	Model: $M9$
Profiling range - distance	0.06 to 40 m
Profiling range - velocity	± 20 m/s
Profiling range - accuracy	$\pm 0.25\%$ of measured velocity, ± 0.2 cm/s
Velocity - resolution	0.001 m/s
Depth - range	0.20 to 80 m
Depth - accuracy	1%
Depth - resolution	0.001 m
Number of cells	Up to 128
Cell size	0.02 to 4 m
Transducer configuration	9 transducers, dual 4-beam 3.0 MHz/1.0 MHz

performed at the CHTTC site to investigate ADV's performance further.

3.2.1 Water tunnel

The water tunnel is a controlled laboratory testing facility located at the University of Manitoba. The test section of the water tunnel is 61 cm wide and 183 cm long with a maximum water height of 60 cm, as shown in Figure 3.4. The water height in the test section can be adjusted. The bottom and side of the test section of the water tunnel are made of plexiglass for visual observation and video recording. Flow around the water tunnel is circulated by a single stage, axial propeller pump. According to the experimental requirement, the flow velocity in the water tunnel can be adjusted using the frequency converter. At maximum water height of 60 cm and the maximum operating frequency of 60 Hz flow velocity of 1.1 m/s can be achieved in the test section. A series of honeycombs is used before the test section to breaks the large eddies and reduces the TI. The velocity uncertainty of the water tunnel is 2.5% [51].

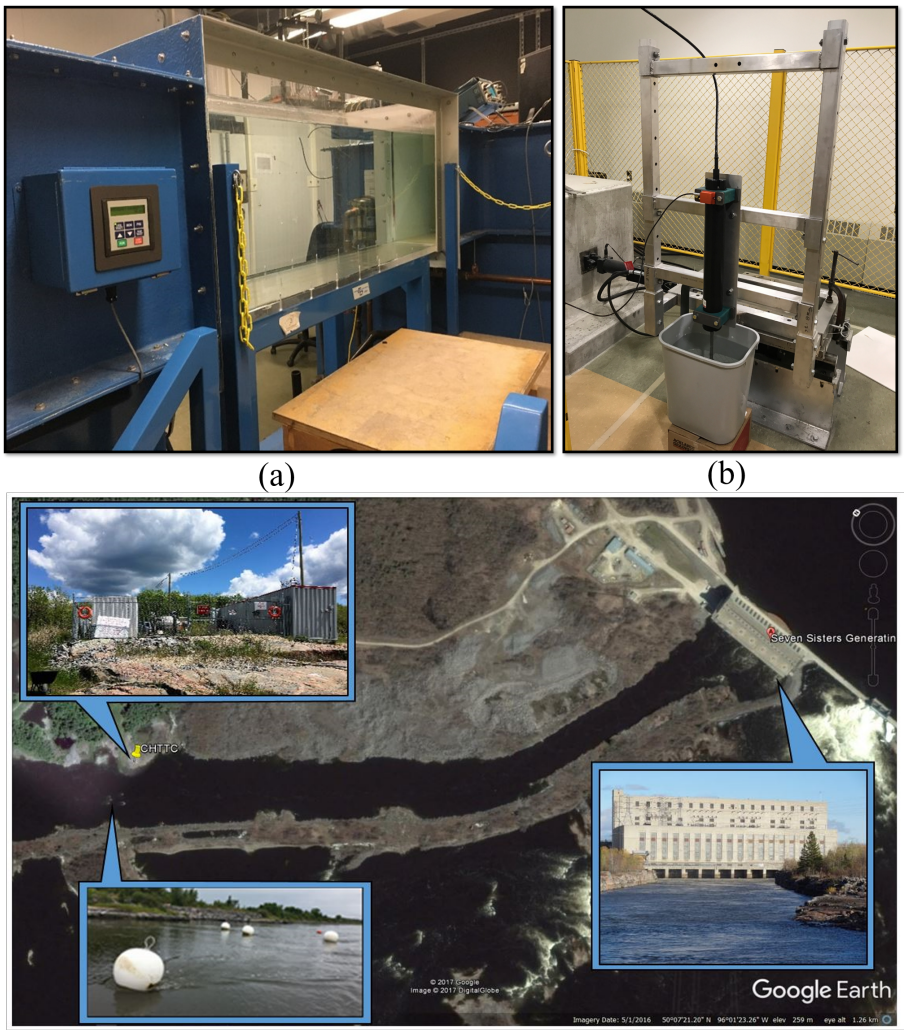

Figure 3.4: Test facilities: (a) Test section of water tunnel, (b) shaker table with ADV mount assembly with IMU located inside the instrument with probe immersed in a water container, and (c) Google Earth view of the CHTTC site showing the location of seven sister dam, CHTTC site office, and the buoys

3.2.2 Shaker table

A uniaxial shaker table provides a controlled movement of the ADV similar to an energetic site where significant motion is transferred to the unit. Different type of periodic and random motion such as ground motion and dynamic signals is simulated to test the performance of the ADV IMU and effectiveness of the developed data processing software.

Table 3.3: Specification of the shaker table

Item	**Specification**
Table	
Size	0.6 × 0.6 m
Weight of the table	0.6 kN
Maximum payload	1 kN
Maximum displacement	± 75 mm
Maximum acceleration	3 g
Frequency range	0.1 - 80 Hz
Actuator	
Model	MTS 242.02
Thrust	10 kN
Stroke length	150 mm
Servo valve	two stages, four-way
Supports	
Shaft diameter	2.54 cm
travel life	50 km

The shaker table consists of a platform table, servo-hydraulic actuator, ball bush bearing, linear support mechanism, and the reaction mass. The overall length and width of the table are 0.6 by 0.6 m. It is moved linearly in the horizontal direction by a servo-hydraulic actuator over a low friction ball bush bearing. The movement frequency range is 0.1 to 80 Hz with a maximum payload of 1 kN. Depending on the input signal the shaker table can have single harmonic, sweep sine or ramp motion. The overall characteristics of the system and individual components are summarized in Table 3.3. A view of the shaker table with ADV mount is shown in Figure 3.4.

Doranga [109] perform several tests using the shaker table and found that in most of the cases the table displacement matches with the input displacement except for low-frequency cases. The tested lowest harmonic frequency is 2.55 Hz with a displace of 1 mm. In that test, a higher order of harmonics was found due to the noise from bearing and the table, while the measured magnitude of the acceleration was found to within acceptable limits.

3.2.3 CHTTC

The Canadian Hydrokinetic Turbine Test Center (CHTTC) is located downstream of the Manitoba Hydro's Seven Sister's dam. It is a man-made channel. Google Earth view of the CHTTC site and Seven Sister Generation Station is shown in Figure 3.4. The CHTTC at the University of Manitoba works with marine energy companies to test HKT. The CHTTC has a depth of approximately 11 m, a width of approximately 60 m, and flow velocity varies from 1.5 to 3.0 m/s. This flow velocity range is ideal to test HKT operations. The hydro dam removes most of the floating debris like tree, and logs, which ensure uninterrupted operation of the turbines. Hourly discharge data is available from Manitoba Hydro which helps to correlate turbine performance throughout the operation of HKT. More details of the CHTTC site activities can be found on the website [110].

3.3 Laboratory tests

Having identified and described the instruments and test facilities a test matrix for laboratory tests was developed to achieve the research objectives and the matrix is shown in Table 3.4. The test matrix is used to evaluate the 5 error terms listed in Table 1.2. Tests 1 to 3 were used to identify the optimum suspended particle size for the water tunnel experiment. Tests 4 and 5 were conducted to identify the effect of ADV's pitch angle on velocity measurement at 0.53 m/s and 1.1 m/s, respectively. More experiments were performed to identify the effect of pitch, roll, and heading angle on the performance of ADV measurements. The focus of the study was given on effect of the pitch angle as ADV's pitch angle dominates during flow measurements in high energetic applications. Shaker table experiments were performed to evaluate the performance of IMU in measuring acceleration. Finally, the performance of ADV was tested by manually applying force on the support structure in the water tunnel.

Table 3.4: Test matrix for water tunnel and shaker table experiment showing location where measurement were taken, and measured parameter on those location. Position, W = z/D represents the measurement location in spanwise direction and depth, H = y/L represents the measurement location in vertical direction.

Water tunnel							
Experiment	**Water height**	**Velocity**	**Particle size (μm)**	**Test specification**			**Tested parameter**
				Region	**Position W = z/L**	**Depth H = y/D**	
Test 1	60 cm	1.1 m/s	<5, 5 20	Upstream	0.25	0.75, 0.73	Suspended water particle
					0.5		
					0.75		
Test 2	60 cm	1.1 m/s	<5, 5 20	Above rocks	0.25	0.75, 0.73, 0.66	Suspended water particle and TI
					0.5		
					0.75		
Test 3	60 cm	1.1 m/s	<5, 5 20	Downstream	0.25	0.75, 0.73, 0.66	
					0.5		
					0.75		
				Instrument orientation			
				Heading (deg)	**Roll (deg)**	**Pitch (deg)**	
Test 4	60 cm	0.53 m/s	20	0	0	0, 5, 10, 15, 20, 25, 30, 35, 40	Pitch angle
Test 5	60 cm	1.1 m/s	20	0	0	0, 5, 7.5, 10, 12.5, 15, 20, 25, 27.5, 30, 32.5, 35, 40, 45	Pitch angle
Test 6	60 cm	1.1 m/s	20	0	10, 20, 30	0	Roll angle
Test 7	60 cm	1.1 m/s	20	10, 20, 30	0	0	Heading angle
Test 8	60 cm	1.1 m/s	20	10, 20, 30	10, 20, 30	0	Roll and heading angle
Test 9	60 cm	1.1 m/s	20	10, 20, 30	0	10, 20, 30	Pitch and heading angle
Test 10	60 cm	1.1 m/s	20	0	10, 20, 30	10, 20, 30	Pitch and roll angle
Test 11	60 cm	1.1 m/s	20	10, 20, 30	10, 20, 30	10, 20, 30	Pitch, roll, and heading angle
Shaker table							
				Settings			
				Displacement (mm)	**Frequency type**	**Frequency (Hz)**	
Test 12	bucket	0 m/s	NA	1	Periodic	2, 5, 7.5, 10, 12, 15	Vibration
Test 13	bucket	0 m/s	NA	0.5	Periodic	2, 5, 7.5, 10, 12, 15	
Test 14	bucket	0 m/s	NA	50	Periodic	2	
Test 15	bucket	0 m/s	NA	1	Periodic	5+10+15	
Water tunnel							
				Manual force applied on ADV			
Test 16	60 cm	0.53 m/s	20	Fast forward force			Motion and vibration
Test 17	60 cm	0.53 m/s	20	Slow forward force			
Test 18	60 cm	0.53 m/s	20	3 small forward force			
Test 19	60 cm	0.53 m/s	20	Mixed force			
Test 20	60 cm	0.53 m/s	20	Vibration			

3.3.1 Suspended particle size

To verify the performance of the ADV on suspended particle size, it is important to understand the relationship between the signal strength and Doppler noise for acoustic flow measurements. The ADV works on the Doppler shift which is related to the change in frequencies between the transmitted and received signals. These reflections come from the scattering particles of the flowing water. If the particles size is too small, the ADV will not receive any reflected signal. Meanwhile, if the signal strength is too weak, the Doppler noise will become prominent, and the performance of the ADV becomes abate. This signal strength can be improved by adding small particles [29]. To examine the effect of the particle size on high energetic flow, the size of the particle is changed while other parameters kept in constant. The Nortek vector ADV can measure the maximum 78 μm sized particle which is calculated from,

$$\frac{2\pi r}{\lambda} = 1 \tag{3.1}$$

$$or, 2r = D_p = \frac{\lambda}{\pi} = \frac{c}{f\pi} \tag{3.2}$$

where D_p = diameter of the particle, c = speed of the sound, and f = frequency of ADV.

Figure 3.5 shows 5, and 20 μm sized particle used in the water tunnel to analyze the effect of particles size on the ADV measurement. Adding these particles does not impact the flow, when the water tunnel is left idle, the suspended water particles are observed which ensures that they are not dissolved. Before applying different sized seeding particles, the water of the tunnel is filtered using a 5 μm filter for at least 48 hr to avoid mixing of different size particles. Experiments are also

(a) (b)

Figure 3.5: Seeding particles size (a) 5 μm, and (b) 20 μm used for analysing the effect of particles size on the ADV performance

conducted without any added particles to compare the results. In general, the size of the particles in a sampling volume increases or decreases the SNR value of the measurement. According to the manufacturer recommendation, if the SNR value is above 10, the ADV measurement is considered valid, and if the value is above 19, then the measurement can be considered as accurate.

3.3.2 Turbulence intensity

To understand the effects of turbulence on the ADV measurements, experiments are performed on a smooth surface water tunnel as mentioned in Section 3.2.1. The large scale of turbulence is generated in the same water tunnel by using the irregular shape of rocks approximately at an order of 10% of the water column height. Pictures of the rocks used in this experiment are shown in Figure 3.6. The approximate average height of the rocks is 10 cm. The rocks are placed after 40 cm of the channel opening, so that creates one upstream region without any obstacle, then a highly turbulent region on top of the rocks, and the downstream region, as shown in Figure 3.6. Then the ADV is mounted on a rigid aluminum structure which is used to make measurements at upstream: Region-1, above rock: Region-2, and downstream: Region-3 which are respectively 6.75, 56.75, and 121.75 cm away from the opening of

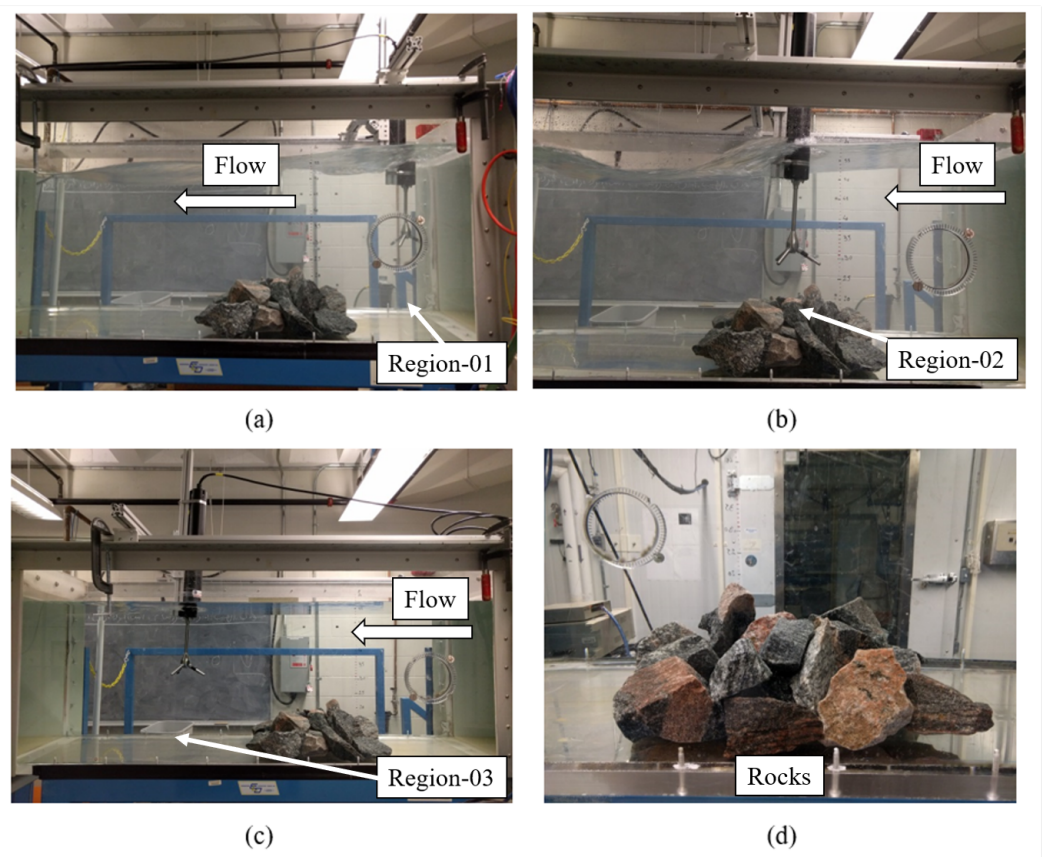

Figure 3.6: Position of the measurements at water tunnel: (a) Region-1: upstream, (b) Region-2: on top of rocks, (c) Region-3: downstream, and (d) the pictures of the rocks used to create high level of turbulence

the water tunnel. The measurements are performed at the height of 31 and 36 cm from the tunnel bed at the upstream, on rocks and downstream of the rock. Additional experiments are also performed at the height of 26 cm at the downstream to check the effect of the obstacle on flow characteristics. Each region divided into three segments and measurements were taken at W = 0.25: first quarter, W = 0.50: second quarter and at the W = 0.75: third quarter along with the width of the tunnel, as shown in Figure 3.7. Reynolds number, R_{eh} of the water tunnel is calculated based on the hydraulic diameter, D_h,

$$R_{eh} = \frac{D_h v}{\mu} \quad = \frac{2whv}{(w+h)\mu} \tag{3.3}$$

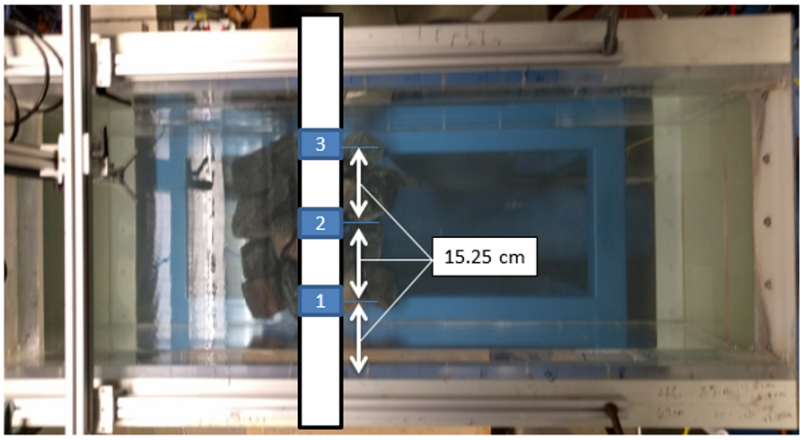

(a)

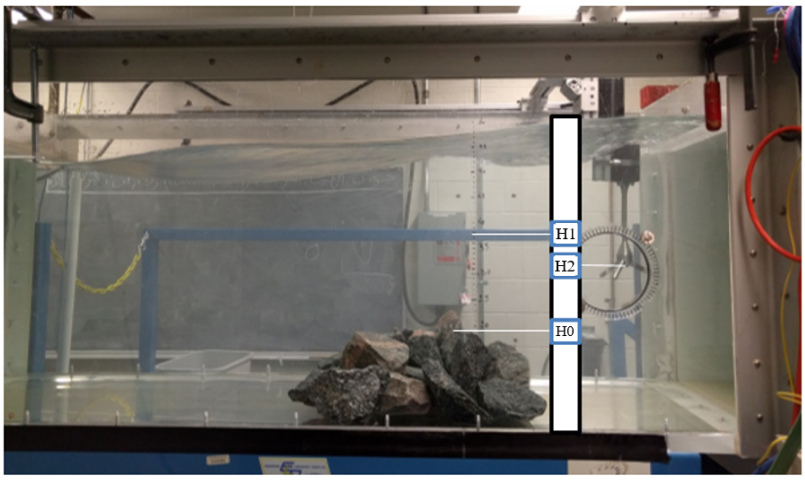

(b)

Figure 3.7: Position of the measurements at water tunnel: (a) ADV lateral position: Position-1, W = 0.25 at the first quarter of the tunnel (15.25 cm from the side wall), Position-2, W = 0.50 at the center (30.50 cm from the side wall), and Position-3, W = 0.75 at third quarter of the tunnel (45.75 cm from the side wall), and (b) ADV vertical position: H0, H = 0.75 average height of rocks, H1, H = 0.73 sampling point 10 mm above H0 and H2, H = 0.66 sampling point 60 mm above H0

where w and h is the width and height of the water tunnel, respectively.

3.3.3 Instrument orientation

Acoustic instruments measure velocity in beam coordinates and then the velocity component is converted into a Cartesian coordinate system (XYZ) or Earth Normal coordinate system (ENU). The XYZ coordinates are also known as instrument fixed

coordinates, and the ENU coordinates are also known as Earth reference coordinates. Coordinates conversion depends on the orientation of the instrument, pitch, roll, and heading angles. In laboratory settings, the instrument orientation and the flow direction are known or can be controlled as per the experiment requirement. However, in a riverine side where flow direction changes frequently and the underwater ADV orientation is unknown, it is recommended to working with ENU coordinates system. If the velocity component in ENU coordinate is known, flow speed and direction can be calculated as

$$Flow\ velocity,\ V = \sqrt{V_E^2 + V_N^2} \tag{3.4}$$

$$Flow\ dircetion,\ \theta = \arctan\left(\frac{V_E}{V_N}\right) \times \frac{180}{\pi} \tag{3.5}$$

where V_E and V_N represent flow speed in East and North direction, respectively.

Then the transformation from ENU to XYZ coordinate system become,

$$V_{XYZ} = T_E^{-1} \times (OM) \times T_L \times V_{ENU} \tag{3.6}$$

where OM is the 4×4 orientation matrix can be found from the ADV recording or can be calculated from the pitch, roll, and heading angle. T_E and T_L are the 3×3 earth and local transformation matrix, respectively. For vector and micro-strain IMU, the transformation matrix is

$$T_E = \begin{bmatrix} 0 & 1 & 0 \\ 1 & 0 & 0 \\ 0 & 0 & -1 \end{bmatrix} \tag{3.7}$$

$$T_L = \begin{bmatrix} 0 & 0 & -1 \\ 0 & 1 & 0 \\ 1 & 0 & 0 \end{bmatrix} \tag{3.8}$$

For flow profile measurements in the riverine environment, the deployment of acoustic instruments from a fixed and steady frame is not possible. In rivers, flow direction does not change significantly, but the alignment of the instruments cannot be controlled. So, before data analysis, the velocity components must be corrected in accordance with flow and instrument orientation. The possible way of angle compensations are:

(a) ENU method: using the East and North velocity component, as in Equation 3.4,

(b) Gravity−g method: using the standard gravitational force and

(c) PRH method: using heading, roll and pitch angle.

The IMU records acceleration in three coordinates. The IMU also records the gravitational force acting on ADV. When the ADV is positioned vertically, the vertical acceleration recorded by the IMU is the gravitational force, $-g$. The negative sign is because of the IMU records in the opposite direction to the actual gravity is acting. Moreover, if the ADV is not placed straight during measurement, the IMU will record some value other than gravitational acceleration. This value can be used to correct the ADV orientation. Note this angle compensation is applicable when pitch or roll angle is present in the ADV deployment. If the deployed ADV contains both pitch and roll angles, this conversion will not produce valid results. This is also true for any measurements with a heading angle.

Another method for angle compensation is using pitch, roll, and heading angles. The value of these angles can be found in IMU recorded data. Although the ADV is

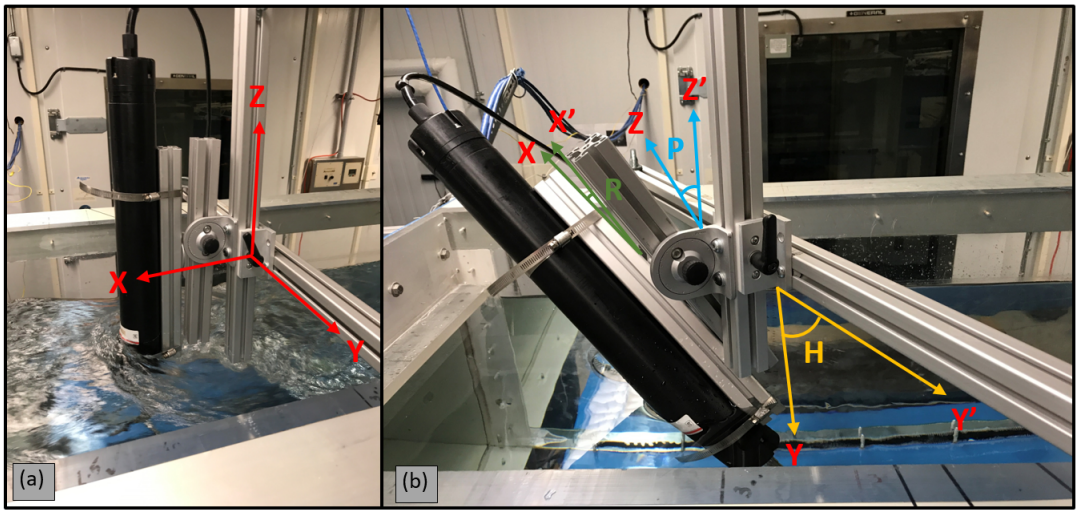

Figure 3.8: Water tunnel test setup for testing effect of different angle on ADV deployment: (a) ADV orientation with the flow direction, and (b) ADV at different pitch (P), roll (R), and heading (H) angle

deployed straight and in line with the flowing water, initial heading angle of the testing site must be considered carefully, as the heading angle is not always zero like pitch and roll angles. The initial heading angle of the ADV can be calculated from the Global Positioning System (GPS) data. Then this angle can be used to correct all the three velocity components.

Tests were performed in the water tunnel with a different angular position to find out their effect on ADV measurements and to estimate the performance of the three angle compensation methods. Figure 3.8 shows the experimental setup for testing the effect of the ADV angle on flow characteristics measurements. For these tests, two Item's angle locking brackets are used for changing pitch and roll angles. However, the heading angle is changed by using the ADV support structure. Results are shown in Section 4.4.

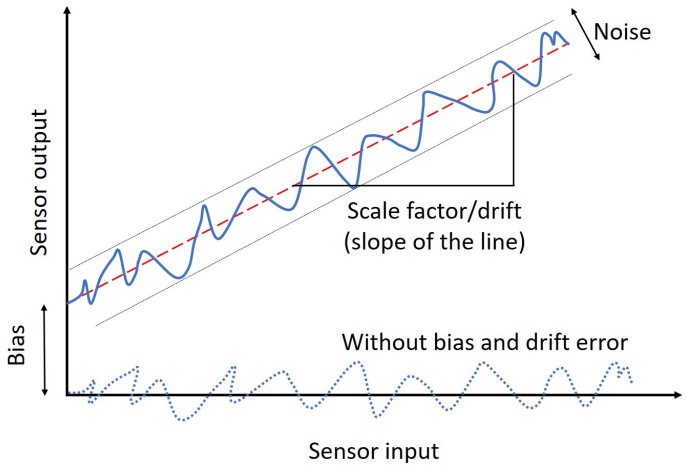

Figure 3.9: Common errors in IMU measurements showing bias, drift, and noise

3.3.4 Vibration and motion

The IMU of the ADV is used to correct for external disturbances to the ADV, but the IMU itself has errors in measurement. Common IMU errors are illustrated in Figure 3.9. The issue with correcting ADV motion with IMU velocity data is that the IMU drifts causing the velocity data to "walk" in one direction and even change the speed or direction of flow measurements. Using a high pass filter the acceleration data from the IMU to eliminate the drift error also does not work as the motion to be used for the correction from the IMU has its peak energy at 0 Hz in the energy spectrum. Consequently applying the filter causes the removal of most of the data. The IMU data is converted instead into the ADV coordinate system using Equation 3.6, or all data is recorded in the ENU coordinate system. Conversion of the coordinate system was presented in Section 3.3.3. Since the ADV records gravity as acceleration, the gravitational force is removed from the IMU recorded linear acceleration data

$$a_{IMU} = [a_y^{IMU} \quad a_x^{IMU} \quad a_z^{IMU}] - [0 \quad 0 \quad g] \tag{3.9}$$

where g is the gravitational force which is a constant.

After this transformation, mean acceleration is removed from the IMU acceleration because it should not have a constant acceleration,

$$A_{IMU} = a_{IMU} - \overline{a_{IMU}} \tag{3.10}$$

IMU acceleration is then converted into velocity by integrating acceleration assuming that the IMU is initially stationary. A low-frequency drift is induced by integrating acceleration. The cumulative integral is performed by the trapezoidal method with unit spacing,

$$v_{IMU} = \int a_{IMU}.dt \tag{3.11}$$

Angular rate, ω, is converted into linear motion by,

$$v_{\omega} = \omega \times r \tag{3.12}$$

where r is the position of the IMU which corresponds to the transducer head of ADV. For this experiment fixed head ADV probe is used and the distance between the ADV transducer head and IMU is 0.36 m.

The water velocity, V_{water}, is then calculated by subtracting IMU velocity, v_{IMU}, and angular velocity, v_{ω}, from the ADV recorded velocity, v_{ADV}, as

$$V_{water} = v_{ADV} - (v_{IMU} + v_{\omega}) \tag{3.13}$$

After removing the IMU recorded velocity and angular movement from the ADV recorded velocity, a trend is observed in each data. These trends are unwanted and resulted from the integration of the IMU acceleration data. These trends are selected

by using Kernel Smoothing Regression (KSR). The theory behind the KSR is that it generates an expected value of a response variable, Y, based on a previously known predictor variable, X. According to Watson [111], it can be presented as,

$$E(Y|X) = f(X) \tag{3.14}$$

where f(X) is a non-parametric function that is unknown. Nadaraya [112] and Watson [111] proposed as a moving average Kernel regression to determine the function as,

$$f_n(x) = \frac{\sum_{i=1}^{n} Y_i K\left(\frac{(x-X_i)}{h(n)}\right)}{\sum_{i=1}^{n} K\left(\frac{(x-X_i)}{h(n)}\right)} \tag{3.15}$$

where K(X) is the Kernel function and h(n)$\rightarrow$0 as n$\rightarrow \infty$. This regression function is commonly referred to as the Nadaraya-Watson Function. Cao [113] implemented the Nadaraya-Watson Function to develop a MATLAB code using the Gaussian kernel and made it available at Mathworks File Exchange. The MATLAB code is used in this thesis for the trend selections. After the trends are selected, they are set to have a shift of zero so that when they are subtracted from the data set only the trends created by the drift error are removed, and no shift is introduced.

3.4 Field experiments

Data collecting in a high energetic riverine environment is associated with many challenges. It is not like experimenting in the laboratory where the test condition is known and can be controlled. For characterization in a riverine environment in addition to the natural obstacles, there are man-made obstacles like a bridge, operating turbines, and mooring lines. Personnel safety with the environment has to

consider during the operation, in addition to not damage the instruments. According to the procedure described in this section the ADV and ADCP are used for velocity and turbulence measurement at the Forks and highly energetic riverine site at the CHTTC, as shown in the test matrix in Table 3.5. The data obtained are analyzed and discussed in Chapter 4. Point F-6 is selected for detail analysis as large boat motion was experienced during the surface measurement at the Forks and the maximum average velocity of 2.52 m/s was measured at CP-D during profile measurement at the CHTTC.

3.4.1 Surface measurements

Initial characterization of the potential hydrokinetic site includes measurement of bathymetry and near-surface free stream velocity. A boat is required for characterizing a site to minimize temporal resolution by quick maneuverability. For this purpose, a zodiac boat is used, as shown in Figure 3.10. A 150 HP engine powers the boat.

The bathymetry helps to identify the shallow region, hazardous region and the potential location of turbine deployment depending on the height of the region. A Humminbird 898c GPS System is used to perform bathymetry. The Humminbird is connected with a sonar system mounted at the bottom of the zodiac boat. A single beam sonar is preferred for narrow channels and one is taken not to hit steep river banks. Sonar system provides a visual representation of the depth and underwater obstruction on the Humminbird display which helps the driver to drive throughout the testing site. This information with GPS tracking is recorded for more detail analysis.

The measurement zodiac boat has a structure to attach the ADV for measuring near surface and free stream velocity. The same structure is also used for the ADCPs to

Table 3.5: Test matrix for field experiments showing location where measurement were taken, and measured parameter on those location. Highlighted measurement point F-6, SP, and CP-D is used for detail analysis in result section.

Experiment	Measurement			Point			Parameters measured
	Method	Instrument	Platform and location	Position		Depth from the surface (m)	
Test 21	Surface	ADV	Zodiac, Forks	F-1		1.23	Velocity and turbulence
Test 22				F-2		1.24	
Test 23				F-3		1.23	
Test 24				F-4		1.22	
Test 25				F-4-2		1.25	
Test 26				F-5		1.20	
Test 27				F-6		1.25	
Test 28	Shore/fixed platform	ADV	Floating mobile platform, CHTTC	SP		0.32	Velocity and turbulence
Test 29	Profile	ADV and ADCP	Floating mobile platform, CHTTC	CP-A	CP-A1	1.2, 2.2, 3.3, 4.3, 5.2, 6.3, 7.3, 8	Velocity and turbulence
Test 30					CP-A2	1.2, 2.3, 3.2, 4.2, 5, 6.2, 7	
Test 31					CP-A3	1.2, 2.2 3, 4.2, 5.1, 6	
Test 32				CP-B	CP-B1	1, 2, 3, 4.3, 5.1, 6, 7.2, 9.2	
Test 33					CP-B2	1.5, 2.4, 3.6, 4.5, 5.8, 6.6, 6.9	
Test 34					CP-B3	1.5, 2.4, 3.5, 4.5, 6.2, 7, 7.5	
Test 35				CP-C	CP-C1	1, 3.1, 4.3, 5.3, 6.2, 7.2, 8.2	
Test 36					CP-C2	2, 3.1, 4.3, 5.3, 6.2, 7.2, 8.2	
Test 37					CP-C3	1.2, 2.2, 3.2, 4.3, 5.3, 6.2, 7.3, 8.5	
Test 38				CP-D	CP-D1	1.2, 2.3, 3.3, 4.3, 5.3, 6.3, 7.4, 8.3	
Test 39					CP-D2	1, 2, 2.9, 3.9, 5.2, 6.4, 7.5	
Test 40				CP-E	CP-E1	1, 2 , 3, 4.2, 5.1, 6.2, 7, 7.5	
Test 41					CP-E2	1.1, 2, 3.1, 4.2, 5, 6, 7, 7.5	
Test 42					CP-E3	1.2, 2.2, 3.2, 4, 5.2, 6.4, 8, 8.4	
Test 43				CP-F	CP-F1	1.5, 2.5, 3.5, 4.5, 5.6, 7, 7.1	
Test 44					CP-F3	1.7, 3, 3.9, 5, 6.2, 7.2, 7.5	
Test 45				CP-G	CP-G1	1, 2, 3.2, 4.2, 5.3, 6.3, 7.3, 8.9	
Test 46					CP-G2	1.1, 2.1, 3.1, 4, 5, 6.2,7.1, 7.8	
Test 47					CP-G3	1.1, 2, 3, 4.3, 5.1, 6, 7.1, 9	
Test 48				CP-H	CP-H1	1.8, 2.7, 3.7, 4.7, 5.8, 6.5, 7.5, 8.5	
Test 49					CP-H2	1.8, 2.5, 3.8, 4.6, 5.6, 6.8, 7.3, 8	

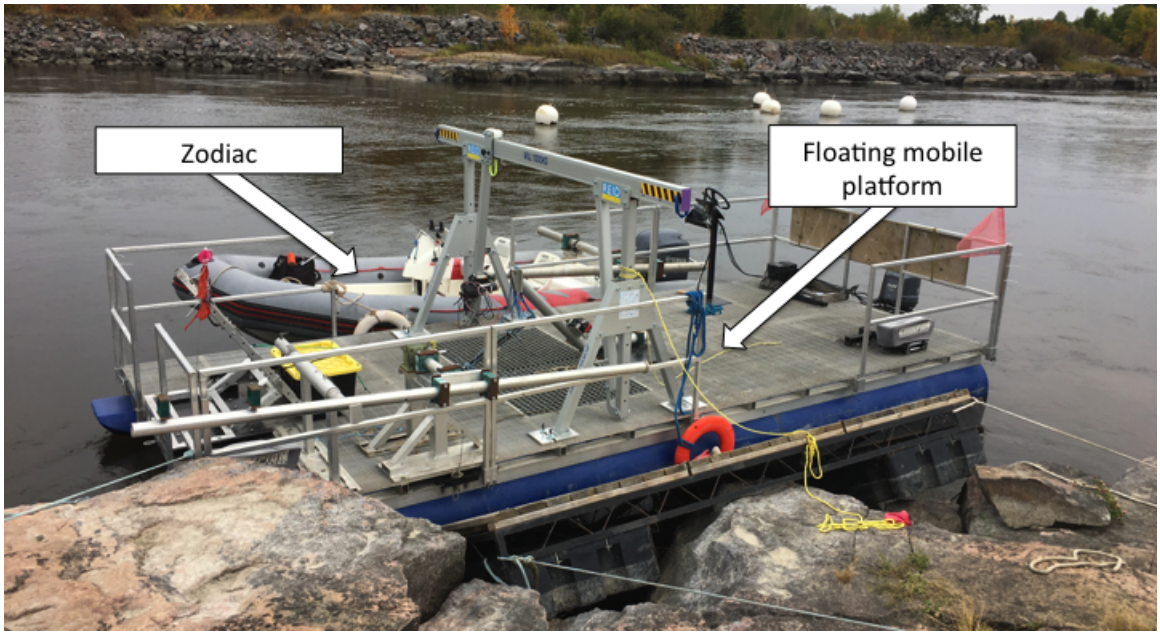

Figure 3.10: Zodiac Pro 650 boat and the floating mobile pontoon platform used for the measurements at the CHTTC. During the experiments the floating mobile platform is not equipped with the gantry shown in the figure and profile measurements by the ADV is performed from the center hatch to keep the pontoon horizontal.

measure flow velocity profile. With this attachment, one instrument can be used at a time for the flow characteristics measurement.

Figure 3.10 shows the floating mobile platform referral to as the blue pontoon, which is also used for surface measurements. Like the zodiac boat, a structure with a horizontal and depth arm on the side of the pontoon is used for instrument deployment. Horizontal ADCP, that is, HADCP or ADV can be installed on the depth arm and then deployed for the flow characterization. When needed a universal structure at the front of the floating mobile platform is used for near surface and free stream velocity measurements by the ADV. There is an arrangement for installing vertical ADCP at the front of the pontoon platform. In this way, the floating mobile platform is used by ADV and ADCPs for flow characterization.

Floating mobile platform is ideal for using different instruments at the same time, and to gather flow information. The step-by-step installation procedure of the

measurement instruments is available at the CHTTC website [110]. A Humminbird can be installed on the pontoon platform. As the pontoon is a slow-moving water-craft, the zodiac is used as a secondary support boat as safety or transporting required items. When the zodiac moves, it creates large wave. So, during measurements process with the pontoon platform, there should not be any movement of the zodiac near the measurement area. Depending upon requirements of the site specification, surface measurement with the pontoon can be performed without or with mooring lines.

Measurements without mooring line

Using a zodiac boat without any mooring line is the simplest way of flow characterization and can cover a large flow area. Before starting the characterization, the ADV is secured to the depth arm at the shore and then moved to the point of interest with the zodiac boat. The ADV is then deployed with the help of the horizontal arm, as shown in Figure 3.11. Data is recorded for 8 minutes as proposed by d'Auteuil [38]. During the measurement time, the boat operator holds the water-craft steady in the flow by using a reference point located along the shoreline. Although the boat driver tries to hold the boat stationary there is some movement. This boat motion creates an error in the ADV measurement. Depending upon the measurement site condition such as heavy wind or high energetic and turbulent flow, the boat driver may find it difficult to hold the boat steady. In that case, it is not feasible to perform characterization as the recorded measurement might be affected by the boat motion, and the safety of the personnel and the instrument is of concern.

The same procedure is also used for surface measurement with the pontoon platform. Experimental setup with the depth arm of the pontoon is shown in Figure 3.12. For this study, measurement data of the Red River near the Forks is analyzed. Zodiac boat with the Nortek ADV attached with depth arm is used for the measurements.

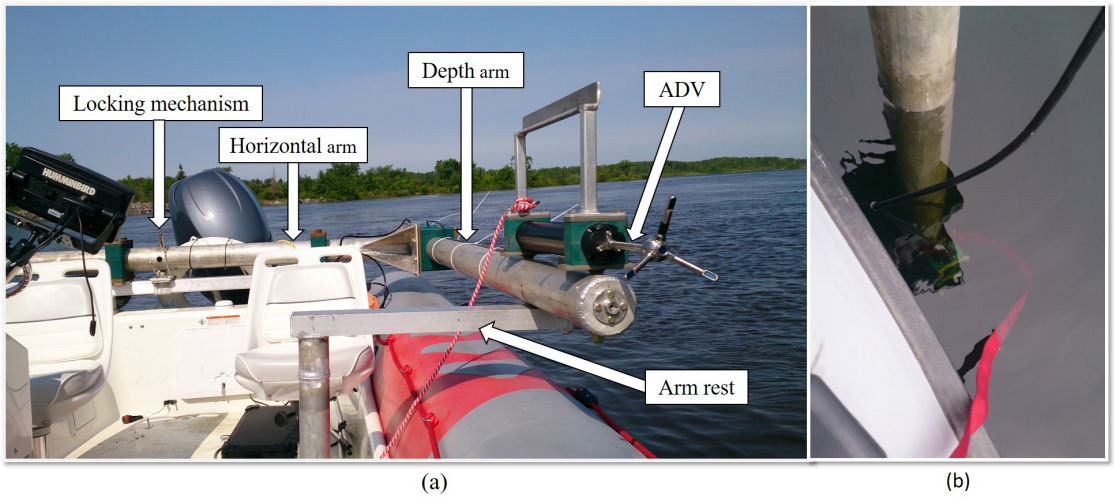

Figure 3.11: Surface measurement at the Forks: (a) Experimental setup used from Zodiac, and (b) deployment of the ADV using depth arm

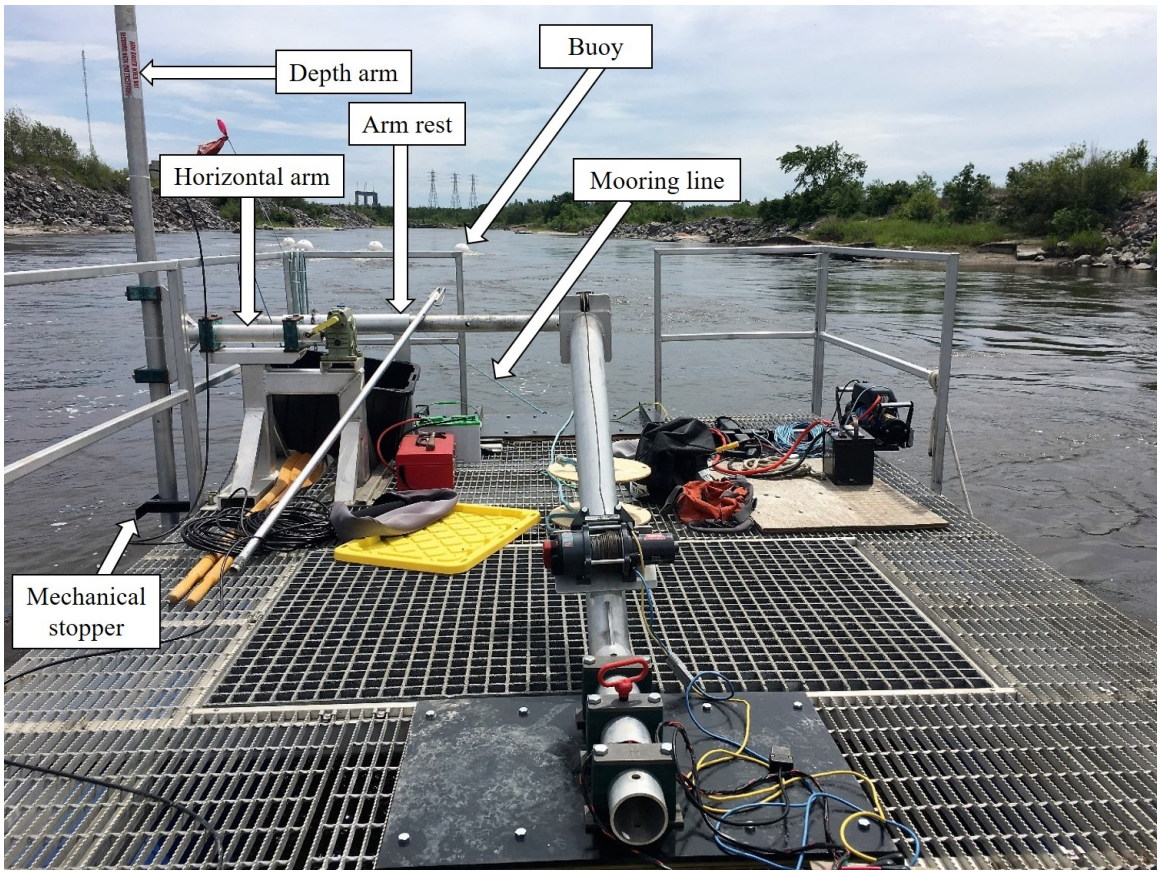

Figure 3.12: Experimental setup used for surface measurement at the CHTTC from the floating mobile platform

Measurements with mooring line

Anchor points are used for turbine deployment at a potential HKT site. These anchor points also used for mooring of the measurement platform. At CHTTC site both the shore anchors and bottom mounted anchoring system are available. As the CHTTC is a man-made channel composed of large and stable granite rocks at the shore, these rocks are used as drilling point for anchors, as shown in Figure 3.15b. Solid reinforced concrete blocks, metal structure or even tree also used as an anchoring point for mooring lines. Bottom mounted anchors are made of three concrete blocks heavy enough to hold moored HKT. Each anchor blocks are attached to a buoy and a common D-ring. This D-ring is used as an anchoring point for mooring lines. For this experiment, the mooring line helps to hold the floating measurement platform steady. Three types of mooring system as introduced here,

(a) Single point mooring from D-ring,

(b) Two-point mooring using shore anchor, and

(c) Two-point mooring with support from the step.

Schematic view of the mooring system is shown in Figure 3.13. For single point mooring measurements, both the zodiac boat and pontoon platform are used. During tests, enough distance from the measurement point and the anchoring point is maintained so that, the mooring structure and the buoys do not influence the flow.

For other cases, the pontoon platform is used. Like surface measurement without any mooring line, side measurement arm of the pontoon is used for single and two-point mooring measurements. However, the measurement arm side of the pontoon cannot be used during the measurement from the steps as the steps block it. The universal mount at the front of the pontoon is used, as shown in Figure 3.14. Using universal

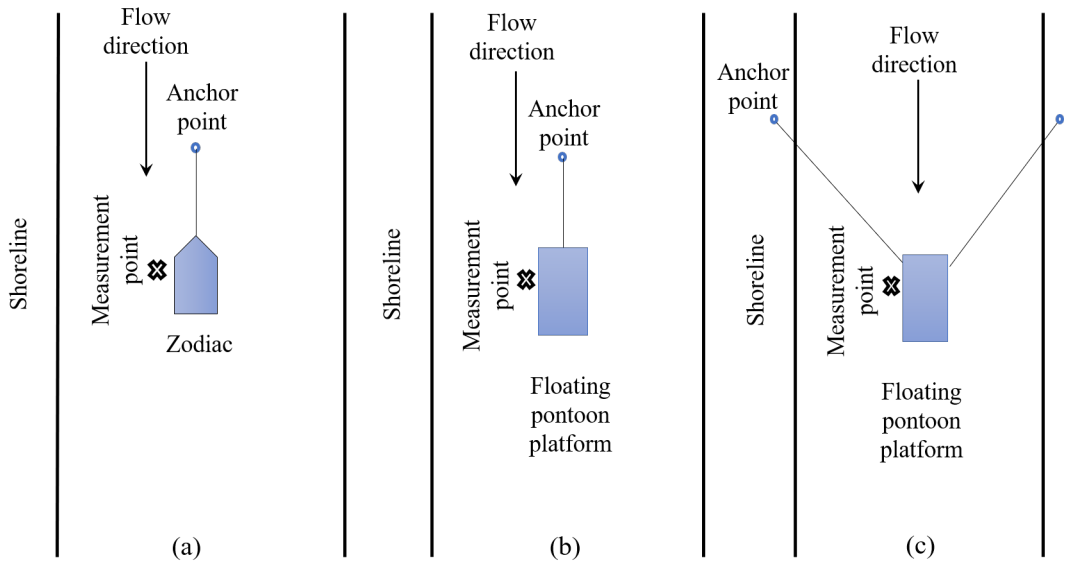

Figure 3.13: Schematic view of anchoring (a) Zodiac using single point mooring, (b) floating mobile platform using single mooring, and (c) floating mobile platform using two point mooring

mount helps to keep the measurement point out of the wake region generated by the steps and the floating measurement platform itself. The floating mobile platform is anchored to two shoreline anchors located on the same side of the shoreline using two electric winches located on the same side of the vessel. One winch is located at the front while the other winch is moved at the back of the measurement platform. With the help of the winches, the measurement platform is then moved closer to the concrete structure to make the platform more stable. A cylindrical shape floating buoy is used in between the steps and floating mobile platform to avoid solid to solid contact and any physical damage of the measurement platform. The design selected avoids the front of the platform driving below the water surface.

3.4.2 Velocity profile measurements

Profile measurement is performed by the floating mobile measurement platform and using two-point anchoring system. The measurement procedure is shown in the Figure 3.15. The two front winches are used to moor the platform with the two

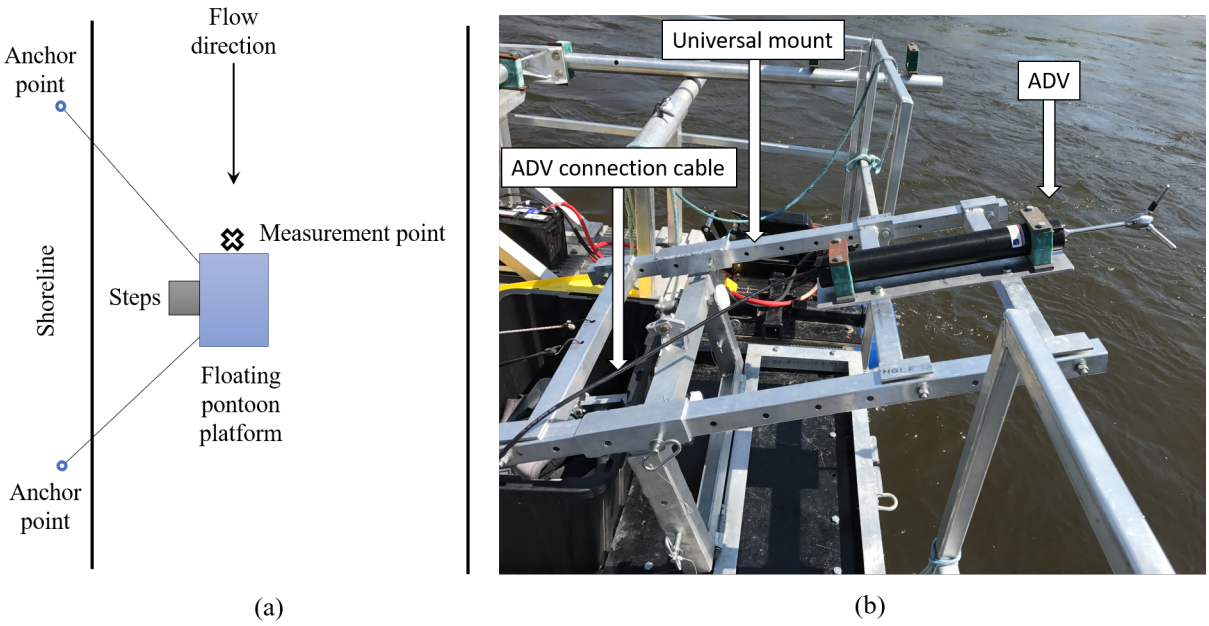

Figure 3.14: (a) Schematic view of anchoring floating mobile platform using two-point mooring with support from steps, and (b) ADV mounted on universal mount

shore anchors, as shown in Figure 3.15a. These winches are used to hold the platform steady and to change the position of the measurement point by providing slack on the winch rope. When the platform is secured, the ADV is deployed from the center of the platform, as shown in Figure 3.15d. The center winch is used to deploy the weight which is connected with it through a steel rope. The weight is used to hold the steel rope downwards and eventually minimizes the ADV alignment. The steel rope is also used as a guideway of the ADV deployment. Schematic view of the weight, steel rope, and ADV is shown in Figure 1.3. The acrylic sheet fin is used to prevent angular rotation of the ADV during measurements. The position of the ADV in different water depth is changed by using a rope. This rope act as safety rope as it is also used for safe retrieval of the ADV. At the same time, the ADCP is deployed from the front of the pontoon boat, as shown in Figure 3.15e. This profile measurement procedure is detailed by d'Auteuil [38], and more details are available at the CHTTC website [110].

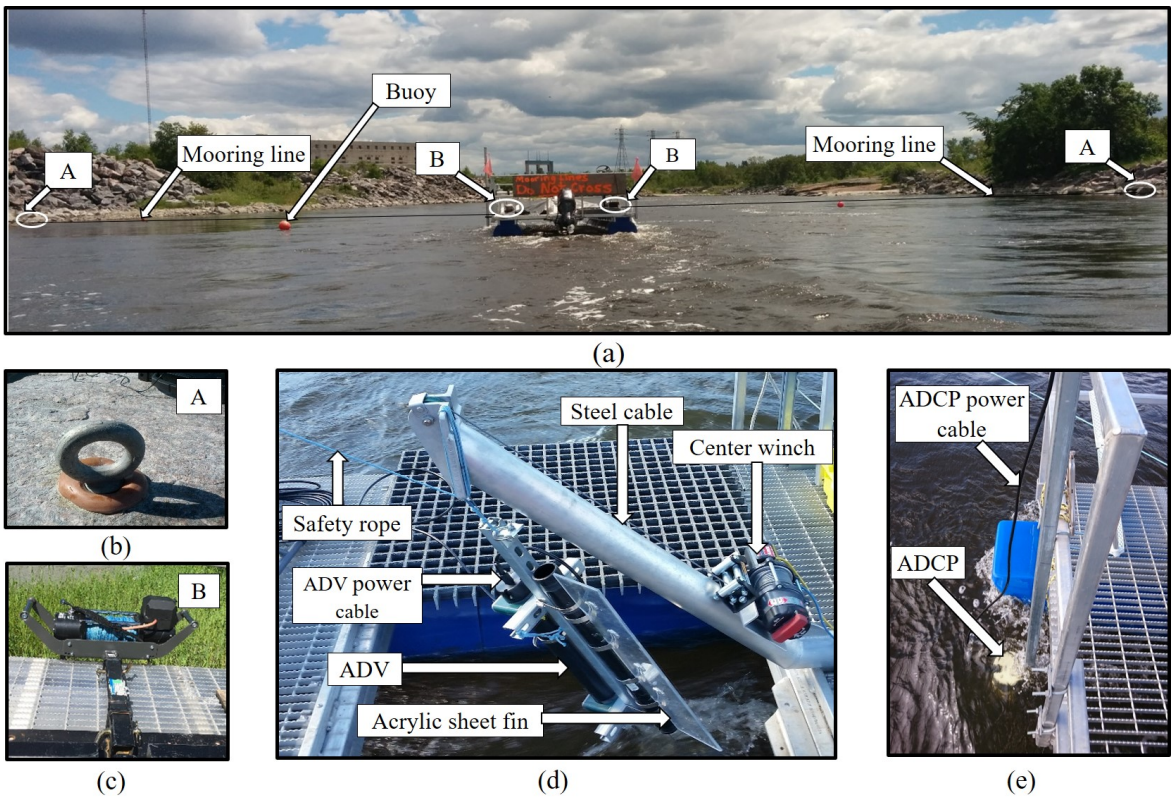

Figure 3.15: Anchoring and deployment system for profile measurement at the CHTTC: (a) Two-point mooring system of floating mobile platform for full velocity profile measurement, (b) anchor point at shore, (c) one of the two front winches used for the pontoon mooring, (d) ADV deployment setup at the center of the measurement pontoon, and (e) deployment of ADCP at front of the pontoon

Chapter 4

Laboratory and field measurement results

4.1 Laboratory test results and analysis

In this section, the data collected from the experiments are presented, and findings from the analysis are discussed to develop a complete uncertainty analysis of these flow measurement in energetic flows. Data is analyzed using a MATLAB code developed by our research group. Excel is used for final calculations and presentation of tables and graphs. The test matrix and procedures are detailed in Sections 3.3 and 3.4, respectively.

4.2 Suspended water particle tests (Tests 1 to 3 in Table 3.4)

The test matrix, as shown in Table 3.4, sets the velocity of the water tunnel at 1.1 m/s for suspended particle tests. The experiments are performed upstream and downstream of the rough surface generated by rocks. Figure 4.1 shows the streamwise velocity measured upstream of the rough surface. The velocity is measured at the

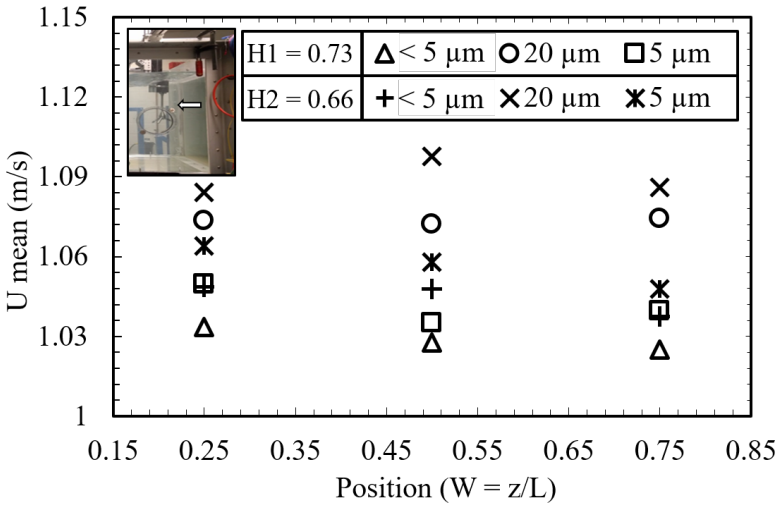

Figure 4.1: The ADV measured streamwise velocity with the particle size of lees then 5 μm, 5 μm, and 20 μm at upstream of the water tunnel at height ratios, H, of 0.73 and 0.66

centerline of the water tunnel, W = 0.50 and closer to the walls, W = 0.25 and 0.75. With the particle size of 20 μm at H = 0.73 and W = 0.50, the measured mean velocity is 1.08 m/s, surpassing the velocity with the particle size of less then 5 μm, and 5 μm. Moving near to the surface at H = 0.66, W = 0.50, and with a particle size 20 μm, the ADV measured velocity is 1.1 m/s which equals the set velocity.

Due to the wake from the rocks downstream of the water tunnel, the flow is more turbulent compared to the upstream location. A higher velocity is measured in the streamwise direction while the spanwise velocity remains negligible and the vertical velocity component fluctuates with depth. Near the bottom of the tunnel at a height ratio of H = 0.75, the U velocity is 1.04 m/s. However, this increases as the ADV position moves towards the surface, as shown in Figure 4.2a. The average SNR of the ADV measurements is 51 with the particle size of less then 5 μm, 5 μm, and 20 μm, which is above the recommended value of 19 [2]. At the bottom surface of the water tunnel, the ADV estimates a lower correlation with the particle size of 20 μm as a result of the turbulent flow. The correlation increases from 60.9% to 87.5% as ADV

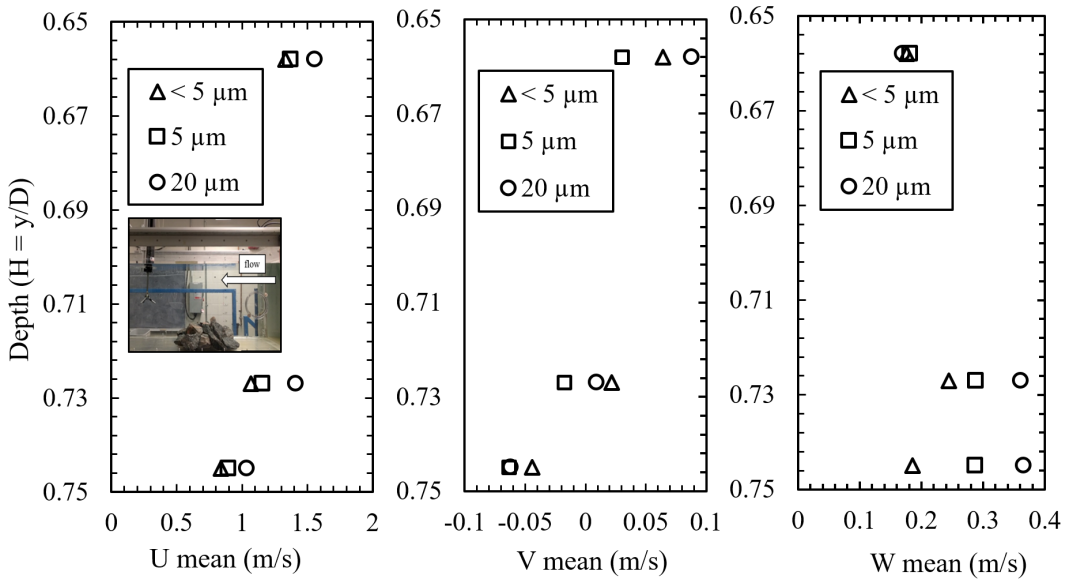

Figure 4.2: The ADV measured velocity component a) U (left), b) V (middle), and c) W (right) with particle size less then 5 μm, 5 μm, and 20 μm measured downstream of the rough surface at water tunnel

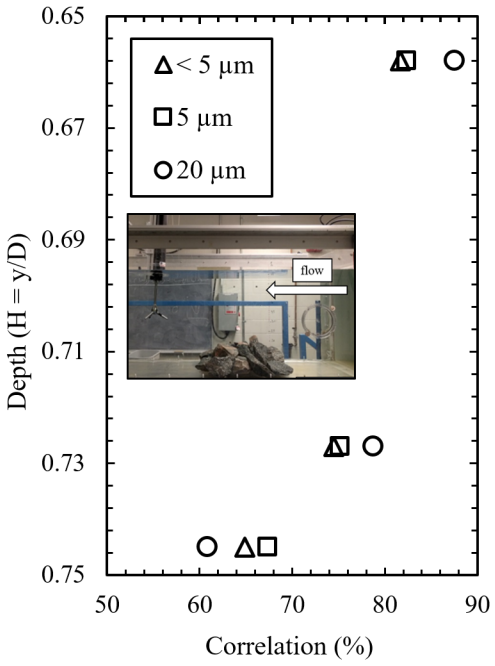

Figure 4.3: Effect of the particle size of less then 5 μm, 5 μm, and 20 μm on the correlation of ADV measurement conducted downstream of the rough surface at water tunnel

Table 4.1: Summary of the flow statistics measured with the particle size of less then 5 μm, 5 μm, and 20 μm at a height ratio of H = 0.66, and an axial position ratio of W = 0.50

Parameter	Upstream Particle size (μm)			Above rocks Particle size (μm)			Downstream Particle size (μm)		
	<5	**5**	**20**	**<5**	**5**	**20**	**<5**	**5**	**20**
U (m/s)	1.05	1.06	1.10	0.62	0.73	0.90	1.33	1.37	1.56
V (m/s)	0.04	0.04	0.06	-0.09	-0.07	-0.11	0.06	0.03	0.09
W (m/s)	0.03	0.02	0.01	-0.07	-0.10	-0.20	-0.18	-0.18	-0.17
Urms	1.05	1.06	1.10	0.97	1.01	1.11	1.35	1.39	1.57
Vrms	0.08	0.08	0.11	0.62	0.65	0.62	0.21	0.21	0.17
Wrms	0.04	0.03	0.02	0.22	0.24	0.28	0.21	0.21	0.18
TKE (m^2/s^2)	0.00	0.00	0.01	0.49	0.48	0.41	0.05	0.05	0.02
TI (%)	5.22	5.19	5.74	91.2	76.9	56.7	13.4	12.9	8.14
Correlation (%)	94.7	94.8	94.5	45.7	46.3	47.2	81.7	82.4	87.5
SNR	53.2	52.9	52.0	51.3	52.1	50.7	52.6	52.5	52.2

moves upward towards the surface at H = 0.66, as shown in Figure 4.3. Summary of the flow statistics with a particle size of less then 5 μm, 5 μm, and 20 μm are shown in Table 4.1. With the particle size of 20 μm, the highest correlation of 87.5% is achieved downstream of the rough surface while the upstream streamwise velocity corresponds to the set velocity. Based on these results, the 20 μm sized particle was selected for the lab experiments to minimize the uncertainty. The uncertainty interval of 4.8% is reduced to 0.2% by using particles size of 20 μm.

4.3 Water tunnel turbulence intensity tests (Tests 2 and 3 in Table 3.4)

Water flowing in the water tunnel passes through a series of honeycombs before entering the test section. These honeycombs assist in breaking eddies generated by the pump while maintaining the turbulence intensity between 3% to 6% at a set velocity of 1.1 m/s. With the introduction of rocks to create a rough surface, as

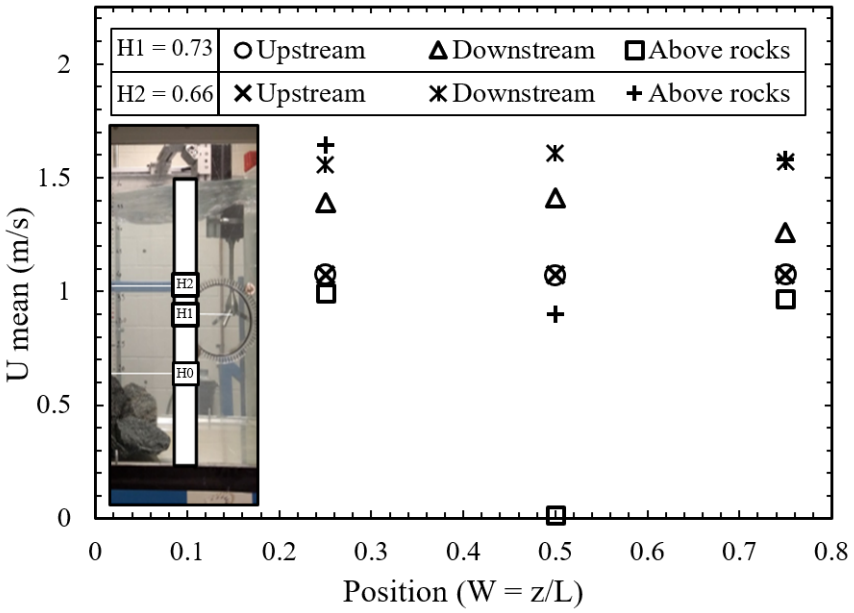

Figure 4.4: Streamwise velocity measured by the ADV upstream, above, and downstream of the rough surface at a height ratio of H = 0.73 and 0.66 as measured in the water tunnel using 20 μm particles

shown in Figure 3.6, the turbulence intensity in the water tunnel increases by 113%. At centerline of the water tunnel and upstream of the rough surface, the streamwise velocity is 1.1 m/s, but over the rough surface, at H = 0.73, and W = 0.5 velocity obtained within the boundary layer. However, over the rough surface and closer to the wall at W = 0.25 and 0.75, an increase in velocity is obtained at the height of H = 0.73 and 0.66 due to uneven roughness as velocity increases from 0.01 m/s to 0.98 m/s. The 41.8% streamwise velocity increase is obtained downstream of the rough surface, as shown in Figure 4.4. This increase in streamwise velocity is due to the wake of the surface roughness.

Figure 4.4 shows the turbulence intensity obtained upstream, above, and downstream of the rough surface while corresponding correlation coefficient is shown in Figure 4.5. A medium TI between 5% to 6% is observed at the upstream of the rough surface and increase above 15% at downstream and a height ratio of H = 0.73. However, TI

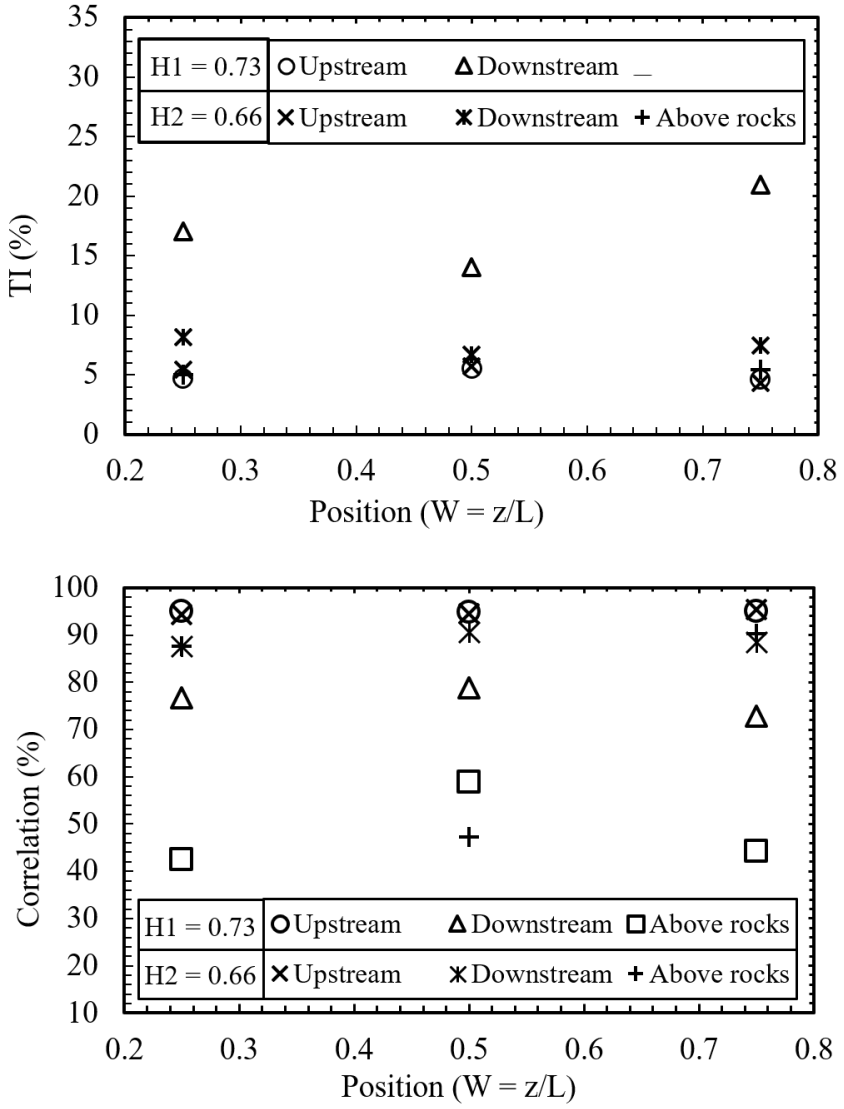

Figure 4.5: The ADV measured a) TI (top), and b) correlation (bottom) at upstream, above, and downstream of the rough surface at a height ratio of H = 0.73 and 0.66. At H = 0.73 and above the rough surface no data point is presented for TI, as the minimum TI of 71% is outside the scale of the figure which could be consider as outlier.

decreases when moving upwards towards the surface. Above the rocks at H = 0.73, the TI is higher than 70%. Although ADV has a good signal strength with an SNR over 51, the correlation is lower than 70%. This low correlation is associated with flow turbulence. Near the walls and H = 0.73, the TI and correlation improves, while at center, the TI increases to 56% due to the boundary layer condition. The summary

of the results obtained upstream, above, and downstream of the rough surface are stated in Table 4.1. A relationship between TI and correlation is observed as when TI increases, there is a decrease in correlation.

4.4 Instrument orientation tests (Tests 4 to 11 in Table 3.4)

According to the measurement procedure developed for the CHHTC site, when the ADV is deployed to different water column heights, it creates an angle with the flow. The Gravity−'g', ENU, and PRH angle compensation methods are used to reduce the uncertainty, as discussed in Section 3.3.3. To implement PRH method, GPS heading angle of the testing site had to be determined first. GPS heading angle of the water tunnel is 58° identified from the GPS location and Google Earth. This angle is used as an initial heading angle. This heading angle along with the ADV measured pitch, roll, and heading angles is used to compensate the orientation of ADV.

Experimental results of the ADV measurements at different pitch angle shows that without angle compensation, deviation from the expected streamwise velocity increases with increase in pitch angle, as shown in Figures 4.6 and 4.7. From the experimental analysis, it is observed that the ADV has an angle compensation mechanism up to 10° as mentioned in the manuals [2]. Further corrective action is required beyond 10° to minimize the measurement uncertainty.

At a velocity of 0.53 m/s, the three angle compensation methods are effective at reducing instrument orientation uncertainty. From Figure 4.6, a maximum deviation of 20% is observed between the measured and expected streamwise velocity at a pitch angle of 40°. After implementing the PRH angle compensation, the uncertainty interval reduces to 2%; the Gravity−'g', and ENU methods agree within 1%.

Increasing the velocity to 1.1 m/s, the effect of the orientation angle becomes

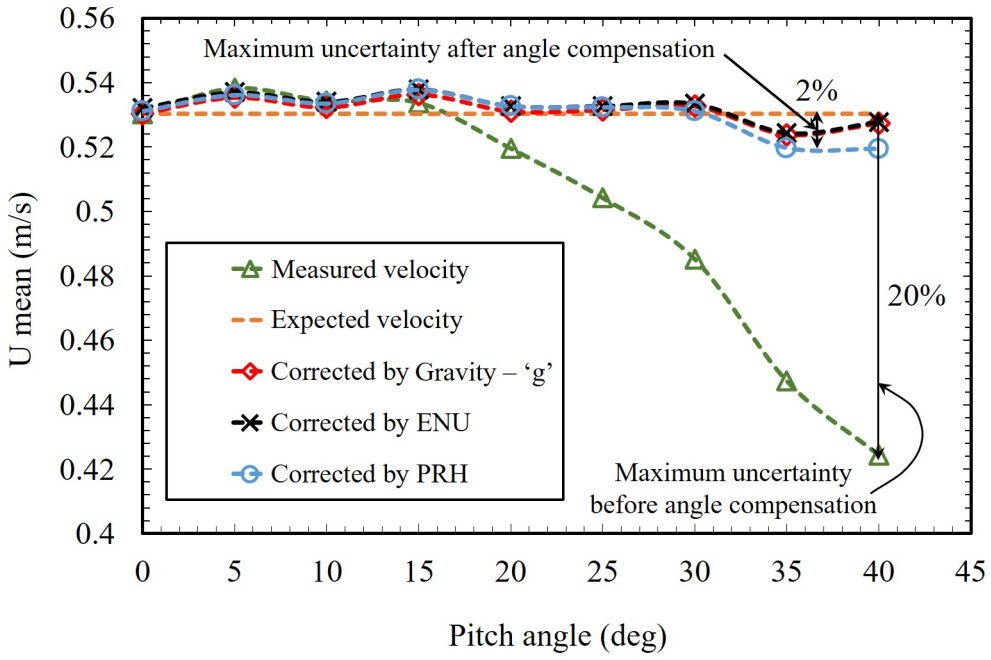

Figure 4.6: Effect of ADV's pitch on streamwise velocity measurements before and after applying Gravity−'g', ENU, and PRH angle correction methods at a water tunnel set velocity of 0.53 m/s

dominant and increases the velocity uncertainty. In this situation, the three angle compensation methods have identical results. A maximum uncertainty reduces from 23% at a 45° pitch angle to 4% at a 27.5° pitch angle, as shown in Figure 4.7.

However, for the W velocity component of the ADV measurement, the ADV's auto-alignment error varies, as shown in Figure 4.8. In this case, angle compensation with ENU and PRH method shows better performance in reducing uncertainty compared to the Gravity−'g' method. The U and W velocity component can be corrected by using the ENU and Gravity−'g' methods. However, all three velocity components can be compensated by using the PRH method. It should be highlighted that for the static ADV, the IMU has a ±0.5° error in PRH altitude calculation while in dynamic condition the error is ±2.0° [2].

In field measurements with a variable pitch angle, there is an effect of the ADV

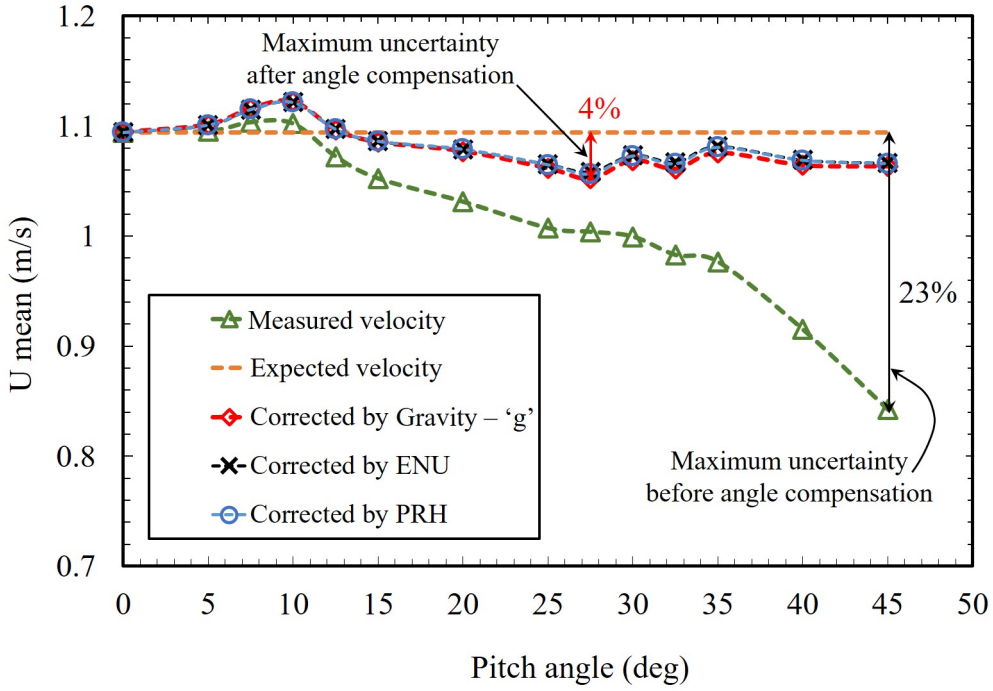

Figure 4.7: Effect of ADV's pitch on streamwise velocity before and after applying Gravity−'g', ENU, and PRH angle correction methods at a water tunnel set velocity of 1.1 m/s

heading and roll angle. The ENU and PRH method works well with pitch, roll and heading angles because in these methods three angles are used to correct the ADV orientation. However, Gravity−'g' compensation only works if there is a pitch or roll angle present in the deployed instrument. It is not efficient if there is a heading angle, or both pitch and roll angle, or if all 3 angles are present during tests. From Table 4.2 a maximum uncertainty interval of 12.25%, 4.60%, and 2.72% is observed in the compensated streamwise velocity using Gravity−'g', ENU, and PRH method, respectively.

Table 4.2: Performance comparison of Gravity−'g', ENU, and PRH angle compensation methods on the ADV orientation during velocity measurement at the water tunnel

Angle			**Measured mean velocity**	**Corrected by Gravity-'g'**		**Corrected by ENU**		**Corrected by PRH**	
P (deg)	**R (deg)**	**H (deg)**	**U (m/s)**	**U (m/s)**	**Diff (%)**	**U (m/s)**	**Diff (%)**	**U (m/s)**	**Diff (%)**
0	0	0	1.108	1.109	0.12	1.117	0.84	1.104	0.35
0	10	0	1.114	1.097	1.03	1.120	1.11	1.110	0.22
0	20	0	1.110	1.047	5.54	1.118	0.89	1.109	0.07
0	30	0	1.110	0.972	12.25	1.120	1.05	1.112	0.32
10	0	0	1.117	1.136	2.56	1.144	3.28	1.125	1.51
20	0	0	1.054	1.125	1.53	1.133	2.23	1.110	0.19
30	0	0	0.967	1.125	1.49	1.132	2.19	1.096	1.10
0	0	10	1.115	1.115	0.67	1.118	0.89	1.110	0.17
0	0	20	1.084	1.084	2.21	1.119	1.02	1.117	0.77
0	0	30	1.024	1.024	7.57	1.126	1.63	1.123	1.37
10	0	10	1.116	1.137	2.61	1.139	2.76	1.126	1.63
20	0	20	1.020	1.106	0.21	1.131	2.05	1.122	1.29
30	0	30	0.887	1.027	7.34	1.133	2.27	1.129	1.86
0	10	10	1.112	1.101	0.63	1.117	0.81	1.111	0.30
0	20	20	1.102	1.090	1.60	1.140	2.86	1.127	1.68
0	30	30	1.020	1.068	3.61	1.134	2.36	1.078	2.72
10	10	0	1.118	1.127	1.75	1.143	3.17	1.128	1.81
20	20	0	1.037	1.085	2.12	1.128	1.84	1.111	0.23
30	30	0	0.943	1.038	6.30	1.159	4.60	1.125	1.51
10	10	10	1.117	1.136	2.51	1.140	2.91	1.131	2.11
20	20	20	1.021	1.127	1.68	1.139	2.76	1.130	1.95
30	30	30	0.869	1.109	0.10	1.122	1.25	1.104	0.35
Maximum uncertainty					12.25		4.60		2.72
Average uncertainty					2.97		2.03		1.07

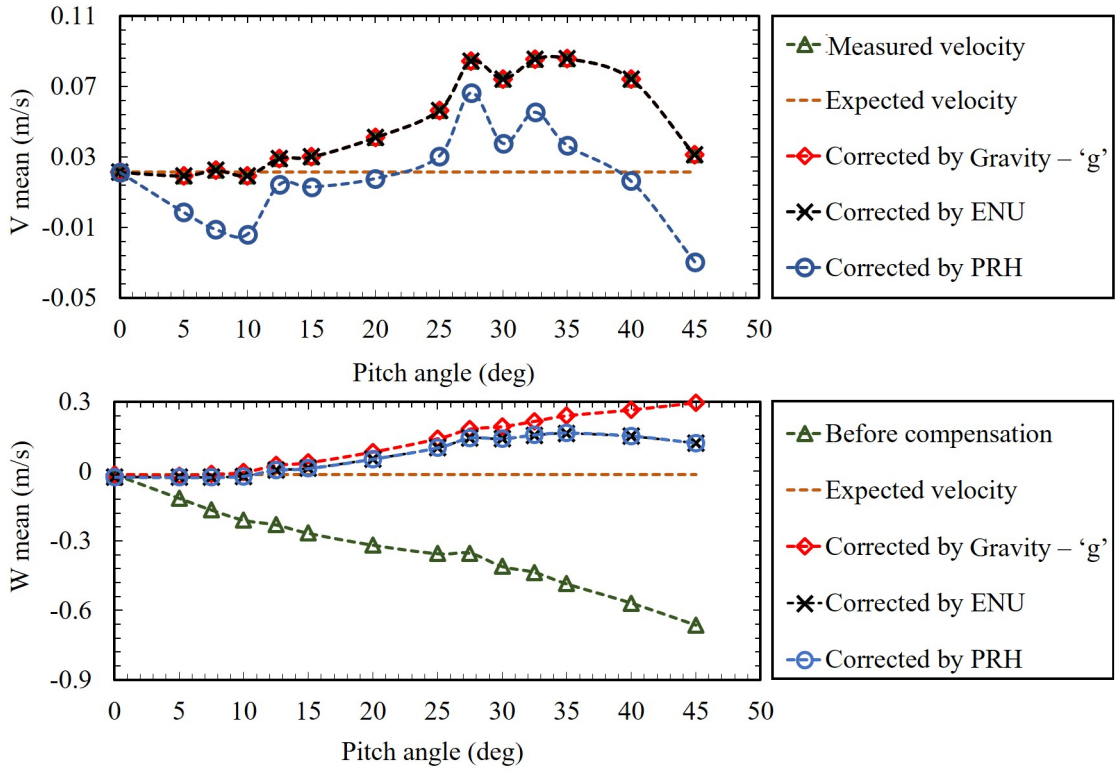

Figure 4.8: Effect of ADV's pitch angle on a) V, and b) W component of the velocity before and after applying Gravity−'g', ENU, and PRH angle correction methods at a water tunnel set velocity of 1.1 m/s

4.5 Vibration and motion tests (Tests 12 to 20 in Table 3.4)

The performance of the ADV's IMU is analyzed using a shaker table at the vibration lab by utilizing a sine wave signal with known displacement to asses the uncertainty of measurement for correction. The resulting vibration is measured by the IMU for validation. Numerous test at different frequencies were conducted, as listed in the test matrix in Table 3.4. Amongst them, the results of tested frequencies 2 and 5 Hz, as shown in Figure 4.9, with Figure 4.9a showing the linear acceleration spectrum of the tested frequency of 2 Hz. Along with the excitation frequency, several higher order frequencies are registered by the IMU accelerometer. These higher order frequencies are visible also at an exciting frequency of 5 Hz, as shown in Figure 4.9b. The exciting frequency of 5 Hz is reported at the highest peak, and corresponding higher orders

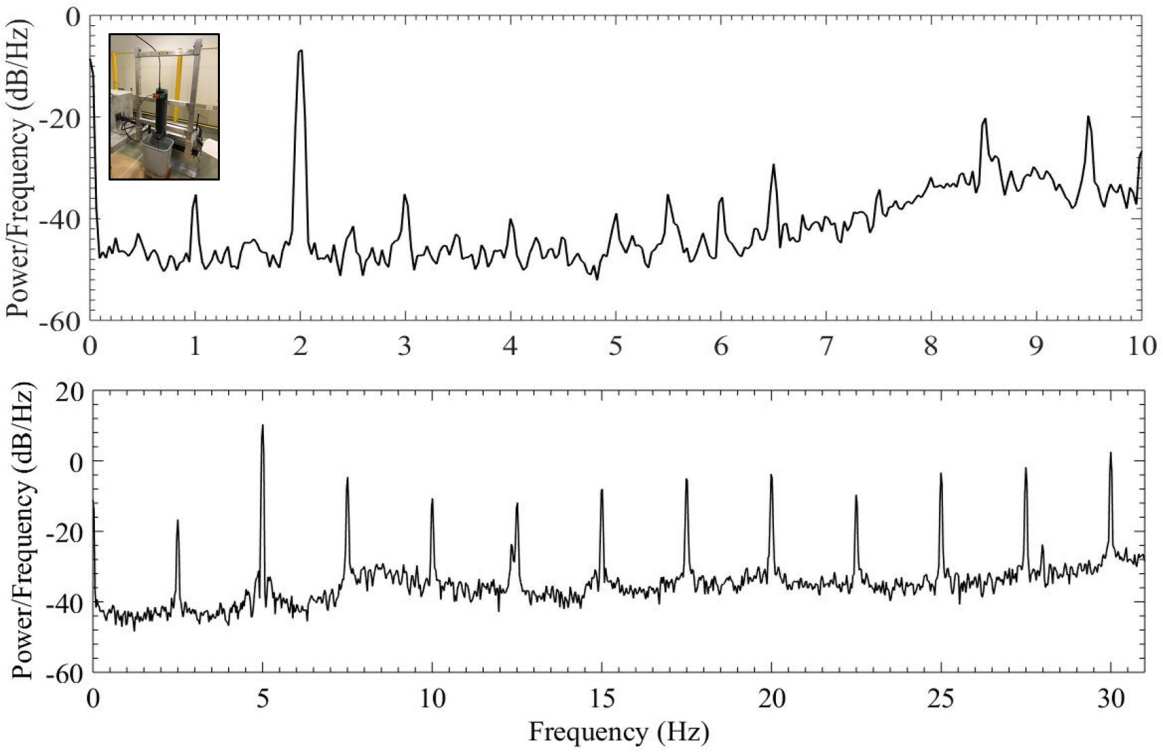

Figure 4.9: Linear acceleration spectrum as measured by IMU of ADV recoding data at 64 Hz while the shaker table has an excitation frequency of (a) 2 Hz, and (b) 5 Hz which are characteristics of Boat and ADV motion in energetic river

of harmonic frequencies are obtained at 7.5, 10, 12.5, 15, 17.5 Hz, and so on. As reported by Doranga [109], these higher order harmonic frequencies also occur when using the shaker table due to the low-performance bearing and table noise. For the IMU performance test, the ADV support mounting adds to the harmonic vibration noise.

To further investigate the IMU's accuracy on ADV motion correction, additional tests are performed in the water tunnel. Starting with the ADV at rest, a force is applied in the direction of the flow to the ADV support structure to create motion and create an error the velocity measurement. This additional motion is detected by the IMU accelerometer and is noticeable in Figure 4.10. IMU obtained velocity is then subtracted from the ADV velocity. The trend in IMU corrected ADV velocity is detected by the Kernel Regression (see Section 3.3.4), as shown in Figure 4.11. This

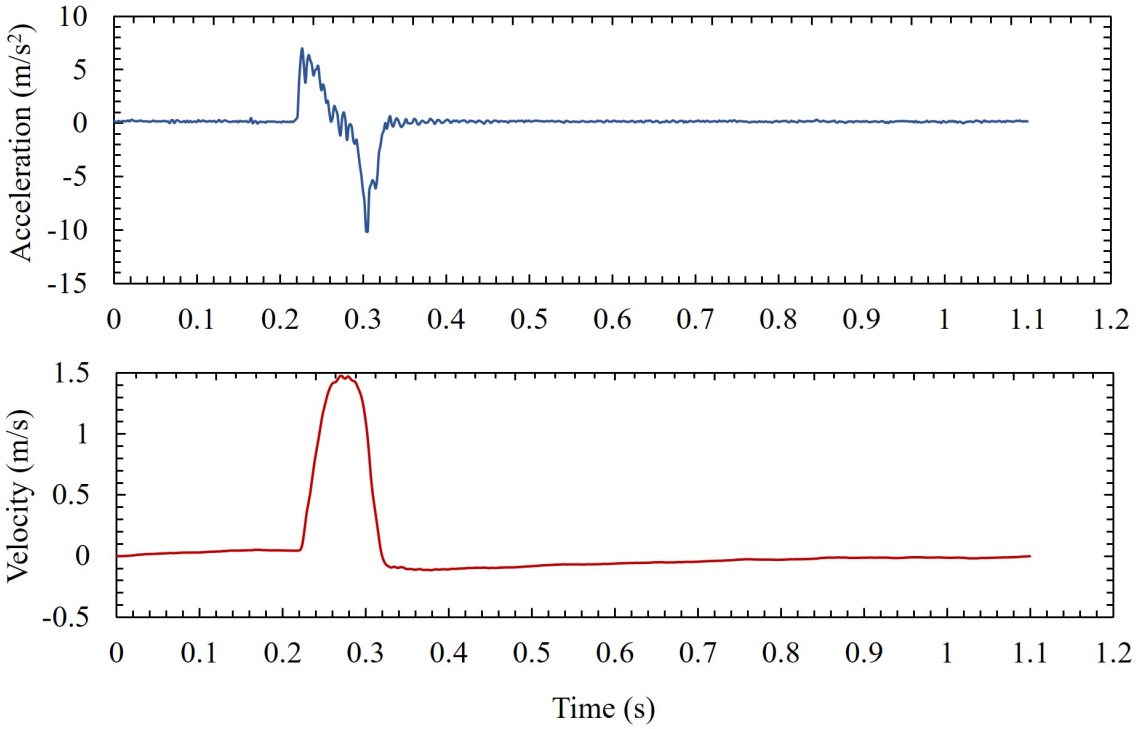

Figure 4.10: Effect of an additional force applied to the ADV support structure: (a) IMU obtained streamwise acceleration, and (b) IMU acceleration converted into velocity

trend is then removed from the ADV velocity, and the final ADV corrected velocity together with the ADV measured velocity is shown in Figure 4.12. The task is to determine the uncertainty in such measurements having disturbance as found in field tests and corrected with IMU.

The set streamwise velocity of the water tunnel is 0.53 m/s. Due to the addition of the external force, the velocity at that point reaches to 1.23 m/s at 2.29 s, as shown in Figure 4.12. The difference between the set and the applied velocity is 1.5 m/s. This additional velocity is detected by the IMU, as shown in Figure 4.10. The final velocity after motion compensation is shown in Figure 4.12. After implementing motion compensation, the ADV measurement total uncertainty decreases from 15.6% to 3.26%.

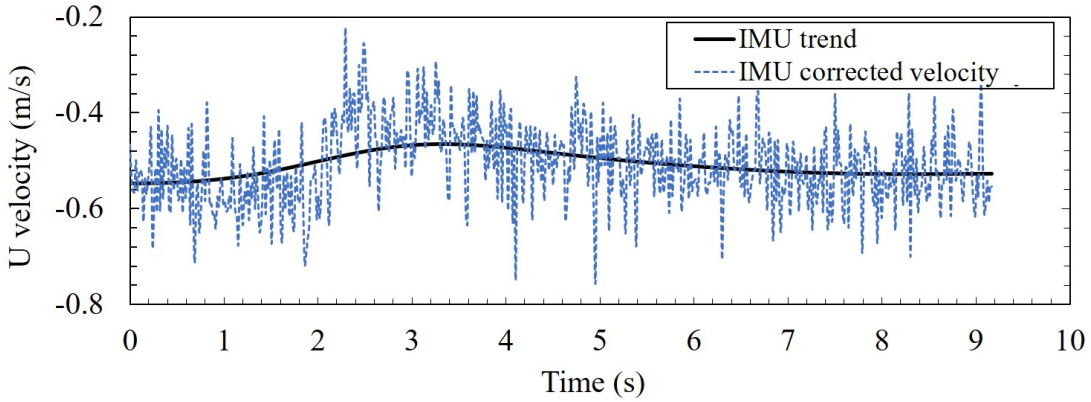

Figure 4.11: The IMU corrected ADV streamwise velocity with quantified IMU drift seen as trend to element motion uncertainty from ADV measured velocity

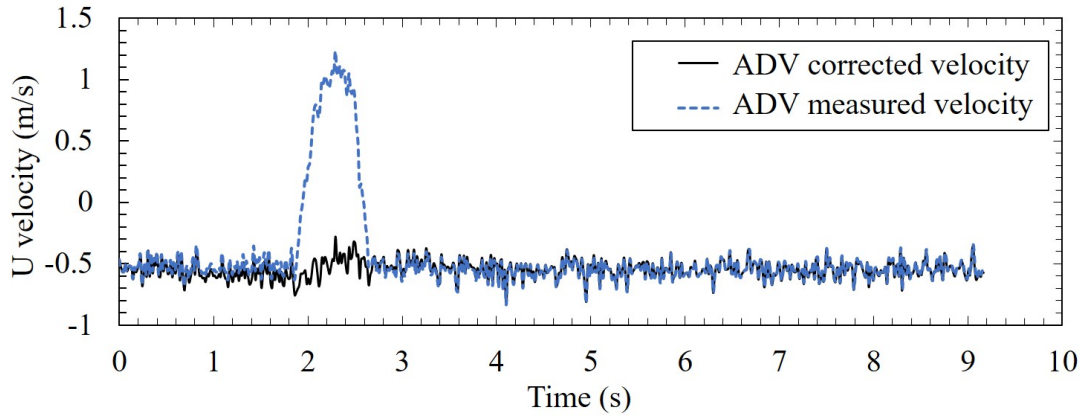

Figure 4.12: Contrast between ADV measured streamwise velocity during additional force applied on the ADV support structure and streamwise velocity obtained after removing uncertainty using motion compensation routine

The same method is applied to the span and vertical velocity components. As the ADV is rigidly mounted on the support structure, the only possible way for its movement was in the lateral direction. Due to this reason, there is no significant difference observed in the span and vertical directions before and after motion compensation, as shown in Figure 4.13.

Forces of different amplitudes are applied to the ADV during measurement. In this case, forces are applied in opposite direction of the flow. The IMU detect the effects and compensates the additional motions applied during measurement, as shown in

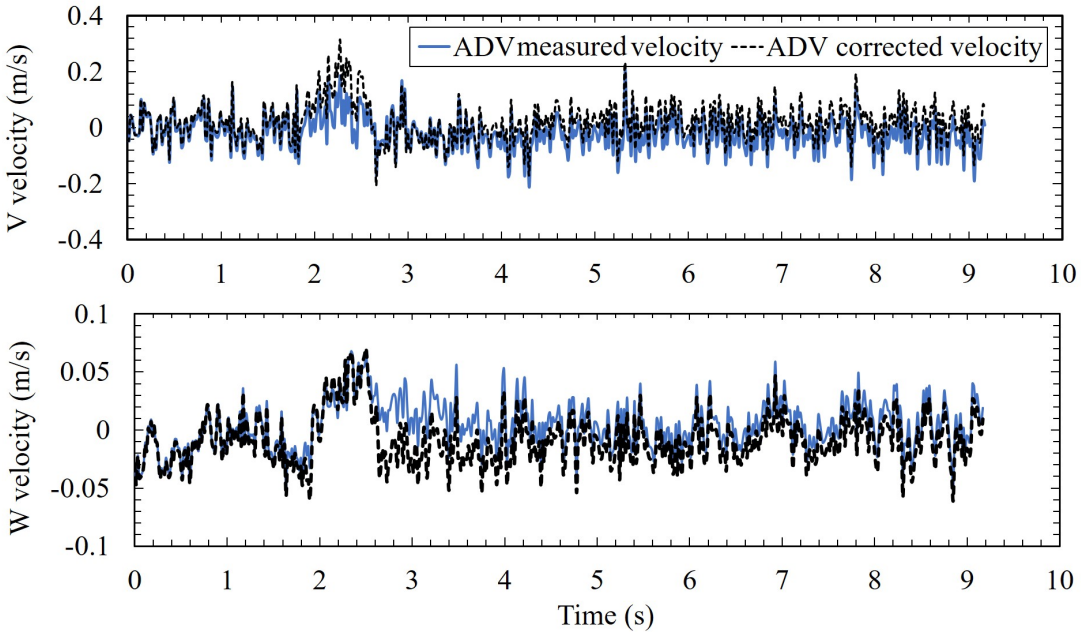

Figure 4.13: Contrast between ADV measured a) V, and b) W velocity component during additional force applied on the ADV support structure and the velocities obtained after removing uncertainty using motion compensation routine

Figure 4.14. For this case, uncertainty of the streamwise velocity measurement is reduced to 0.96% from 18.5%. Different cases and conditions are tested in the water tunnel to investigate the performance of the motion compensation method, as mentioned in the test matrix in Table 3.4. Satisfactory results are obtained from examined cases in the laboratory and it can be observed that uncertainty of the measurement depends upon the applied forces on the ADV and the intensity of the turbulence being measured. We therefore conclude that with ADV motion induced in the field, The IMU and data processing system produces an uncertainty of 3.3%.

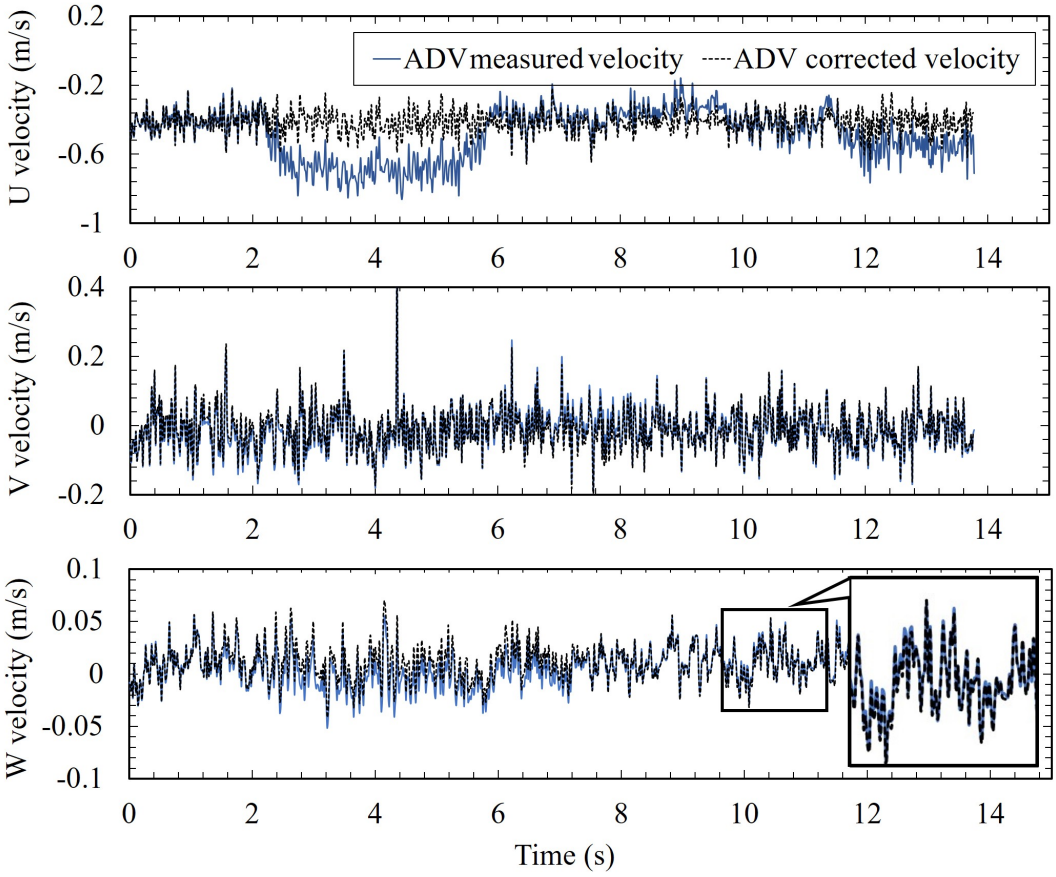

Figure 4.14: Comparison of ADV measured time series of a) U (top), b) V (middle), and c) W (bottom) velocity components during additional force of different amplitude is applied on the ADV support structure and the corrected velocities obtained after implementing motion compensation routine

4.6 Field experiment results and analysis

4.6.1 Surface measurements (Tests 21 to 27 in Table 3.5)

As a part of preliminary test, surface measurements from the zodiac arm structure (shown in Figure 3.11) were performed at six selected points on the Assiniboine river at the Forks, Winnipeg, Manitoba in 2015. The measurements were performed near the bridge at the Forks. A Google Earth view of the selected locations is shown in Figure 4.15. The points were chosen based on their apparent velocity, position, depth, presence of obstruction, and distance from the previous measurement points.

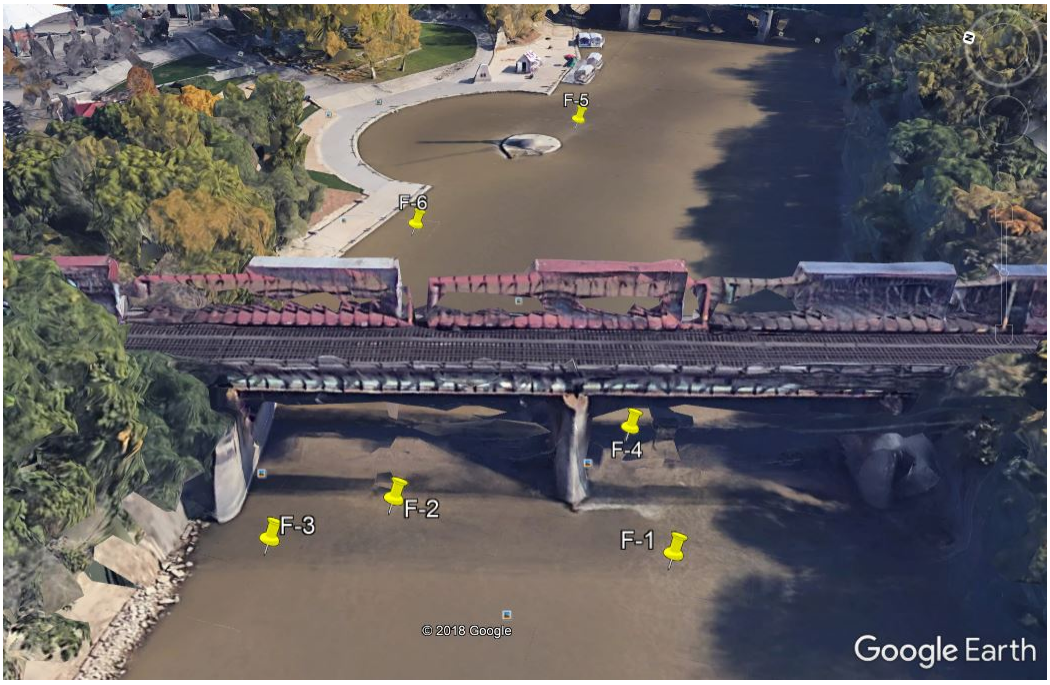

Figure 4.15: Location of the surface measurement points on the Assiniboine River at the Forks in Winnipeg. Multiple points are selected to capture the range of velocities occurring in the river.

The measurements were performed to investigate the velocity variation across the river.

The data was measured for three minutes with an average SNR of 49.6 and correlation of 92.6%. From this we conclude that the naturally occurring seeding particles are sufficient ADV measurement, based on results in section 4.2 As the measurement arm is lowered into the water, the pitch and roll angle varied due to movement of the boat. In most cases, the IMU measured pitch agrees with the calculated pitch angle calculated using the Gravity−'g' method with a maximum difference of 1.27°. The pitch and roll angle of the measurement varies within 10°. All of these indicate that the quality of the data collection was excellent. A summary of the ADV raw data without motion correction is shown in Table 4.3. The larger velocity region has a TI exceeding 30%, while the low-velocity region has comparatively lower TI with a range of 5.60% to 16.4%. For hydrokinetic turbine deployment, these results are

Table 4.3: Summary of results obtained from the preliminary survey of surface measurements at the Forks

ID	Correlation (%)	SNR	Pitch angle measured by		U (m/s)	V (m/s)	W (m/s)	TI (%)
			Gravity-'g' (deg)	PHR (deg)				
F-1	94.7	49.8	5.97	4.70	1.05	-0.20	-0.23	31.02
F-2	94.2	48.8	8.50	7.40	2.51	-0.56	-0.13	10.3
F-3	95.5	49.3	9.04	7.93	2.67	-0.68	-0.23	5.60
F-4	90.5	50.5	7.96	6.95	1.87	-0.53	-0.12	16.4
F-5	85.2	49.1	6.17	5.31	1.62	-0.64	-0.13	30.5
F-6	95.3	49.9	7.80	6.78	2.36	-0.45	-0.15	8.31

used to select the fastest flowing area of the river for detailed characterization. Even though more power can be extracted from the high flow region, the TI is considered for shelf-life and performance of the turbine.

Performing surface measurement at high flow regions is a challenge because during that period the boat driver has to hold the measurement platform as steady as possible which requires expertise and the full consciousness of the driver. Unwanted platform motion can affect the result and make it difficult to select the highest flow region accurately. At measurement Point F-6 a peak is observed due to the movement of the measurement platform, as shown in Figure 4.16. This motion is also captured by the IMU as instrument acceleration and used to compensate velocity uncertainty.

Figure 4.17 shows the IMU corrected ADV velocity with the selected trend of the IMU internal error. Trend selection works accurately except near the location with the spike as marked in Figure 4.17.The spike causes a slight deviation in the trend selection and the final ADV velocity correction. These spikes can be removed by using the hybrid despiking method [37]. From analyses, it can be observed that using despiking method removes valid data points if there is any platform or instrument or both motion presents during the measurement process. It is recommended to use motion compensation before using any despiking routine. Final compensated U,

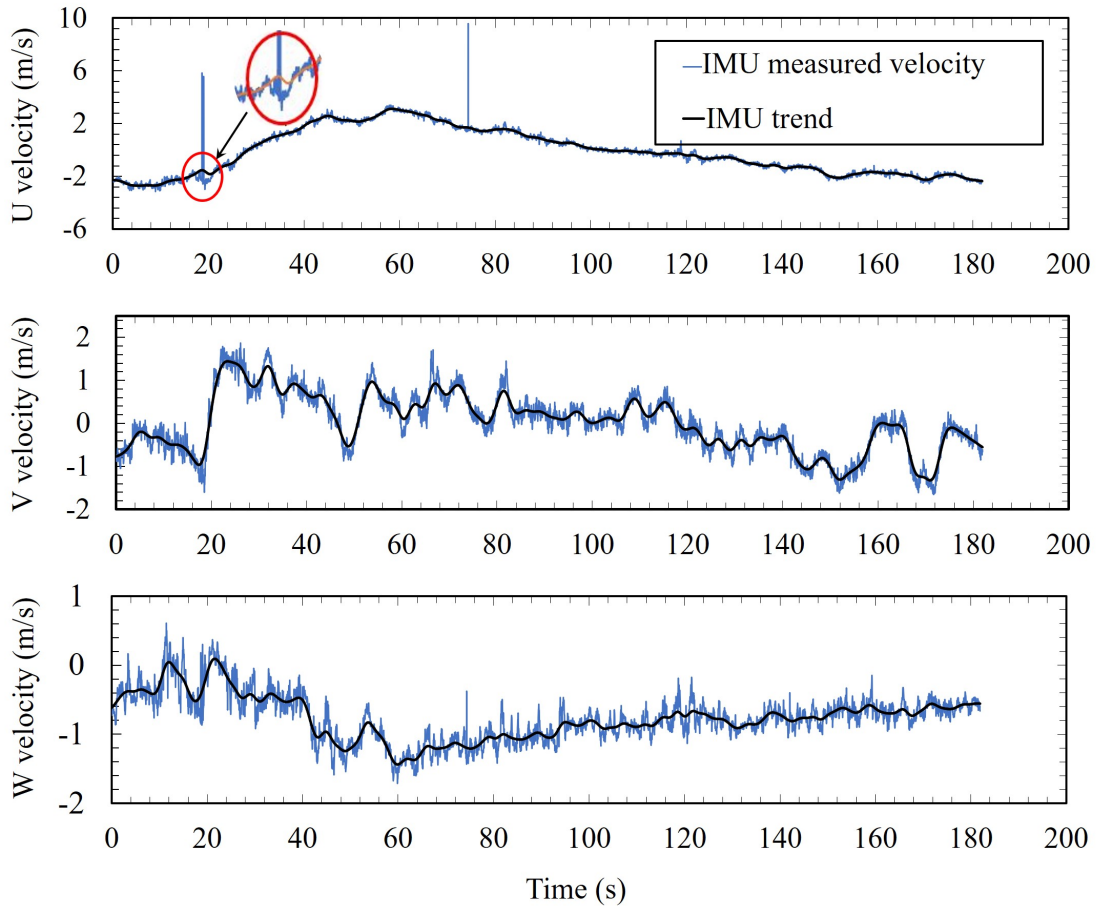

Figure 4.16: Time series of IMU measured ADV velocity components a) U, b) V, and c) W of measurement point F-6, with trend selection. In the measured time series acoustic noise is observed as spikes. Such noise adds undesirable skewness in trend selection of the U velocity component as marked with a circle.

V, and W velocity components along with the ADV measured velocity is shown in Figure 4.18. After motion compensation and despiking, the mean streamwise flow velocity obtained is 2.29 m/s with an total uncertainty interval of 2.92%.

Energy spectra of the ADV for streamwise velocity with and without motion correction is presented in Figure 4.19. Results demonstrate the ability of the motion compensation using IMU acceleration to remove the motion from the ADV measurements. Motion compensation removes the higher order of the harmonics and also reduces the magnitude of the peaks induced by the instrument movement.

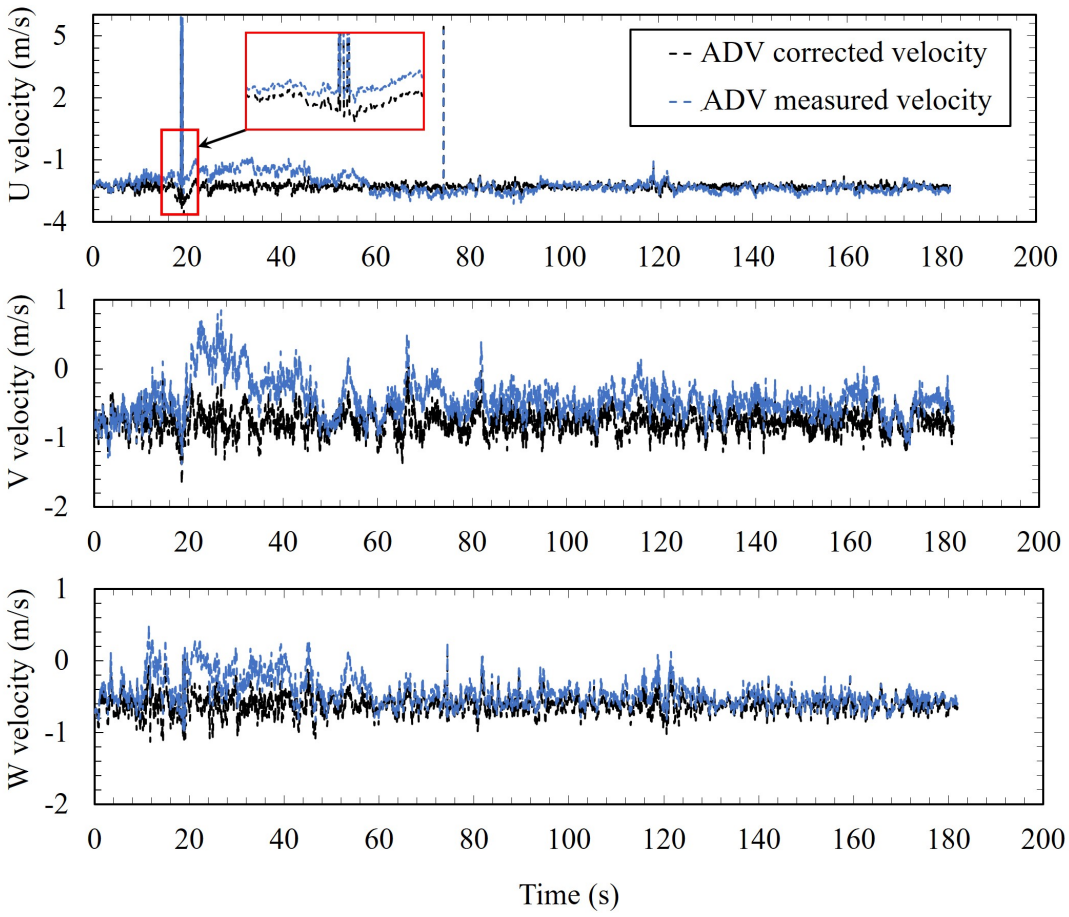

Figure 4.17: Time series of IMU measured ADV velocity components a) U, b) V, and c) W of measurement point F-6, without any compensation, and with motion compensation. Unwanted skewness is observed in the corrected streamwise velocity as marked with a box.

At a frequency of 0.2 Hz, when there is no motion and harmonics, the motion compensated results shows divergence from the ADV measurement. This discrepancy is due to the IMU accelerometer's low-frequency bias drift which was observed by Kilcher [47].

Results as shown in Table 4.4 indicates a significant improvement in TI measurement from the ADV after motion compensation. The TI increases from 5.60% to 15.6% at Point F-2 due to the noisy dataset. As shown in Figure 4.16, spikes in the measurement results divergence in trend selection and at the end, it increases the

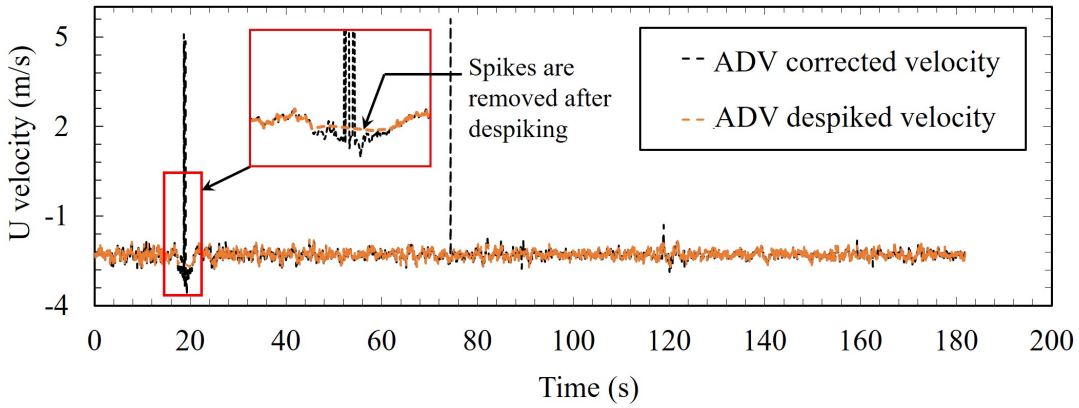

Figure 4.18: Time series of ADV measured streamwise velocity components of measurement point F-6, with motion compensation, and with despiking. Unwanted spikes are removed from the corrected streamwise velocity as marked with a box. The task is to access the uncertainty of the measurement with a despiked data set and the contribution of the uncertainty added by the despiking routine.

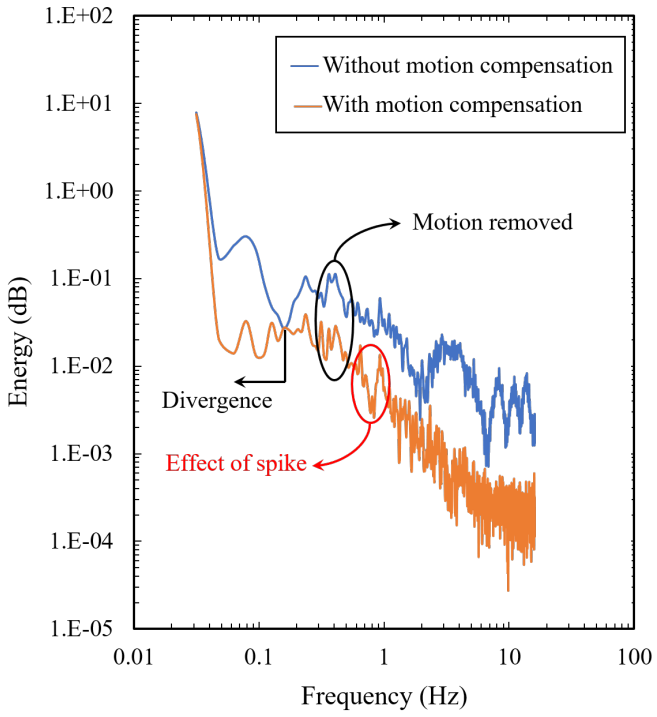

Figure 4.19: Energy spectra of measurement at Point F-6 with, and without motion compensation showing ADV velocity removed from the measured velocity, effect of the spikes, and the divergence in corrected velocity

Table 4.4: Comparison of average flow statistics before, and after motion compensation of the data measurements at the Forks

ID	Before motion compensation		After motion compensation		Uncertainty of	
	U (m/s)	TI (%)	U (m/s)	TI (%)	U (%)	TI (%)
F-1	1.05	31.0	0.74	7.13	29.3	77.0
F-2	2.51	10.3	2.68	6.43	6.89	37.8
F-3	2.67	5.60	2.52	3.68	5.58	34.3
F-4	1.87	16.4	2.26	10.5	21.0	36.1
F-5	1.62	30.5	1.87	18.5	15.5	39.5
F-6	2.36	8.31	2.29	5.66	2.92	31.9
Maximum uncertainty					29.3	77.0
Minimum uncertainty					2.92	31.9

uncertainty of the motion correction. For noisy dataset without large boat motion, the results can be improved by using despiking routine first and then the motion compensation. In this case, the final compensated TI is 3.68%. Although TI decreases in every case, the streamwise velocity decreases in some cases and increases in others. This distinction is due to the dynamics of the measurement platform and support structure of the ADV. The average uncertainty of the surface measurement from Zodiac, before and after motion compensation is 13.5% and 42.8% for streamwise velocity and TI, respectively.

4.6.2 Shore/fixed platform measurements (Test 28 in Table 3.5)

Shore Point (SP) measurements were taken to compare the results with site characterization data and to verify the effect of movement of the measurement platform and deployment procedure on ADV performance. Three-point mooring support system, two from the shore and one from the steps, were used for this process. Location of the SP is shown in Figure 4.20. Therefore, minimal movement of the platform will affect the measurement. The ADV used to take surface measurements

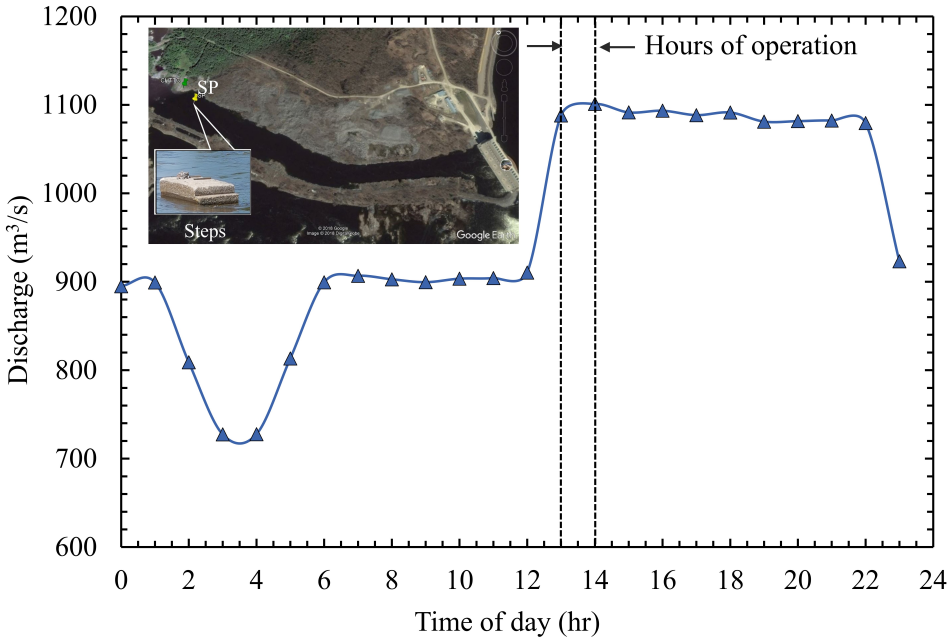

Figure 4.20: Discharge from the Seven Sisters dam during the days of measurement from the Point SP. Location of the measurement point SP is marked in the plot. Vertical line shows the time period of the measurement.

only. The statistics of the measurement is given in Table 4.5. The collected data quality was good as average SNR of 24.4 and correlation of 95.6% were obtained. The average pitch and roll angle of the measurements were below 10°. A satellite view of the measurement point and hourly flow-rate during the day of measurement is shown in Figure 4.20.

Initial analysis shows that the measured dataset has fewer spikes compared to the surface measurement procedure used at the Forks. This is because of reduced platform motion and instrument's vibration. Still, movement of the measurement platform is observed which is later corrected by using the motion compensation routine, as shown in Figure 4.21.

The obtained discharge rate of the dam during the measurement time was approximately $1,100\ m^3/s$, as shown in Figure 4.20. The average velocity from measurement point SP was 0.98 m/s, which was lower than the expected velocity. There are two

Table 4.5: Comparison of average flow statistics between before and after motion compensation of the measurements from SP at CHTTC

	Before motion compensation	**After motion compensation**	**Uncertainty interval(%)**
U velocity (m/s)	1.10	0.98	11.0
V velocity (m/s)	-0.33	-0.13	60.6
W velocity (m/s)	0.16	0.12	26.3
TI (%)	17.6	12.5	29.0
TKE (m^2/s^2)	0.05	0.02	58.2
	Measured by Gravity–'g'	**Measured by PRH**	**Uncertainty interval (%)**
Pitch angle (deg)	6.52	7.22	10.6

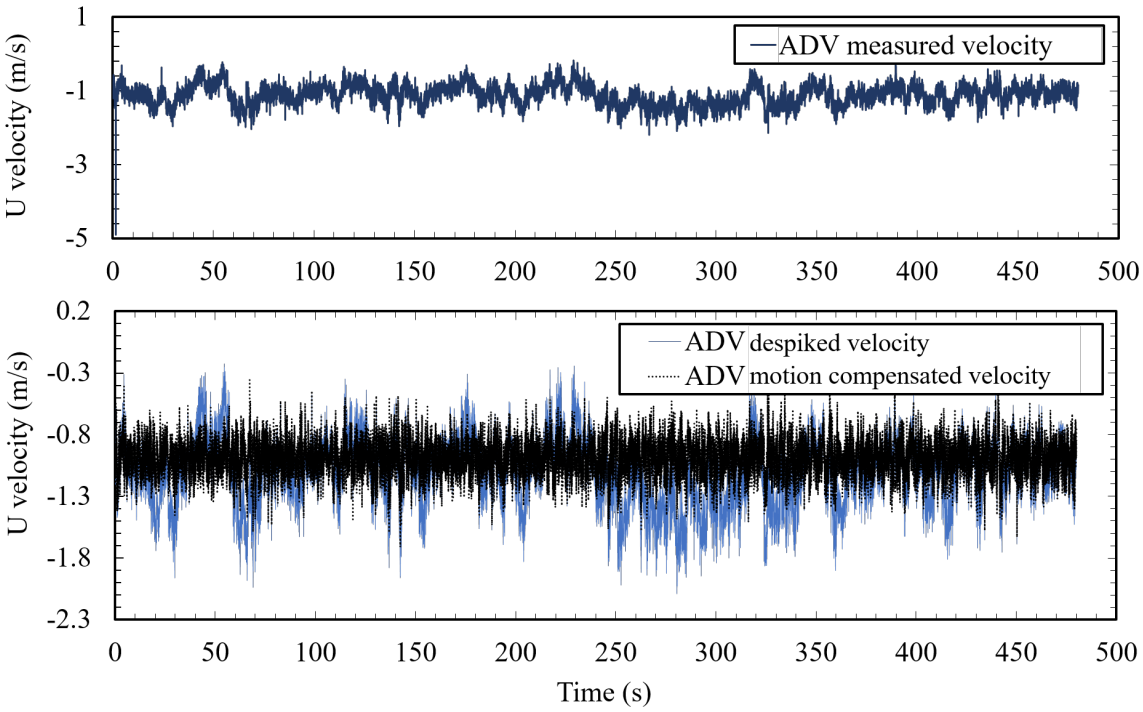

Figure 4.21: Time series of ADV measured a) streamwise velocity, U, and b) corrected velocity after despiking and the motion compensation at Point SP measured from a fixed platform

possible reasons behind that, the first one being that the depth of the SP measurement was only 0.3 m while the second been that the steps were closer to shore area which may also have caused the measurement point to fall into the lower velocity region.The

Figure 4.22: Location of the flow Characterization Point (CP) at downstream of the Seven Sisters dam on the Winnipeg River at CHTTC. Each day's CP labeled in a alphabetic order from A to H.

uncertainty interval of the measurement before and after motion compensation for streamwise velocity is 11.0% which is 20.1% lower than the uncertainty for the surface measurement at the Forks and TI is smaller by 38.22%. This difference in uncertainty is due to less platform motion or lower velocity of the measurement location.

4.6.3 Profile measurements (Tests 29 to 49 in Table 3.5)

As a part of a flow characterization campaign, 20 velocity profiles were measured in the CHTTC channel [110]. Characterization points are marked as CP and shown Figure 4.22. Each day's characterization points are labeled in alphabetical order from A to G where CP-A is the farthest upstream and CP-G is the farthest downstream measurement points. Depending upon the width, depth and physical obstructions such as rocks at the channel, 2 or 3 measurement points were selected at each CP for full profile measurement. At each measurement point, ADCP is used to take full velocity profile from the surface whereas the ADV is placed at a different height to measure the flow statistics. The procedures are detailed in Reference [38, 110]. Each point took approximately one day to setup and take measurements is all went well.

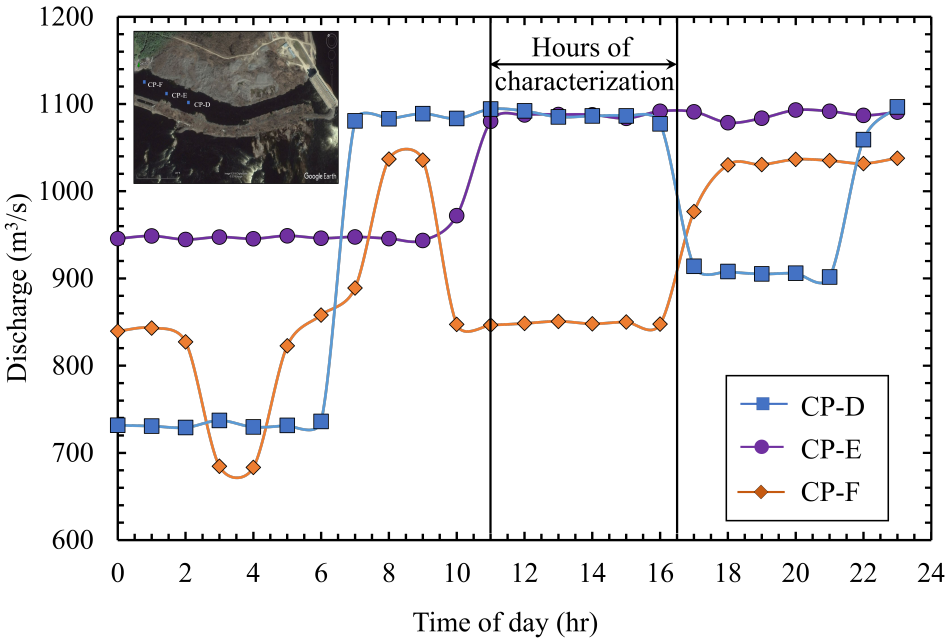

Figure 4.23: Discharge from the Seven Sisters dam during site characterization days. Vertical line shows the time period of the measurement. To simplify the plot, three out of eight days of data are shown.

The CP's are located downstream of the Seven Sisters dam. The hourly discharge rate is available from the Seven Sisters hydro dam and discharge data of measurement days of CP-D, E and F are presented in Figure 4.23. From Figure 4.23 it is observed that during characterization period, there is no significant change in discharge rate. Hence there should not be any significant change in flow velocity. This makes it easy to identify the motion of the measurement platform or instrument during the measurement period.

The ADV pitch angle and the rotational angle during the measurements are shown in Figure 4.24. These angles depend upon the deployment procedure, flow velocity, turbulence statistics, surrounding environments of the measurement region and the expertise of the operator. If there is less slack between the surface measurement platform and the bottom weight, the pitch angle will be less. The opposite is true for large slack. The pitch angle of the CP-D1 and CP-D2 varies from 2.72° to 37.7° with

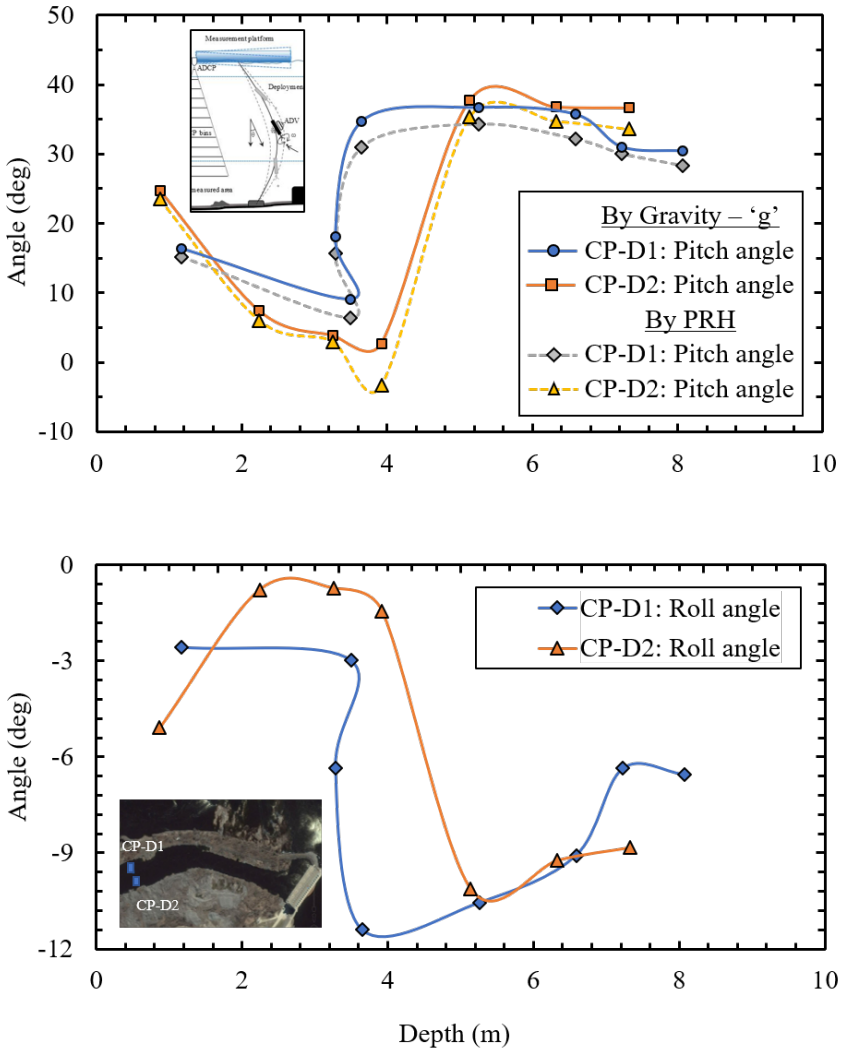

Figure 4.24: Comparison Gravity−'g' and PRH method in measuring ADV orientation at different depth of measurement Point CP-D1, and CP-D2: a) pitch angle, and b) roll angle

an average difference of 2.02° between the pitch angles measured by the Gravity−'g' and PRH method. At 3.9 m depth of CP-D2, the measured pitch angle is − 3.0°. This is because of the ADV alignment in the opposite direction to the flow velocity. This may occur if the measurement platforms move too much towards the flow direction to make ADV as much as vertical as possible. However, the roll angle for both characterization point CP-D1 and CP-D2 are within the acceptable limit of 10°. If the measured angle is within 10° no angle compensation routine is applied.

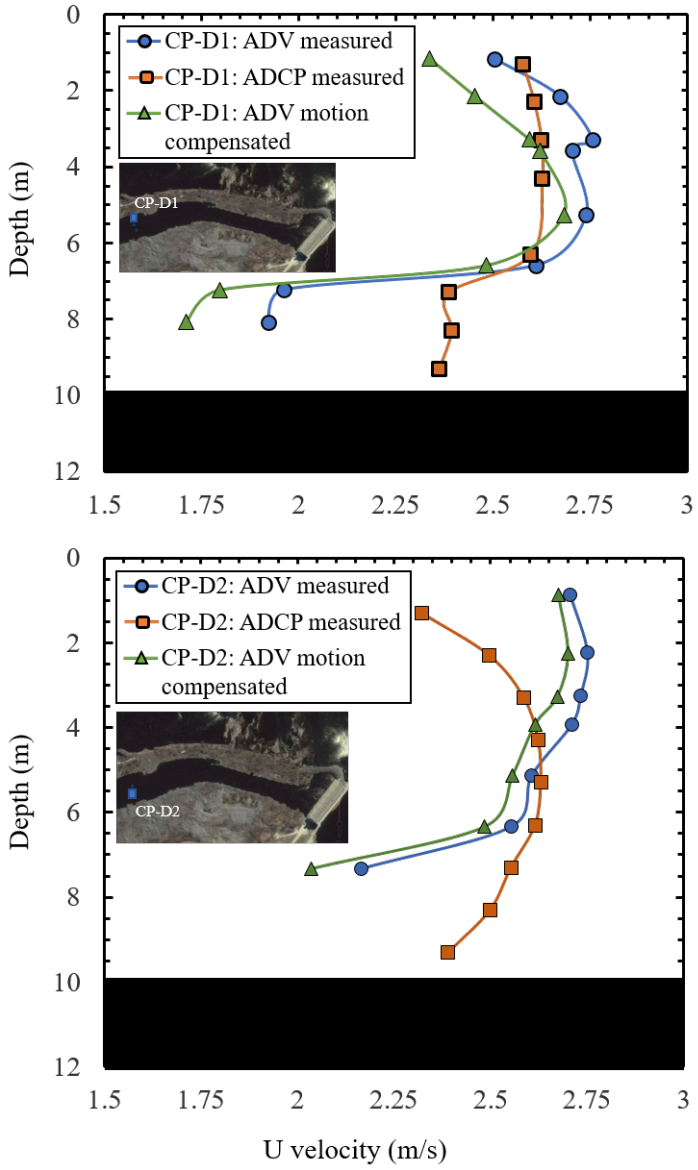

Figure 4.25: Comparison of streamwise velocity profile measured by ADV, ADCP, and ADV after motion correction, at measurement Point a) CP-D1, and b) CP-D2. The dark area indicates the bed of the river. The mean value obtained from a time series at the corresponding depth is indicates as a data point along the spline of each profile.

The mean streamwise velocity profile and TI profile of the characterization point CP-D1 and CP-D2 are shown in Figure 4.25 and Figure 4.26 respectively. Although the approximate depth of the channel is 12 m, the maximum depth of the ADV measurement is 8.1 m. However, the maximum depth of the ADCP measurement is

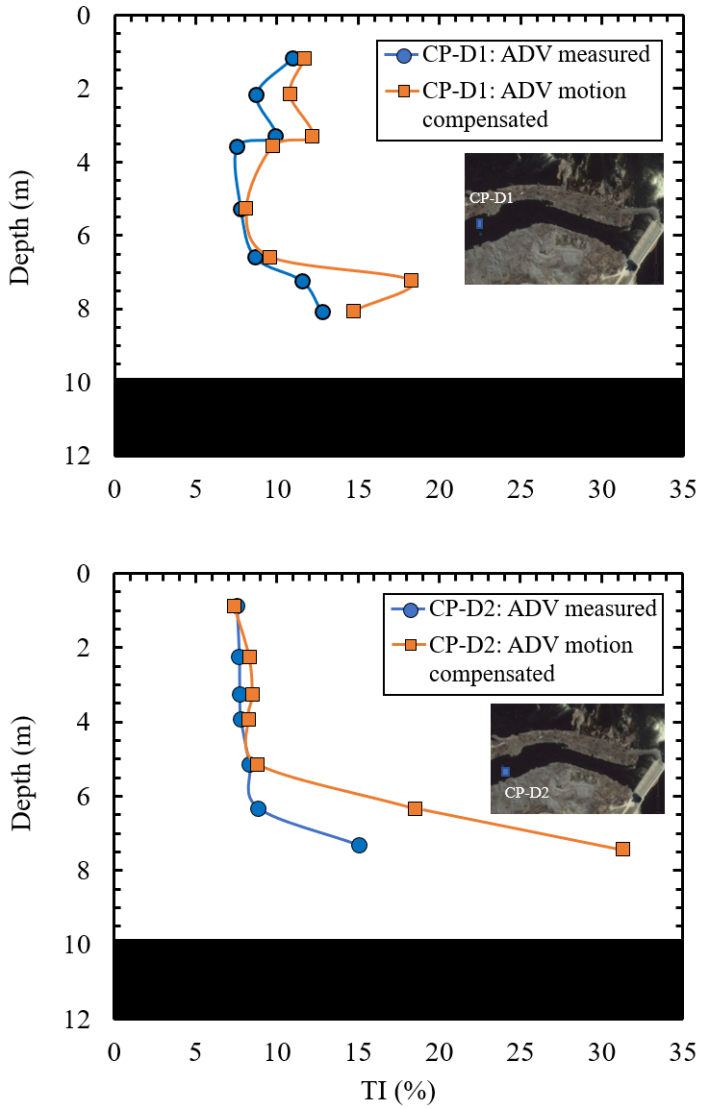

Figure 4.26: Comparison of TI profile measured by ADV before, and after motion correction at measurement Point a) CP-D1, and b) CP-D2. The dark area indicates the bed of the river. The mean value obtained from a time series at the corresponding depth is indicates as a data point along the spline of each profile.

10.5 m. From Figure 4.25, it is observed that in some cases ADCP under-predicts while in other cases it over-predicts the mean streamwise velocity compared to the ADV measured velocity. In the middle section, where turbulence is low compared to the near surface and boundary layer, ADV measured mean velocity is most likely to agree with the ADCP measurements. This is because the ADCP uses spatial averaging and also does have enough high resolution to calculate flow velocity.

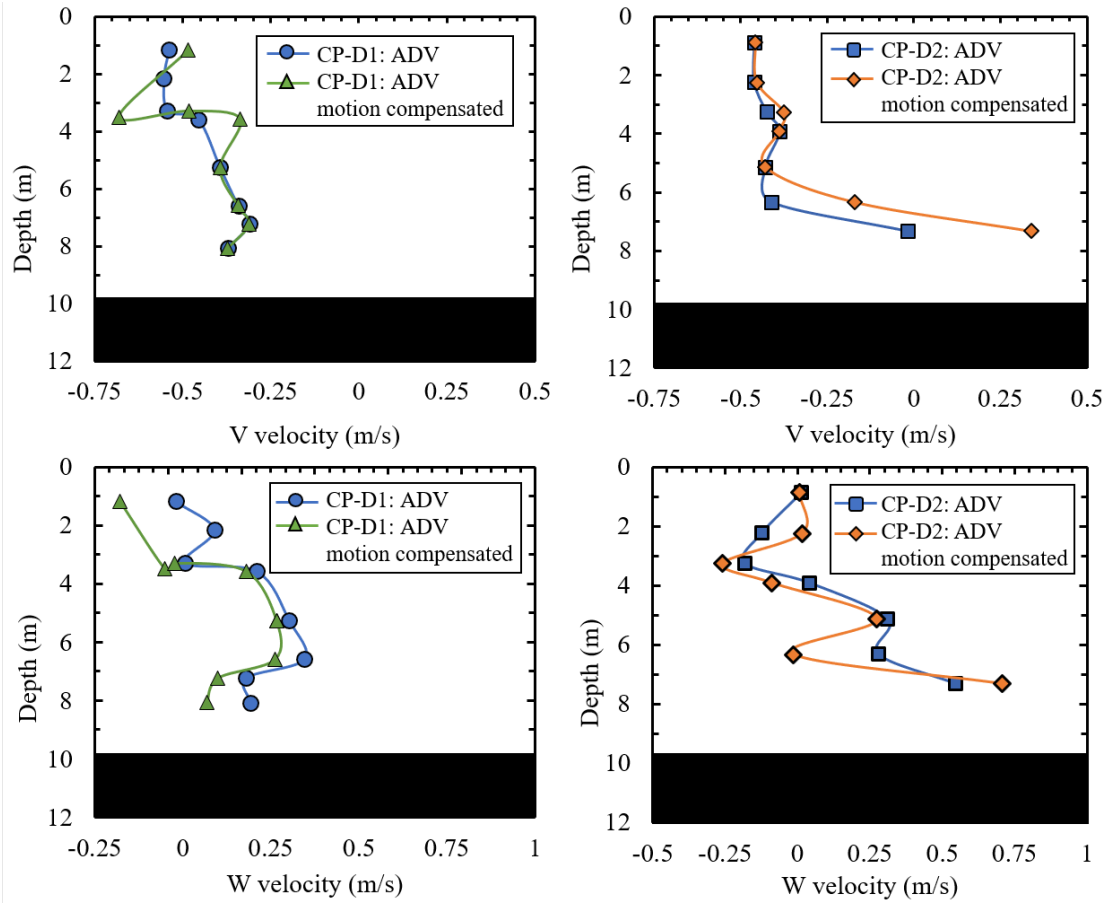

Figure 4.27: Comparison of spanwise and vertical velocity profile measured by ADV, before and after motion correction, at the CHTTC. From left to right: CP-D1, and CP-D2. The dark area indicates the location of river bed.

Figure 4.27 shows the spanwise and vertical velocity profiles measures by the ADV, before and after motion compensation at CP-D1 and CP-D2. The average uncertainty interval between the measured and motion compensated spanwise and vertical velocity at CP-D1 is 8.89% and 190%, respectively, while for CP-D2 the uncertainty interval is 12.1% and 96.7%. For CP-D2, the spanwise velocity measurement at a depth of 7.33 m is ignored as the value is unexpectedly high and could be considered as outlier. Similar to the streamwise velocity profile, near to the surface and bottom of the river bed where turbulence is high, spanwise velocity vary between the ADV measured, and motion compensated velocity.

It is observed that the ADV velocity profile without motion correction overpredicts the

Table 4.6: Average flow statistics of the characterization points CP-D1, and CP-D2; before, and after motion compensation

Depth (m)	Before motion compensation		After motion compensation		Uncertainty of	
	U (m/s)	TI (%)	U (m/s)	TI (%)	U (%)	TI (%)
CP-D1						
1.17	2.50	11.0	2.34	11.7	6.66	6.59
2.15	2.67	8.73	2.45	10.8	8.19	23.4
3.29	2.76	9.91	2.59	11.4	5.86	15.5
3.65	2.70	7.52	2.62	9.72	3.07	29.1
5.26	2.74	7.76	2.68	8.08	2.06	4.15
6.59	2.61	8.65	2.48	9.58	4.82	10.8
7.23	1.96	11.6	1.80	18.3	8.32	58.0
8.07	1.92	12.8	1.71	14.7	11.0	15.0
CP-D2						
0.87	2.71	7.55	2.67	7.38	1.18	2.19
2.24	2.75	7.69	2.70	8.30	1.87	7.99
3.25	2.73	7.71	2.67	8.48	2.23	10.0
3.92	2.71	7.78	2.61	8.24	3.53	5.88
5.14	2.61	8.31	2.56	8.82	1.91	6.12
6.33	2.55	8.88	2.48	18.5	2.74	108
7.33	2.17	15.0	2.04	31.2	6.00	107
Maximum uncertainty					11.0	109
Minimum uncertainty					1.18	2.29

mean streamwise velocity. This is because of the flowing water which adds additional velocity to the ADV measurement. The motion compensation removes this added velocity. The CHTTC characterization data contains a large number of spikes in the data due to the suspended water particles, deployment cable vibration, instrument vibration and motion, and measurement platform motion. These spikes are removed by using the hybrid despiking method. As there was no significant change in the flow rates, despiking will not affect valid data points. Findings are summarized in Table 4.6.

There was a maximum of 11.0% difference observed between streamwise velocity with and without motion compensation. It is worth noting that the location with the

highest turbulence intensity has the highest uncertainty between the compensated and non-compensated velocity while the maximum uncertainty for TI is 109.0%. Near the bottom of the riverbed, the ADV measured TI is lower, but after motion compensation, the value gets higher due to the spikes in data. However, compare to the near surface, more spikes were observed at the bottom of river bed due to the obstruction and surface roughness. Another possible reason could be the effect of the boundary layer. The average uncertainty interval of the measurement before and after motion compensation for streamwise velocity and the TI is 4.63% and 27.4%, respectively.

4.7 Summary

Moffat method, which is also known as the Guide to the expression of Uncertainty in Measurements (GUM) is used to quantify the uncertainty of the ADV velocity measurement for the 3 application used in this study − laboratory, field platform, and cable in a river. For any given calculated parameter, y, and N number of measurements, the combined uncertainty $u_c(y)$ is calculated by

$$u_c^2(y) = \sum_{i=1}^{N} \left(\frac{\partial f}{\partial x_i} \right)^2 u^2(x_i) \tag{4.1}$$

where the partial derivative, $\frac{\partial f}{\partial x_i}$, is the sensitive coefficient, and $u(x_i)$ is the uncertainty of each measurement x_i.

For laboratory experiments, it is considered that each of the measurement is independent, and the repeated observation of each measurement follows Gaussian distribution. The combined uncertainty of the ADV's laboratory experiment can be expressed through measured uncertainty of the speeding particle $u(S)$, orientation, $u(O)$, and motion and vibration, $u(MV)$ as,

$$u_c^2(y) = \left(\frac{\partial f}{\partial S}\right)^2 u^2(S) + \left(\frac{\partial f}{\partial O}\right)^2 u^2(O) + \left(\frac{\partial f}{\partial MV}\right)^2 u^2(MV) \tag{4.2}$$

The expanded uncertainty, U is obtained using the following equation:

$$U = k u_c(y) \tag{4.3}$$

where k is the coverage factor. The value of k depends upon the level of confidence. The range of k value is 2 to 3. If $k = 2$ the level of confidence is approximately 95% and if $k = 3$ the level of confidence is approximately 99%.

The measured value of each term in this study are presented in Figure 4.28 and Table 4.7. Figure 4.28 reflects the cases where laboratory settings matches with the field experiment conditions. There is an improvement in ADV measurement is observed before and after implementing best practice and compensation routines where dominating uncertainties are instrument orientation, and motion and vibration with an uncertainty of 4.60% and 3.26%, respectively. For field experiment speeding particle, instrument orientation, motion, and vibration are variables depending on site specification and the time of operation. So the uncertainty is calculated based on the ADV measured velocity, with the angle and motion compensated velocity.

With best practice and controlled laboratory working condition the uncertainty of the ADV measurement is less then 2.5% [51]. However, based on Equation 4.2 the combined uncertainty interval of the water tunnel measurements increases to 7.44% with the flow velocity of 1.1 m/s and implementing field conditions in the water tunnel. The calculated uncertainty can be high as 27.2% with the maximum instrument orientation uncertainty interval of 12.3% for a roll angle of 30° using Gravity−'g' method, while from the riverine surface and profile measurements shows that the roll angle of the ADV varies within 10°, as shown in Table 4.4 and Figure 4.24,

Table 4.7: Uncertainties associated with the ADV streamwise velocity measurements in the water tunnel, surface measurements at the Forks, and profile measurement at CHTTC

Source	**Uncertainty**	**Measurement specification**			
		Water tunnel		**River**	
		Standard condition	**Field condition**	**Profile**	**Surface**
Instrument	Doppler noise	Variable	Variable	Variable	Variable
	Sampling volume	Variable	Variable	Variable	Variable
	Sampling frequency	Variable	Variable	Variable	Variable
	Sampling time	Variable	Variable	Variable	Variable
	Spatial and temporal resolution	NA	NA	NA	NA
Environment	Particle size	Variable	4.86%	Variable	Variable
	Turbulence	Variable	Variable	Variable	Variable
	Air bubbles	NA	NA	Variable	Variable
	Sound speed	Variable	Variable	Variable	Variable
	Presence of magnetic field	NA	NA	NA	NA
Deployment	Instrument orientation	NA	4.60%	Variable	Variable
	Motion and vibration	NA	3.26%	Variable	Variable
Data analysis	Coordinate transformation	NA	NA	NA	NA
	Post processing	Variable	Variable	Variable	Variable
Combined uncertainty interval		<2.50%*	7.44%	11.0% **	29.3% ***

* Reference [51]

** Combined uncertainty calculated based on the ADV measured velocity before and after angle, and motion compensation of measurement Point CP-D1 and CP-D2.

***Combined uncertainty calculated based on the ADV measured velocity before and after angle, and motion compensation of measurement Point F-1 to F-6.

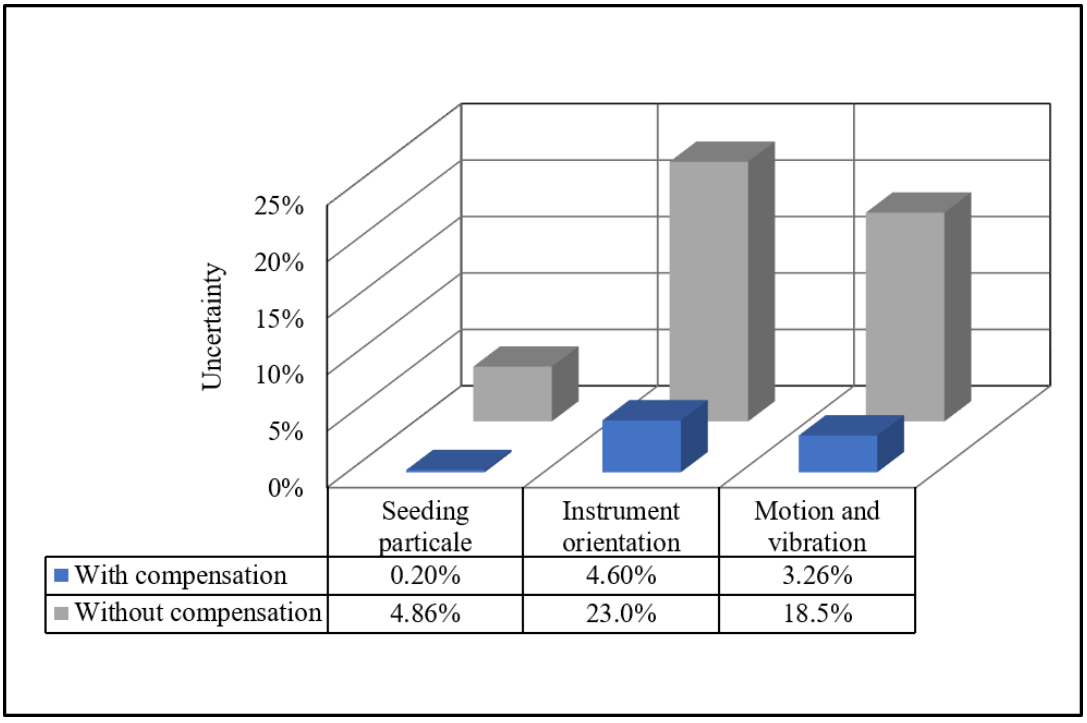

Figure 4.28: ADV measurement uncertainty in the water tunnel due to presence of seeding particle, instrument orientation, motions, and vibration before, and after implementing corrective action, and compensation routine developed in this study

respectively. With this, the maximum orientation uncertainty interval is reduced to 4.60% while the associated combined uncertainty interval reduced to 7.44%. Hence, the uncertainty interval for laboratory measurement is obtained as 14.2% with a 95% confidence interval.

From Table 4.7, it it can be seen that the highest measurement uncertainty interval of 29.3% is obtained from surface measurement at the Forks due to irregular motion of the measurement platform, and the high turbulence level of the flow. For the profile measurements, the maximum uncertainty interval is obtained as 11.0%, which is lower than the surface measurement. This difference can be attributed to less irregular movement of the measurement platform during measurement. However, for profile measurement, the uncertainty interval of 6.66% is obtained near the river surface and 10.6% near the bottom of the river at measurement Point CP-D1, while at measurement Point CP-D2, 6% measurement uncertainty interval is obtained near

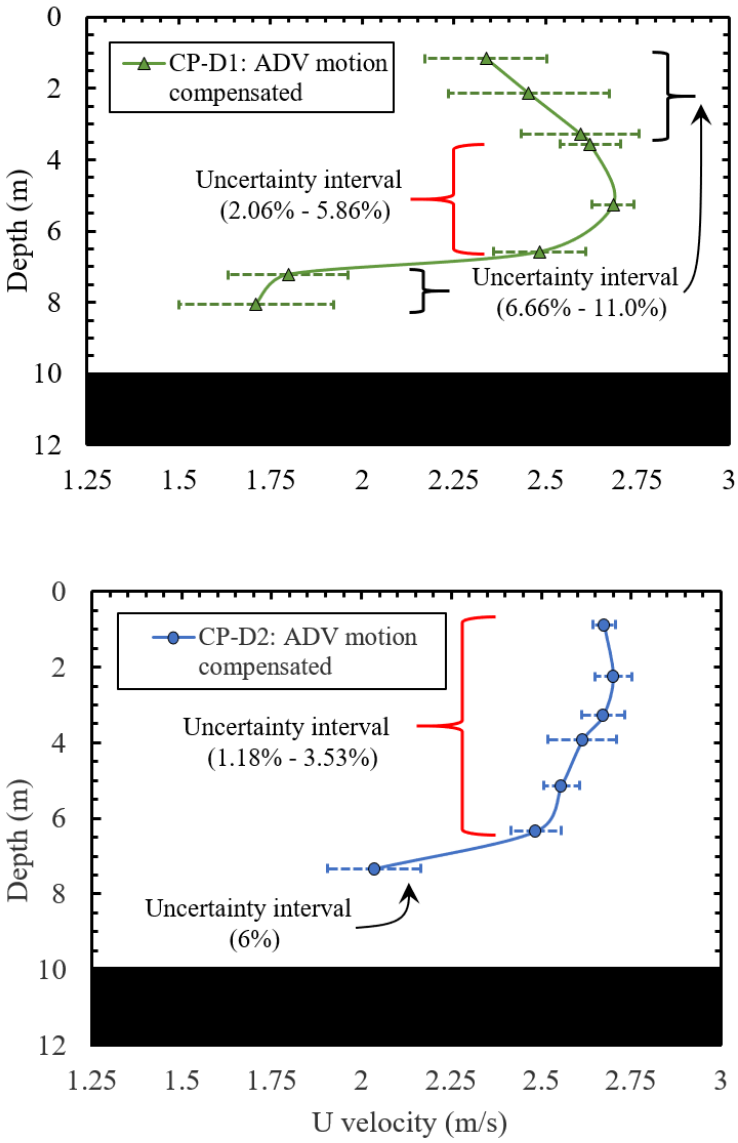

Figure 4.29: The streamwise velocity profile measured by ADV after angle, and motion compensation, at measurement point a) CP-D1, and b) CP-D2 at CHTTC. The error bar shows the uncertainty interval compare with the ADV measured velocity. The dark area indicates the location of river bed.

the bottom of the river, and 1.18% is obtained towards the surface, as shown in Figure 4.29. Comparing both positions, higher uncertainty is observed at the locations with higher turbulence intensity.

Chapter 5

Conclusions, best practice, and recommendations

5.1 Conclusion

A series of tests are performed in the shaker table and water tunnel to identify the effect of seeding particles, instrument orientation, surface roughness, instrument vibration and motion on ADV measurements. Initial assessment of vibration tests shows that with the increasing vibration frequency, the acceleration data fluctuate more intensely. Such an increase in vibration, create additional fluctuation in the measurement and hence increases the uncertainty. A MATLAB code is developed and implemented to correct instrument orientation and motion. At a velocity of 0.53 m/s, a maximum deviation of 20% is observed between the measured and expected streamwise velocity at a pitch angle of 40°. After implementing the PRH angle compensation, the uncertainty interval reduces to 2%; the Gravity−'g', and ENU methods agree within 1%. The water tunnel results show that with the implementation of the angle and motion compensation the maximum uncertainty

interval of the streamwise velocity measurement is reduced to 14.2% from 21.6% at a set velocity of 1.1 m/s.

For surface measurement at the Forks, the ADV orientation angle varies within the range of 10°. In such cases, no angle compensation routine is applied to the measurement. By implementing motion compensation, the platform motion is removed from the ADV surface measurements at Point F-6 where relatively large platform motion is observed in the streamwise velocity measurement. Further, with motion compensation, TI of F-1 and F-2 measurement points are reduced to 7.13% and 18.5% from 31.0% and 30.2%, respectively. The average uncertainty interval of the measured and motion compensated streamwise velocity and TI is 13.5% and 42.8%, which decreases to 11.0% and 20.1%, corresponding to 11.0% and 53.0% decrease, respectively using a three-point mooring system.

In case of profile measurements at CHTTC, the measurement platform is in motion with the flow velocity which adds additional motion in the ADV measurement. These motions are observed in the ADV measured streamwise velocity and removed using motion compensation routine. Near the center of the velocity profile, the ADV measured velocity agrees with the motion compensated velocity within a range of 1.18% to 5.86%, while the range is 6.66% to 11.0% for near the surface and river bed. This higher uncertainty near the surface and the river bed is due to the higher TI and spikes in the data. However, TI is overpredicted by a maximum of 109% near the river bed due to spikes in the data.

There are some limitations in the motion compensation routine which will be addressed in future works. If the starting point of the measurement is a spike or in relatively large motion, the trend selection routine does not work correctly, as it is not a spike detection and replacement mechanism. Currently, this is addressed by removing the starting data points until the first data point is no longer a spike or in

motion. If there is a significant change in flow velocity throughout the measurement, motion correction routine may detect it as a platform motion and remove it. In such cases, motion compensation may remove valid data points. For this study, the maximum length of measurement is 8 minutes, and it is assumed that there is no significant change in flow velocity during this period. Findings were summarized in Table 4.7.

Finally, instrument uncertainty can be reduced by implementing best practices. For field measurements, it has to be ensured that there are sufficient sized particles available in the water to conduct experiments with the ADV. In a situation were there are not enough sized particles, milk can be added to increase the signal strength of the ADV. Also two-point anchoring of the measurement platform should be ensured to minimize platform movement. Furthermore, proper deployment of the measuring instruments has to be maintained by ensuring the instrument is perpendicular as much as possible with the flow. For cable deployment, instrument orientation is governed by providing appropriate length of the deployment cable. If required underwater imaging instrument- sonar camera can be used to observe instrument orientation, and take corrective action.

5.2 Recommendation and future work

To determine the impact of the ADV orientation during deployment, two Item's angle locking Bracket is used in the water tunnel. These brackets are mechanically interlocked, and the precision of their angle measurement is unknown. Additionally, laboratory tests of ADV motion are done by adding manual forces which are not measured independently. Instead, an automated or semi-automated traversing system is recommended to use in the water tunnel to achieve more accurate and precise results.

For the scope of this project, the Kernel Square Regression technique is implemented to identify the drifting trends in the IMU measurement. The trend is then removed so that the underlying data may be used to correct for external motions of the ADV measurements. However, in the future, it is recommended to test the Kalman filter as a replacement as it is already in use in some applications to adjust for the IMU inherent errors and could be used to predict the IMU error better.

The ADV measurement is also affected by vibration. The source of this vibration could be due to the extensive force applied by flowing water or vibration of the deployment cable of the ADV. The IMU accelerometer measurement is affected by these vibrations. If the acceleration measurement is not accurate, it will ultimately affect the performance of the motion compensation routine. This vibration must be isolated from the acceleration measurement to remove the platform motion accurately. However, the effect of vibration on IMU acceleration measurement is discussed in this thesis; a detailed analysis is required to identify the impact of vibration on the ADV and IMU measurements.

Finally, it is also recommended to perform the characterization process for extended periods if possible for a full day or some days. This will help to understand the change in flow statistics over a long period, and the ability of the ADV to determine flow velocity and the turbulence statistics. This will further help to understand the performance of the motion compensation routine in removing platform motion over a significant change in flow rate.

Bibliography

[1] M. Muste, K. Yu, J. A. Gonzalez-Castro, M. Ansar, and R. Startzman, "Methodology for Estimating ADCP Measurement Uncertainty in Open-Channel Flows," in *Critical Transitions in Water and Environmental Resources Management*, no. 2002. Reston, VA: American Society of Civil Engineers, jun 2004, pp. 1–13. [Online]. Available: https://doi-org.uml.idm.oclc.org/10.1061/40737(2004)268 http://ascelibrary.org/doi/10.1061/40737%282004%29268

[2] Nortek, "ADV user manual," no. August, 2005.

[3] SonTek a Xylem brand, "RiverSurveyor S5 / M9 System Manual," no. 858, p. 154, 2013.

[4] I. I. Data, "Renewable 2016 global status report: key findings," *Innovation*, 2016.

[5] T. Pedersen, "Microstrain IMU coordinates Nortek coordinates 16 cm," 2014.

[6] D. of Economic and P. D. Social Affairs, "World population prospects: The 2015 revision, key findings and advance tables," 2015, working Paper No. ESA/P/WP.241.

[7] L. E. Doman and E. al., *International Energy Outlook 2016*, 2016, vol. 0484, no. May.

[8] International Energy Agency, "Key World Energy Statistics 2009," *Statistics*, p. 82, 2015.

[9] P. Charriau and N. Desbrosses, "2015 Global Energy Trends Towards a Peak in Energy Demand and CO_2 Emissions ?" *Enerdata Publications*, p. 34, 2016.

[10] I. Dincer, "Renewable energy and sustainable development: a crucial review," *Renewable and Sustainable Energy Reviews*, vol. 4, no. 2, pp. 157–175, 2000.

[11] Dr. Martin Kaltschmitt; Dr. Wolfgang Streicher; Dr. Andreas Wiese, Ed., *Renewable energy technology, economics and environment.* Springer-Verlag Berlin Heidelberg 2007, 2007.

[12] J. McGowan, "Large-scale solar/wind electrical production systems-predictions for the 21st century." January 1990.

[13] N. Bullard, J. Isola, and E. Zindler, "February 2013.","*Renewable Energy Now Cheaper Than New Fossil Fuels in Australia." Bloomberg New Energy Finance. Retrieved*, vol. 15, 2013.

[14] International Energy Agency, "Renewable energy medium-term market report 2015. Market Analysis and Forecasts to 2020 - Executive Summary," p. 14, 2015.

[15] M. J. Khan, M. T. Iqbal, and J. E. Quaicoe, "River current energy conversion systems: Progress, prospects and challenges," *Renewable and Sustainable Energy Reviews*, vol. 12, no. 8, pp. 2177–2193, 2008.

[16] M. S. Güney and K. Kaygusuz, "Hydrokinetic energy conversion systems: A technology status review," *Renewable and Sustainable Energy Reviews*, vol. 14, no. 9, pp. 2996–3004, 2010.

[17] M. J. Khan, G. Bhuyan, M. T. Iqbal, and J. E. Quaicoe, "Hydrokinetic energy conversion systems and assessment of horizontal and vertical axis turbines for river and tidal applications: A technology status review," *Applied Energy*, vol. 86, no. 10, pp. 1823–1835, 2009.

[18] A. S. Bahaj and L. E. Myers, "Fundamentals applicable to the utilisation of marine current turbines for energy production," *Renewable Energy*, vol. 28, no. 14, pp. 2205–2211, 2003.

[19] L. I. Lago, F. L. Ponta, and L. Chen, "Advances and trends in hydrokinetic turbine systems," *Energy for Sustainable Development*, vol. 14, no. 4, pp. 287–296, 2010. [Online]. Available: http://dx.doi.org/10.1016/j.esd.2010.09.004

[20] M. I. Yuce and A. Muratoglu, "Hydrokinetic energy conversion systems: A technology status review," *Renewable and Sustainable Energy Reviews*, vol. 43, pp. 72–82, 2015. [Online]. Available: http://dx.doi.org/10.1016/j.rser.2014.10.037

[21] M. Balat, "Hydropower Systems and Hydropower Potential in the European Union Countries," *Energy Sources, Part A: Recovery, Utilization, and Environmental Effects*, vol. 28, no. 10, pp. 965–978, 2006. [Online]. Available: http://www.tandfonline.com/doi/abs/10.1080/00908310600718833

[22] P. Action, "River turbines," vol. 44, no. 871954, 2008.

[23] E. A. Nystrom, K. A. Oberg, and C. R. Rehmann, "Measurement of turbulence with acoustic Doppler current profilers - Sources of Error and laboratory results," *Hydraulic Measurements and Experimental Methods Specialty Conference, Estes Park, Colorado, United States*, pp. 1–10, 2002. [Online]. Available: http://ascelibrary.org/doi/abs/10.1061/40655(2002)55

[24] J. a. González-Castro and M. Muste, "Framework for Estimating Uncertainty

of ADCP Measurements from a Moving Boat by Standardized Uncertainty Analysis," *Journal of Hydraulic Engineering-ASCE*, vol. 133, no. 12, pp. 1390–1410, 2007.

[25] H. Toniolo, P. Duvoy, S. Vanlesberg, and J. Johnson, "Modelling and field measurements in support of the hydrokinetic resource assessment for the Tanana river at Nenana, Alaska," *Proceedings of the Institution of Mechanical Engineers, Part A: Journal of Power and Energy*, vol. 224, no. 8, pp. 1127–1139, 2010.

[26] A. E. Hay, J. M. McMillan, R. Cheel, and D. J. Schillinger, "Turbulence and Drag in a High Reynolds Number Tidal Passage Targetted for In-Stream Tidal Power," *Oceans 2013 San DIego*, pp. 1–10, 2013. [Online]. Available: ftp://128.171.151.230/bhowe/outgoing/IEEEOES_2013/papers/130503-133.pdf

[27] R. Karsten, V. Klaptocz, T. Waung, and Greg Trowse, "Characterizing tidal flows and turbine power production in Petit Passage using oceanographic and CFD models validated based on ADCP data," *Offshore Energy Research Association of Nova Scotia*, 2016.

[28] J. Woods, "Hydrokinetic Turbine Systems for Remote River Applications in Cold Climates," Doctor of Philosophy (Ph.D.), University of Manitoba, 2017. [Online]. Available: http://hdl.handle.net/1993/32079

[29] A. Lohrmann, R. Cabrera, and N. Kraus, "Acoustic-doppler velocimeter(ADV) for laboratory use," pp. 351–365, 1994.

[30] G. N. Underwood, "Evaluation of a new laboratory acoustic doppler velocimeter," Master's thesis, Texas A and M University, 1994.

[31] B. V. I. Nikora and D. G. Goring, "ADV Measurements of Turbulence: Can

We Improve Their Interpretation?" *Journal of Hydraulic Engineering-ASCE*, vol. 124, no. 6, pp. 2–6, 1998.

[32] G. Voulgaris, J. H. Throwbridge, and J. H. Trowbridge, "Evaluation of the Acoustic Doppler Velocimeter (ADV) for Turbulence Measurements," *Journal of Atmospheric & Oceanic Technology*, vol. 15, no. 1, p. 272, 1998. [Online]. Available: http://journals.ametsoc.org/doi/abs/10.1175/1520-0426(1998)015%3C0272:EOTADV%3E2.0.CO;2%5Cn

[33] J. N. P. Stuart, "A new method for evaluating erors in high frequency ADV measurements," vol. 366, no. February 1999, p. 2007, 2000.

[34] *An Experimental Study of Tidal Bores and Positive Surges: Hydrodynamics and Turbulence of the Bore Front.* Department of Civil Engineering, University of Queensland, 2005.

[35] D. Hurther and U. Lemmin, "A Correction Method for Turbulence Measurements With a 3-D Acoustic Doppler Velocity Profiler Using a Constant Beam Width Transducer," *Journal of Atmospheric and Oceanic Technology*, vol. 18, no. 3, pp. 446–458, 2001.

[36] A. H. Birjandi and E. Bibeau, "Bubble Effects on the Acoustic Doppler Velocimeter (ADV) Measurements," in *Volume 2: Fora*. ASME, 2009, pp. 27–32. [Online]. Available: http://proceedings.asmedigitalcollection.asme.org/proceeding.aspx?articleid=1637693

[37] A. H. Birjandi and E. L. Bibeau, "Improvement of Acoustic Doppler Velocimetry in bubbly flow measurements as applied to river characterization for kinetic turbines," *International Journal of Multiphase Flow*, vol. 37, no. 8, pp. 919–929, 2011. [Online]. Available: http://dx.doi.org/10.1016/j.ijmultiphaseflow.2011.05.001

[38] S. d'Auteuil, "Investigation and development of flow and turbulence measurement techniques for riverine hydrokinetic turbine sites," Master's thesis, University of Manitoba, 2017.

[39] E. Mosselman, "Morphological modelling of rivers with erodible banks," *Hydrological Processes*, vol. 12, no. 8, pp. 1357–1370, 1998.

[40] S. M. Wiele, J. B. Graf, and J. D. Smith, "Sand deposition in the Colorado River in the Grand Canyon from flooding of the Little Colorado River," *Water Resources Research*, vol. 32, no. 12, pp. 3579–3596, 1996. [Online]. Available: https://www.scopus.com/inward/record.uri?eid=2-s2.0-0030302099&partnerID=40&md5=0bb12275bcec5da9c190e658d5f2bcfb

[41] D. W. Crowder and P. Diplas, "Using two-dimensional hydrodynamic models at scalse of ecological importance," *J. Hyrdrology*, vol. 230, pp. 172–191, 2000.

[42] R. W. J. Lacey and A. G. Roy, "The spatial characterization of turbulence around large roughness elements in a gravel-bed river," *Geomorphology*, vol. 102, no. 3-4, pp. 542–553, 2008. [Online]. Available: http://dx.doi.org/10.1016/j.geomorph.2008.05.045

[43] H. Schlichting and K. Gersten, *Boundary layer theory*, 8th ed. Springer, 2003.

[44] J. Thomson, B. Polagye, and M. Richmond, "Quantifying turbulence for tidal power applications," no. 4, 2010.

[45] G. N. McCann, S. Hitchcock, and S. Lane, "Implications of Site-Specific Conditions on the Prediction of Loading and Power Performance of a Tidal Stream Device St Vincent's Works," *2nd International Conference of Ocean Energy (ICOE 2008), 15 -17 October 2008, Brest, France*, no. October, pp. 1–9, 2008.

[46] Mit, "Basics of Turbulent Flow," pp. 1–10, 2012.

[47] L. Kilcher, J. Thomson, J. Talbert, A. Deklerk, L. Kilcher, J. Thomson, J. Talbert, and A. Deklerk, "Measuring Turbulence from Moored Acoustic Doppler Velocimeters A Manual to Quantifying Inflow at Tidal Energy Sites Measuring Turbulence from Moored Acoustic Doppler Velocimeters A Manual to Quantifying Inflow at Tidal Energy Sites," no. March, 2016.

[48] P. J. Pritchard, *Fox and McDonald's introduction to fluid mechanics*, 8th ed. John Wiley & Sons, 2011.

[49] J. Bureau International des Poids et Measures (BIPM), "Evaluation of measurement data - Guide to the expression of Uncertainty in Measurement," no. September, 2008.

[50] M. a. Arango, "Resource assessment and feasibility study for use of hydrokinetic turbines in the tailwaters of the priest rapids project," Master's thesis, University of Washington, 2011.

[51] A. H. Birjandi, "Effect of Flow and Fluid Structures on the Performance of Vertical River Hydrokinetic Turbines," p. 238, 2012. [Online]. Available: http://mspace.lib.umanitoba.ca/handle/1993/14401

[52] A. Kalnach, J. Kalnach, A. Mutule, and U. Persis, "Potential of the lower daugava for siting hydrokinetic turbines/daugavas lejteces enerģētiskais potenciāls hidrokinētisko turbīnu izmantošanai," *Latvian Journal of Physics and Technical Sciences*, vol. 50, no. 2, pp. 3–14, 2013.

[53] G. Voulgaris and S. T. Meyers, "Temporal variability of hydrodynamics, sediment concentration and sediment settling velocity in a tidal creek," *Continental Shelf Research*, vol. 24, no. 15, pp. 1659–1683, 2004.

[54] K. M. Thyng and J. J. Riley, "Idealized headland simulation for tidal hydrokinetic turbine siting metrics," *MTS/IEEE Seattle, OCEANS 2010*, 2010.

[55] G. T. R. Corporation, "Assessment of Energy Production Potential from Tidal Streams in the United States Final Project Report Award Number : DE-FG36-08GO18174," pp. 1–109, 2011.

[56] S. Matt, W. Hou, S. Woods, W. Goode, E. Jarosz, and A. Weidemann, "A novel platform to study the effect of small-scale turbulent density fluctuations on underwater imaging in the ocean," *Methods in Oceanography*, vol. 11, no. 2014, pp. 39–58, 2014. [Online]. Available: http://dx.doi.org/10.1016/j.mio.2015.01.001

[57] R. Lueck, F. Wolk, J. Hancyck, and K. Black, "Hub-height time series measurements of velocity and dissipation of turbulence kinetic energy in a tidal channel," *2015 IEEE/OES 11th Current, Waves and Turbulence Measurement, CWTM 2015*, 2015.

[58] H. Chanson, M. Trevethan, and S. ichi Aoki, "Acoustic Doppler velocimetry (ADV) in small estuary: Field experience and signal post-processing," *Flow Measurement and Instrumentation*, vol. 19, no. 5, pp. 307–313, 2008.

[59] M. Trevethan and H. Chanson, "Turbulent mixing in a small estuary: Detailed measurements," *Estuarine, Coastal and Shelf Science*, vol. 81, no. 2, pp. 191–200, 2009. [Online]. Available: http://dx.doi.org/10.1016/j.ecss.2008.10.020

[60] Y. Peltier, S. Proust, N. Riviere, A. Paquier, and K. Shiono, "Turbulent flows in straight compound open-channel with a transverse embankment on the floodplain," *Journal of Hydraulic Research*, vol. 51, no. 4, pp. 446–458, 2013. [Online]. Available: http://www.tandfonline.com/doi/abs/10.1080/00221686.2013.796499

[61] S. Gooch, J. Thomson, B. Polagye, and D. Meggit, "Site characterization for tidal power," *OCEANS 2009, MTS/IEEE Biloxi-Marine Technology for*

Our Future: Global and Local Challenges, pp. 1–10, 2009. [Online]. Available: http://ieeexplore.ieee.org/xpls/abs_all.jsp?arnumber=5422134

[62] M. C. Richmond and V. Durgesh, "Inflow Characterization for Marine and Hydrokinetic Energy Devices . FY-2011 : Annual Progress Report," *Renewable Energy*, no. June, 2011.

[63] V. S. Neary, B. Gunawan, and D. C. Sale, "Turbulent inflow characteristics for hydrokinetic energy conversion in rivers," *Renewable and Sustainable Energy Reviews*, vol. 26, pp. 437–445, 2013. [Online]. Available: http://dx.doi.org/10.1016/j.rser.2013.05.033

[64] A. R. Cowan, "User ' s Guide by," vol. 00, no. March, 2002.

[65] W. Bennett, "Spectra of Quantized Signals," pp. 446–471, 1948.

[66] Nortek, "Comprehensive Manual - Principles of Operation," p. 142, 2015.

[67] P. Rusello, "A practical primer for pulse coherent instruments," *Nortek technical note No.: TN-027*, pp. 1–17, 2009. [Online]. Available: http://scholar.google.com/scholar?hl=en&btnG=Search&q=intitle:A+Practical+Primer+for+Pulse+Coherent+Instruments#0

[68] SonTek/YSI, "Acoustical Doppler Velocimeter (Adv): Sampling Volume Size and Velocity Accuracy," vol. i, no. February, pp. 2–4, 1998.

[69] B. Robertson, C. Hiles, E. Luzko, and B. Buckham, "Quantifying the Wave Energy Resource and Farm Siting Opportunities for Western Canada," *International conference on ocean energy*, vol. 1, no. 250, 2014.

[70] G. Reikard, B. Robertson, B. Buckham, J. R. Bidlot, and C. Hiles, "Simulating and forecasting ocean wave energy in western Canada,"

Ocean Engineering, vol. 103, pp. 223–236, 2015. [Online]. Available: http://dx.doi.org/10.1016/j.oceaneng.2015.04.081

[71] C. E. Hiles, B. J. Buckham, P. Wild, and B. Robertson, "Wave energy resources near Hot Springs Cove, Canada," *Renewable Energy*, vol. 71, pp. 598–608, 2014. [Online]. Available: http://dx.doi.org/10.1016/j.renene.2014.06.020

[72] V. S. Neary, B. Gunawan, C. Hill, and L. P. Chamorro, "Near and far field flow disturbances induced by model hydrokinetic turbine: Adv and adp comparison," *Renewable Energy*, vol. 60, pp. 1–6, 2013.

[73] V. Neary, B. Polagye, B. Gunawan, and K. Colby, "Tidal energy site resource assessment: technical specifications, best practices and case studies," Oak Ridge National Laboratory, Oak Ridge, Tech. Rep., 2013.

[74] B. Gunawan, V. S. Neary, and J. Colby, "Tidal energy site resource assessment in the East River tidal strait, near Roosevelt Island, New York, New York," *Renewable Energy*, vol. 71, pp. 509–517, 2014. [Online]. Available: http://dx.doi.org/10.1016/j.renene.2014.06.002

[75] M. Guerra, R. Cienfuegos, J. Thomson, and L. Suarez, "Tidal energy resource characterization in Chacao Channel, Chile," *International Journal of Marine Energy*, vol. 20, pp. 1–16, 2017. [Online]. Available: https://doi.org/10.1016/j.ijome.2017.11.002

[76] B. Gunawan, V. S. Neary, J. Mortensen, and J. D. Roberts, "Assessing and Testing Hydrokinetic Turbine Performance and Effects on Open Channel Hydrodynamics: An Irrigation Canal Case Study," *U.S. Department of Energy - Energy Efficiency & Renewable Energy*, no. March 2016, pp. 1–6, 2017.

[77] D. G. Goring and V. I. Nikora, "Despiking Acoustic Doppler Velocimeter Data," *Journal of Hydraulic Engineering*, vol. 128, no. 1, pp. 117–126, 2002.

[Online]. Available: http://ascelibrary.org/doi/10.1061/%28ASCE%290733-9429%282002%29128%3A1%28117%29

[78] A. Rodriguez, A. Sánchez-Arcilla, J. M. Redondo, and C. Mösso, "Macroturbulence measurements with electromagnetic and ultrasonic sensors: A comparison under high-turbulent flows," *Experiments in Fluids*, vol. 27, no. 1, pp. 31–42, 1999.

[79] J. B. Richard, J. Thomson, B. Polagye, and J. Bard, "Method for identification of Doppler noise levels in turbulent flow measurements dedicated to tidal energy," *International Journal of Marine Energy*, vol. 3-4, pp. 52–64, 2013. [Online]. Available: http://dx.doi.org/10.1016/j.ijome.2013.11.005

[80] K. Miller and M. Rochwarger, "A covariance approach to spectral moment estimation," *IEEE Transactions on Information Theory*, vol. 18, no. 5, pp. 588–596, September 1972.

[81] V. Durgesh, J. Thomson, M. C. Richmond, and B. L. Polagye, "Noise correction of turbulent spectra obtained from acoustic doppler velocimeters," *Flow Measurement and Instrumentation*, vol. 37, pp. 29–41, 2014. [Online]. Available: http://dx.doi.org/10.1016/j.flowmeasinst.2014.03.001

[82] S. E. Buykx, M. A. Van Den Hoop, R. F. Cleven, J. Buffle, and K. J. Wilkinson, "Particles in natural surface waters: Chemical composition and size distribution," *International Journal of Environmental Analytical Chemistry*, vol. 77, no. 1, pp. 75–93, 2000.

[83] N. Mori, T. Suzuki, and S. Kakuno, "Experimental study of air bubbles and turbulence characteristics in the surf zone," *Journal of Geophysical Research*, vol. 112, no. C5, p. C05014, 2007. [Online]. Available: http://doi.wiley.com/10.1029/2006JC003647

[84] K. Blanckaert and U. Lemmin, "Means of noise reduction in acoustic turbulence measurements," *Journal of Hydraulic Research*, vol. 44, no. 1, pp. 3–17, 2006. [Online]. Available: http://www.tandfonline.com/doi/abs/10.1080/00221686.2006.9521657

[85] M. Martin, V., Fisher, T., Millar, R., and Quick, "ADV Data Analysis for Turbulent Flows: Low Correlation Problem (ASCE)," *Hydraulic Measurements and Experimental Methods 2002*, pp. 1–10, 2002. [Online]. Available: http://ascelibrary.org/doi/abs/10.1061/40655(2002)101

[86] B. Gunawan and V. S. Neary, *ORNL ADCP post-processing guide and matlab algorithms for MHK site flow and turbulence analysis*, 2011, no. September.

[87] ——, *ORNL ADV post-processing guide and matlab algorithms for MHK site flow and turbulence analysis*, 2011, no. September.

[88] B. Ruonan, C. Liekai, W. Xingkui, and L. Danxun, "Comparison of ADV and PIV Measurements in Open Channel Flows," *Procedia Engineering*, vol. 154, pp. 995–1001, 2016.

[89] D. R. Sutherland, D. R. Noble, J. Steynor, T. Davey, and T. Bruce, "Characterisation of current and turbulence in the FloWave Ocean Energy Research Facility," *Ocean Engineering*, vol. 139, no. January, pp. 103–115, 2017.

[90] M. R. Soltani, A. H. Birjandi, and M. Seddighi Moorani, "Effect of surface contamination on the performance of a section of a wind turbine blade," *Scientia Iranica*, vol. 18, no. 3 B, pp. 349–357, 2011. [Online]. Available: http://dx.doi.org/10.1016/j.scient.2011.05.024

[91] K. B. Strom and A. N. Papanicolaou, "ADV measurements around a cluster microform in a shallow mountain stream," *Journal of Hydraulic Engineering*, vol. 133, no. 12, pp. 1379–1389, 2007.

[92] R. D. L. Engle, "Air force institute of technology," no. March, 2015.

[93] R. George, R. E. Flick, and R. T. Guza, "Observations of turbulence in the surf zone," *Journal of Geophysical Research*, vol. 99, no. C1, pp. 801–810, 1994. [Online]. Available: http://doi.wiley.com/10.1029/93JC02717

[94] A. C. Wilcox and E. E. Wohl, "Field measurements of three-dimensional hydraulics in a step-pool channel," *Geomorphology*, vol. 83, no. 3-4, pp. 215–231, 2007.

[95] V. I. Nikora and G. M. Smart, "Turbulence characteristics of New Zealand gravel-bed rivers," *Journal of Hydraulic Engineering*, vol. 123, no. 9, pp. 764–773, 1997.

[96] J. Thomson, J. Talbert, L. Kilcher, M. Richmond, J. Talbert, A. DeKlerk, B. Polagye, M. Guerra, and R. Cienfuegos, "Tidal turbulence spectra from a compliant mooring," *Proceedings of the 1st Marine Energy Technology Symposium, METS 2013*, pp. 1–9, 2013.

[97] M. H. Holmes and M. H. Garcia, "Flow over bedforms in a large sand-bed river: A field investigation," *Journal of Hydraulic Research*, vol. 46, no. 3, pp. 322–333, 2008.

[98] M. N. Egeland, "Spectral evaluation of motion compensated adv systems for ocean turbulence measurements." Master's thesis, Florida Atlantic University, 2014.

[99] L. F. Kilcher, J. Thomson, S. Harding, and S. Nylund, "Turbulence measurements from compliant moorings. Part II: Motion correction," *Journal of Atmospheric and Oceanic Technology*, vol. 34, no. 6, pp. 1249–1266, 2017.

[100] J. Thomson, J. Talbert, A. D. Klerk, S. Zippel, M. Guerra, and L. Kilcher, "Turbulence measurements from moving platforms," *2015 IEEE/OES 11th*

Current, Waves and Turbulence Measurement, CWTM 2015, vol. 3, no. 4, 2015.

[101] J. H. VanZwieten, M. N. Egeland, K. D. Von Ellenrieder, J. W. Lovenbury, and L. Kilcher, "Experimental evaluation of motion compensated ADV measurements for in-stream hydrokinetic applications," *2015 IEEE/OES 11th Current, Waves and Turbulence Measurement, CWTM 2015*, 2015.

[102] M. Muste, D. Kim, and J. a. González-Castro, "Near-Transducer Errors in ADCP Measurements: Experimental Findings," *Journal of Hydraulic Engineering*, vol. 136, no. 5, pp. 275–289, 2010.

[103] C. M. García, M. I. Cantero, Y. Niño, and M. H. García, "Turbulence Measurements with Acoustic Doppler Velocimeters," *Journal of Hydraulic Engineering*, vol. 131, no. 12, pp. 1062–1073, 2005. [Online]. Available: http://ascelibrary.org/doi/10.1061/(ASCE)0733-9429(2005)131:12(1062)

[104] V. Nikora and D. Goring, "Flow Turbulence over Fixed and Weakly Mobile Gravel Beds," *Journal of Hydraulic Engineering*, vol. 126, no. 9, pp. 679–690, sep 2000. [Online]. Available: https://doi-org.uml.idm.oclc.org/10.1061/(ASCE)0733-9429(2000)126:9(679) http://ascelibrary.org/doi/10.1061/%28ASCE%290733-9429%282000%29126%3A9%28679%29

[105] R. K. R. K. Otnes and L. Enochson, "Applied time series analysis," Wiley, New York, p. 1, Tech. Rep., 1978.

[106] R. Duraiswami, "Bubble counting using an inverse acoustic scattering method," *The Journal of the Acoustical Society of America*, vol. 104, no. 5, p. 2699, 1998.

[107] S. Elgar, B. Raubenheimer, and R. T. Guza, "Current Meter Performance in the Surf Zone," *Journal of Atmospheric and Oceanic Technology*, vol. 18, no. 10, pp. 1735–1746, oct 2001. [Online]. Available: https://search-

proquest-com.uml.idm.oclc.org/docview/222489324?accountid=14569 http://journals.ametsoc.org/doi/abs/10.1175/1520-0426%282001%29018%3C1735%3ACMPITS%3E2.0.CO%3B2

[108] ——, "Quality control of acoustic doppler velocimeter data in the surfzone," *Measurement Science and Technology*, vol. 16, no. 10, p. 1889, 2005. [Online]. Available: http://stacks.iop.org/0957-0233/16/i=10/a=002

[109] S. Doranga and C. Q. Wu, "Development and performance analysis of single axis simulation table for durability testing," in *Dynamics of Civil Structures, Volume 4*, F. N. Catbas, Ed. Cham: Springer International Publishing, 2014, pp. 227–234.

[110] "http://www.chttc.ca/," 2016.

[111] G. S. Watson, "Smooth Regression Analysis," *Sankhya: The Indian Journal of Statistics*, vol. 26, no. 4, pp. 359–372, 1964.

[112] E. A. Nadaraya, "On Estimating Regression : Theory of Probability & Its Applications," *Society for Industrial and Applied Mathematics*, vol. 9, no. 1, pp. 141–142, 1964. [Online]. Available: https://doi.org/10.1137/1109020

[113] Y. Cao, "A non parametrical regression tool using gaussian kernel," in *Kernel Smoothing Regression*. MathWorks File Exchange, 2008.

Appendix A

Fundamental

A.1 Dimensionless parameters

A.1.1 Reynolds number

The Reynolds number, R_e is used to determine the flow regime; turbulent or laminar and can be calculated by

$$R_e = \frac{\rho R_h u}{\mu} \tag{A.1}$$

where μ is the dynamic viscosity, R_h is the hydraulic radius defined as;

$$R_h = \frac{A_s}{P_{wt}} \tag{A.2}$$

where A_s is cross-section area of the flow, and P_{wt} is the wetted parameter.

Laminar flows are simple, slow and associated with low Reynolds number while turbulent flows are irregular with random spatial and temporal variation and are

associated with high Reynolds number. In a riverine environment, turbulent flow regimes are predominant and have to be measured in a comprehensive way for proper HTKs operations.

A.1.2 Froude number

The Froude number Fr is another parameter used to determining flow conditions and is define as

$$Fr = \frac{u}{\sqrt{gR_h}} \tag{A.3}$$

where gravitational force, g, is 9.81 m/s^2

Froude number compares the actual water velocity with speed of the surface gravitational wave. When Froude number is less than one $Fr < 1$, the flow is sub-critical. This means that the flow is slow and has low energy. When $Fr = 1$ the flow is said to be critical flow means there is a perfect balance between energy. But when $Fr > 1$, the flow is said to be super-critical which is typical of energetic river sites.

Appendix B

MATLAB code

B.1 Motion compensation code

This motion compensation code is the part of the MATLAB code developed for the post processing of ADV dataset.

```
function motionCompensation(~,~)

        %{
        ---------------------------------------------------------------------
        Function: motionCompensation
        ---------------------------------------------------------------------
         The function motionCompensation used the built in ADV Vector IMU
         to compensate for motion induced onto the ADV during the recording
         process. The IMU drift error is removed using a KSR (Kernel
         Smoothing Regression). Note - The KSR operation is a bottleneck
         operation and this routine can be very time consuming.
        ---------------------------------------------------------------------
        %}

        % Declare global variables
        global FilePathName;
        global U V W t frequency;
        global accel_x accel_y accel_z;

        % If no file path is loaded end without doing anything
        if isempty(FilePathName), return, end
        % Change the cursor to a loading animation and update the statusbar
        % to display that the data is being motion compensated.
        set(main.window, 'pointer', 'watch');
        set(main.status_UpdateLabel, 'String'...,
            'Status: Please wait - Preforming motion compensation...');
        drawnow;
```

```
    % Merge several global vectors together into a matrix to faciliate
    % iterating over the three velocity components.

    vel_ADV = [U, V, W];
    IMU = [accel_x, accel_y, accel_z];
    assignin('base', 'vel_ADV', vel_ADV)
    assignin('base', 'IMU', IMU)

    vel_ADV = [U, V, W]';
    IMU = [accel_x, accel_y, accel_z]';
    % Perform motion compensation by iterating over the three velocity
    % components.
for compCount = 1:3

        ADV_tmp = vel_ADV(compCount,:);
        IMU_tmp = IMU(compCount,:);
    size(ADV_tmp)
        size(IMU_tmp)

        IMU_meanSub = IMU_tmp-mean(IMU_tmp);
        IMU_velocity = cumtrapz(IMU_meanSub)./frequency;
        basicCorr = ADV_tmp-IMU_velocity;

        % The following section of code performs a KSR (Kernel
        % Smoothing Regression) on the data. Note: h is the bandwidth
        % of the data and N is the number of samples for the output.



        x = t;
        y = basicCorr;

        x=x(:);
        y=y(:);

        h = 0.5;
        N = length(t);
    % Note: The following line is creating a Gaussian kernel
        % function. @(z) is a function handle. It defines an anonymous
        % function 'kerf' that takes z as an input.
    kerf=@(z)exp(-z.*z/2)/sqrt(2*pi);

        ksr.x = linspace(min(x),max(x),N);
        ksr.f=zeros(1,N);
        for k=1:N
            z=kerf((ksr.x(k)-x)/h);
            ksr.f(k)=sum(z.*y)/sum(z);
        end

        % End of the KSR code.

        % Calculate the corrected velocity.
        cumTrend = ksr.f;
        assignin('base', 'cumTrend', cumTrend)
        cumTrend = cumTrend-cumTrend(1);
        minimalCorrection = basicCorr-cumTrend;
        assignin('base', 'IMU_velocity', IMU_velocity)
        assignin('base', 'basicCorr', basicCorr)
```

```
        % Reassign the corrected velocity to the appropriate velocity
            % component.
            if compCount == 1
                U = minimalCorrection';
        assignin('base', 'U', U)
            elseif compCount == 2
                V = minimalCorrection';
                assignin('base', 'V', V)
            else
                W = minimalCorrection';
                assignin('base', 'W', W)
            end

        end

        % Disable the motion compensation and angle compensation buttons.
        % Angle compensation must be preformed prior to motion
        % compensation.
        set(main.compensate_AngleButton, 'Enable', 'off');
        set(main.compensate_MotionButton, 'Enable', 'off');

        % Reset the cursor after the data and update the statusbar
        set(main.window, 'pointer', 'arrow');
        set(main.status_UpdateLabel, 'String', 'Status: ');

    end
```

B.2 Trend selection code

```
function r=ksr(x,y,h,N)
% KSR   Kernel smoothing regression
%
% r=ksr(x,y) returns the Gaussian kernel regression in structure r such that
%   r.f(r.x) = y(x) + e
% The bandwidth and number of samples are also stored in r.h and r.n
% respectively.
%
% r=ksr(x,y,h) performs the regression using the specified bandwidth, h.
%
% r=ksr(x,y,h,n) calculates the regression in n points (default n=100).
%
% By Yi Cao at Cranfield University on 12 March 2008.

x=x(:);
y=y(:);
clean missing or invalid data points
inv=(x~=x)|(y~=y);
x(inv)=[];
y(inv)=[];
Check input and output
error(nargchk(2,4,nargin));
error(nargoutchk(0,1,nargout));
if numel(x)~=numel(y)
    error('x and y are in different sizes.');
end
Default parameters
if nargin<4
    N=100;
```

```
elseif ~isscalar(N)
    error('N must be a scalar.')
end
r.n=length(x);
if nargin<3
    optimal bandwidth suggested by Bowman and Azzalini (1997) p.31
    hx=median(abs(x-median(x)))/0.6745*(4/3/r.n)^0.2;
    hy=median(abs(y-median(y)))/0.6745*(4/3/r.n)^0.2;
    h=sqrt(hy*hx);
    if h<sqrt(eps)*N
        error('There is no enough variation in the data. Regression is
meaningless.')
    end
elseif ~isscalar(h)
    error('h must be a scalar.')
end
r.h=h;

Gaussian kernel function
kerf=@(z)exp(-z.*z/2)/sqrt(2*pi);

r.x=linspace(min(x),max(x),N);
r.f=zeros(1,N);
for k=1:N
    z=kerf((r.x(k)-x)/h);
    r.f(k)=sum(z.*y)/sum(z);
end

end
```